REMTECH

RTR 249-01

RAREFIED GAS EFFECTS ON AEROBRAKING/REENTRY VEHICLES WITH WAKES

February 28, 1995

Contract:

NAS8-39368

Prepared by:

Amolak C. Jain

Prepared for:

National Aeronautics and Space Administration
George C. Marshall Space Flight Center
Marshall Space Flight Center, AL 35812

FOREWORD

This technical report partially fulfills the reporting requirements of work conducted under SBIR Phase II contract NAS8-39368 for Marshall Space Flight Center, National Aeronautics and Space Administration. The work presented here was performed by REMTECH, Inc., Huntsville, AL, and is titled, "Rarefied Gas Effects on Aerobraking/Reentry Vehicles with Wakes."

The project manager from REMTECH was Dr. Amolak C. Jain. The project was very much aided by the technical support of the NASA Technical Monitor, Mr. Werner K. Dahm, Chief Aerodynamicist, Structures and Dynamics Laboratory.

ABSTRACT

The purpose of the present investigation is to understand the basic nature of the wake flow behind an Aeroassisted Space Transfer Vehicle (ASTV) or Aeroassisted Flight Experiment Vehicle (AFE). The astronauts were supposed to fly in the bay of an ASTV or AFE. This problem of thermal environment on the bay of the vehicle becomes important to ensure the safety of the astronauts.

A computer code based on the full Navier-Stokes equations with surface slip and temperature jump boundary conditions is developed. The governing equations are expressed in spherical-cylindrical coordinates and a third order accurate upwind-biased scheme with provision to use a second order accurate central-difference scheme of numerical integration, is used. To ensure a high order of accuracy, complete flowfield from the stagnation line to the wake flow is computed. For this purpose, the computer code is divided into three parts, viz., stagnation part, forepart and aftpart and has the provision to converge each part to provide boundary conditions to the next part or we can compute the entire flow in each iteration.

Extensive numerical computations have been carried out for a number of prescribed conditions, but for the sake of brevity, the results of computations for SR3 tunnel conditions of CNRS, France, are reported here. Computations have been carried out on a cylindrical body with a spherical nose (also called sphere-cylinder body) and on a hemisphere with a cylindrical bay with radius equal to a quarter of the radius of the base of hemisphere, to simulate a generic AFE configuration. Comparison of the results on sphere-cylinder and on the generic AFE body helps us to understand the rarefaction effects and the effect of wake flow on the main flowfield. Comparison with the DSMC data from NASA LaRC indicates general agreement about the nature of wake, but our results differ quantitatively with the DSMC results. At the present moment, the results from the CNRS tunnel are not available. As such, a quantitative comparison of the present results with the experimental data is not possible.

In general, it is found that the wake on a generic AFE is a slow moving, high temperature, low density and, consequently, low pressure fluid.

CONTENTS

List of Figures

NOMENCLATURE

u	Velocity component in the direction of θ-increasing for spherical coordinate system and in the direction of z-increasing for cylindrical coordinate system.
v	Velocity component in the radial direction
u_s	Velocity at the top of Knudsen layer
p, ρ, T	Pressure, density and temperature, respectively.
$\bar{T}_{o\infty}$	Total temperature
T_w	Dimensionless wall temperature = $\bar{T}_w / \bar{T}_{o\infty}$
T_s	Temperature at the top of Knudsen layer
r, θ	Spherical-polar coordinates of a point P in Fig. 6.1b
r, z	Cylindrical coordinates of a point Q in Fig. 6.1b
$\bar{r}_B$	Represents the body of revolution and defined by Eqs. (6-2) in spherical coordinate system and (6.4) in cylindrical coordinate system
$\bar{r}_e$	Represents the outer edge of the domain of integration and defined by Eqs. (6.1) and (6.3)
$\bar{r}_N$	Nose radius of curvature
ne	Merged layer thickness = $r_e - r_B$
η, θ	Transformed variables in spherical coordinates defined by Eq. (2.10)
η, ζ	Transformed variables in cylindrical coordinate system and defined by Eq. (4.10)
c	$= r_B + \eta \cdot ne$
c'	$= \frac{\partial r_B}{\partial \theta} + \eta \frac{\partial ne}{\partial \theta}$ for spherical coordinate system
c'	$= \frac{\partial r_B}{\partial \zeta} + \eta \frac{\partial ne}{\partial \zeta}$ for cylindrical coordinate system
c''	$= \frac{\partial^2 r_B}{\partial \theta^2} + \eta \frac{\partial^2 ne}{\partial \theta^2}$ for spherical coordinate system
c''	$= \frac{\partial^2 r_B}{\partial \zeta^2} + \eta \frac{\partial^2 ne}{\partial \zeta^2}$ for cylindrical coordinate system
ζ, ϕ	Coordinates in the computational plane for the forepart of the body and defined by Eq. (2.16)

y,x	Coordinates in the computational plane for the aftpart of the body and defined by Eq. (4.17)
c_p	Specific heat at constant pressure
c_v	Specific heat at constant volume
γ	Ratio of specific heats = c_p/c_v
M	Mach number
Λ	$= \frac{1}{2} + \frac{1}{(\gamma-1)M_\infty^2}$
μ	Viscosity coefficient
k	Thermal conductivity
σ	Prandtl Number = $\frac{\mu c_p}{k}$
Re0	Reynolds number based upon total temperature = $\bar{\rho}_\infty \bar{u}_\infty \bar{r}_N / \bar{\mu}(\bar{T}_{o\infty})$
α, θ	Momentum and thermal accommodation coefficients
$\dot{q}$	= Heat transfer for unit area to the wall (=$k\frac{\partial T}{\partial n}$, n being normal to the wall)
C_H	= Heat transfer coefficient = $\dot{q} / \left(\frac{1}{2}\rho_\infty u_\infty^3\right)$
τ	= Skin friction per unit area at the wall
C_f	= Skin friction coefficient = $\tau / \left(\frac{1}{2}\rho_\infty u_\infty^2\right)$
C_p	= Pressure coefficient = $(p - p_\infty) \Big/ \left(\frac{1}{2}\rho_\infty u_\infty^2\right)$
a, b	Semi-major and semi-minor axis of the conic section
c	Focal distance from the center of conic section
e	Eccentricity = c/a
e_1, e_2	Eccentricities of the conic sections generating the body of revolution and outer edge of the domain of integration
a_1, a_2	Nose radii of curvature of the conic sections generating the body of revolution and the outer edge of the domain of integration
u_o, v_o, ρ_o, T_o, p_o, p_2	Defined by Eq. (3.8)

Subscripts and Superscripts

$\bar{}$	Bar over a quantity represents the dimensional value of the variable

∞	Represents the value of the variable at free-stream conditions
$o\infty$	Represents the value of the variables at the stagnation condition in free stream

Section 1
INTRODUCTION

1.1 Statement of Problem

The purpose of this investigation is to understand the structure of the wake of an aeroassisted flight type vehicle when it reenters the atmosphere . The aeroassisted vehicles were supposed to traverse the upper atmosphere for a sustained period of time. These vehicles were called Aeroassisted Space Transfer Vehicle (ASTV) and also Aeroassisted Flight Experiment (AFE) Vehicle. The generic shape of an AFE essentially consists of a hemisphere with a cylindrical bay. The problem is extremely important from the point of view of understanding the basic nature of wake under rarefied conditions. Particularly important is the question as to when the wake is formed and how it grows with reduced rarefaction. Also, the AFE was supposed to fly with human beings in the bay of the vehicle. As such, it was important to know the thermal environment of the vehicle so as to ensure the safety of the astronauts. In view of the importance of the problem, Working Group 18 of the international organization AGARD of NATO has taken this problem as one of the prime problems for investigation by the international scientific community. Some of the organizations that are participating to solve the problem of wake through experimental and theoretical procedures are the following:

1. NASA Langley Research Center
2. NASA Marshall Space Center
3. CNRS, Meudon, France
4. DLR Gottingen, Germany
5. DRA Farnborough
6. Imperial College, UK

Working Group 18 had several meetings and the efforts are still continuing to resolve the problem.

In the present investigation, we decided to compute the complete flow field including wakes on a generic AFE type configuration so that the upstream effects if any can be detected. A highly accurate, fastly converging computer code based upon the full Navier-Stokes equations with surface slip and temperature jump boundary conditions is developed. The code uses a third order accurate upwind biased numerical scheme with provision to use second order accurate central-difference scheme of numerical integration near the boundary points of the domain of integration. Other salient features of the code are the following:

1. The code uses the Navier-Stokes equations in spherical coordinate system to compute the forepart flow and cylindrical coordinate system to compute the aft part flow. In this procedure, the singularity that often arises in the body oriented coordinate system at the sharp corner of the sphere is not present. In the body oriented coordinate system, the corner of the hemisphere has an infinite number

of normals and as such cannot be uniquely solved. In our approach, the flow at the corner can be uniquely determined.

2. The computer code is divided into the three parts:
   a. STAG PART: Here, special solution of stagnation line flow have been obtained with a view to provide accurate description of the stagnation line flow and to provide one of the boundary conditions to compute the flow downstream [1,2].
   b. FORE PART: Here, the Navier-Stokes equations in spherical coordinate system are computed using a central-difference scheme of numerical computation. As we do not expect any separation of the flow on the fore part of the body, the central-difference scheme is found adequate for our purposes.
   c. AFT PART: Here, the Navier-Stokes equations in cylindrical coordinate system are computed using a third-order accurate upwind biased scheme to compute the main flow and a second-order central-difference scheme to compute the flow adjacent to the boundary.

The code is so developed that each part converges and provides boundary conditions to compute the next part or we can compute the complete flowfield in each iteration. Various grid generation schemes i.e. algebraic (exponential and trapezoidal) and adaptive are incorporated to give the much needed flexibility of resolving the flow. In most of the cases, the computations converge in less than 1000 iterations and it takes less than three hours of CPU time on SUN work station of REMTECH, Inc.

In the present report, computations have been carried out under experimental conditions of SR3 low-density tunnel at Centre National da la Recherche Scientific (CNRS), Meudon, France. The computations have been carried out on a cylindrical surface with a hemispherical nose (called sphere-cylinder in this report) and on a hemisphere with a cylindrical bay with radius of the cylinder equal to a quarter of the radius of the base of hemisphere. In this way, we can understand the basic features of the flowfield on sphere-cylinder under rarefied conditions and find out the effect of dropping the cylindrical surface to a quarter of the size of the radius of the base of hemisphere on the main flowfield. Besides the thermal environment of the complete vehicle can be computed with reasonable accuracy.

In Chapters 2, 3 and 4, the basic mathematical formulation is described in brief. In Chapter 5, a description of numerical scheme is given. In Chapter 6, grid generation procedure is described .In Chapter 7, the development of initial conditions is presented. In Chapter 8, the Successive Accelerating Replacement Method of numerically integrating the finite-difference form of the governing equations is given. In Chapter 9, discussion of the results is presented followed by conclusion.

1.1 Review of Relevant Literature

In 1990, Jain and Dahm [3] investigated the wake flows on blunt bodies described as sphere and sphere-cone under hypersonic rarefied conditions. The flow was predicted on the basis of the full Navier-Stokes equations with surface slip and temperature jump boundary conditions. They found that on a spherical surface, separation of the fluid takes place at the denser end of the transitional regime. Using DSMC calculations, Brewer[4] and Dogra et al. [5] investigated the wake structure on a sphere and found that under prescribed conditions similar to those used in Ref. [3], there is no flow separation. They attributed this discrepancy to the inaccuracy of the Navier-Stokes equations to predict flow in the wake where the flow is very rarefied. In Refs. [6-9], Moss et al., computed the flow on a 70 degree blunted cone with a round corner and having a cylindrical bay, under three test conditions at SR3 tunnel of CNRS, France, using DSMC particulate method developed by Bird and the Navier-Stokes continuum method described by LAURA code. They compared the results from the particulate and continuum approaches on the 70 degree blunted cone for Knudsen numbers (Ku. No.) ranging from .03 to .001. They found that for Kn. No. = .03, DSMC method predicts a small vortex on the sting while LAURA code predicts no separation [Fig. 16(A) of Ref. 6]. From the above discussion, it is clear that there are significant quantitative differences in the predictions of the flowfield based upon the particulate and continuum approaches. Qualitatively, the behavior of the flow quantities from the predictions of the particulate and continuum approaches is very similar.

At the present moment, extensive numerical experiments on 70 degree blunted cone are taking place at Imperial College, London, CNRS, France, and DFL, Germany. It is expected that the results of these experiments will be available soon and help us to decide the degree of accuracy of different approaches to predict wake flows behind blunt bodies.

In Ref. [4], Brewer computed the flow with DSMC method on an ASTV type configuration. Essentially, his body consisted of a hemisphere with and without a cylindrical bay. He computed flow under flight conditions for Kn. No. = .0104, .0302, .1180, .6548. He found that a hemisphere with a sting forms a closed wake in the entire transitional regime while a hemisphere without a sting has attached flow right up to the continuum limit of the transitional regime. In particular, Brewer showed in Fig. 12 of Ref. [6], the completely attached flow on the after part of the hemisphere without a sting, for Knudsen No. = .0302.

In Ref. [7], Dogra et al., also computed the wake flow on a 70 degree blunted cone with and without sting, under wind tunnel conditions for Kn. No. = .0317, .0107 and .0012. They found that the flow on a hemisphere without a sting separates for Kn. No. = .0107 and .0012, while the flow remains attached at Kn. No. = .0317.

For the case of hemisphere with a sting, Fig. 10 of Ref. [4] shows that the separated vortex extends up to x/d = .15 under flight conditions of Kn. No. = .0302, while Fig. 6 of Ref. [6] indicates that the length of the vortex is much smaller, viz., $x/d \leq .05$ under wind tunnel conditions and Kn. No. = .0317. In Ref. [4], hemisphere corner is sharp, which ought to increase slightly (about 15 percent, Ref. [7]) the size of the vortex. Since am-

bient temperatures in the computations are not exactly the same in Refs. [4] and [6], it is difficult to draw any conclusions about the accuracy of these computations. However, there seems to be substantial differences in the prediction of DSMC results from various places.

Section 2
GOVERNING EQUATIONS OF MOTION IN SPHERICAL COORDINATE SYSTEM

The non-dimensional forms of the steady state Navier-Stokes equations in spherical-polar coordinates with axial symmetry are the following:

Continuity Equation

$$(\rho v)_r + \frac{2\rho v}{r} + \frac{(\rho u)_\theta}{r} + \frac{\rho u \cot\theta}{r} = 0 \tag{2.1}$$

Tangential Momentum Equation

$$\begin{aligned}
&\frac{p_\theta}{r} + \rho\left(v u_r + \frac{u}{r}u_\theta + \frac{uv}{r}\right) \\
&= \frac{2}{\mathrm{Re}_0}\frac{1}{r}\left[\frac{\mu}{r}(u_\theta + v) - \frac{\mu}{3r}(r v_r + 2v + u_\theta + u\cot\theta)\right]_\theta \\
&+ \frac{1}{\mathrm{Re}_0}\left\{\mu\left[r\left(\frac{u}{r}\right)_r + \frac{v_\theta}{r}\right]_r + \frac{3\mu}{r}\left[r\left(\frac{u}{r}\right)_r + \frac{v_\theta}{r}\right]\right. \\
&\left. + \frac{2\mu}{r^2}\cot\theta\left[u_\theta - u\cot\theta\right]\right\}
\end{aligned} \tag{2.2}$$

Radial Momentum Equation

$$\begin{aligned}
&p_r + \rho\left(v v_r + u\frac{v_\theta}{r} - \frac{u^2}{r}\right) \\
&= \frac{2}{\mathrm{Re}_0}\left[\mu v_r - \frac{\mu}{3r}(r v_r + 2v + u_\theta + u\cot\theta)\right]_r \\
&+ \frac{1}{\mathrm{Re}_0}\frac{1}{r}\left\{\mu\left[r\left(\frac{u}{r}\right)_r + \frac{v_\theta}{r}\right]\right\}_\theta \\
&+ \frac{2}{\mathrm{Re}_0}\frac{\mu}{r}\left(2v_r - \frac{u_\theta + v}{r}\right) \\
&+ \frac{1}{\mathrm{Re}_0}\frac{\mu}{r}\left\{\cot\theta\left[r\left(\frac{u}{r}\right)_r + \frac{v_\theta}{r}\right] - \frac{2}{r}(v + u\cot\theta)\right\}
\end{aligned} \tag{2.3}$$

Energy Equation

$$\Lambda\,\rho\left(v\,T_r+\frac{u}{r}T_\theta\right)=\left(v\,p_r+u\,p_\theta\right)$$
$$+\frac{\Lambda}{\mathrm{Re}\,0}\,\frac{1}{\sigma}\,\frac{1}{r}\left\{\left(\mu\,r\,T_r\right)_r+\left(\frac{\mu T_\theta}{r}\right)_\theta+\mu\,T_r+\frac{\mu\cot\theta}{r}T_\theta\right\}$$
$$+\frac{\mu}{\mathrm{Re}\,0}\left\{2v_r^2+\frac{2}{r^2}\left(u_\theta+v\right)^2+\frac{2}{r^2}\left(v+u\cot\theta\right)^2+\left[r\left(\frac{u}{r}\right)_r+\frac{1}{r}v_\theta\right]^2\right\} \tag{2.4}$$
$$-\frac{2}{3}\frac{1}{r^2}\frac{\mu}{\mathrm{Re}\,0}\left\{r\,v_r+2v+u\cot\theta+u_\theta\right\}^2$$

Equation of State

$$p=\frac{\gamma-1}{\gamma}\Lambda\,\rho\,T\quad. \tag{2.5}$$

Boundary Conditions

1. At the edge of the ML, $r = re$

$$u=\sin\theta,\qquad v=-\cos\theta\qquad \rho=1,$$
$$T=1-\frac{1}{2\Lambda},\quad p=\frac{1}{\gamma\,M_\infty^2}. \tag{2.6}$$

2. At the surface, $r = r_B$

$$u_s=A\frac{M_\infty}{\mathrm{Re}\,0}\,\frac{\mu}{\rho}\sqrt{\frac{T_\infty}{T}}\left(u_r-\frac{u}{r}\right)_{r=r_B}+\underbrace{\frac{1}{5}\cdot\frac{\gamma}{\gamma-1}\cdot\frac{1}{\sigma}\cdot\frac{1}{\mathrm{Re}\,0}\cdot\frac{\mu}{\rho T}\times\left(\frac{\partial T}{\partial\theta}\right)_{r=r_B}}_{Creeping\ Term} \tag{2.7}$$

$$T_s=T_w+B\,\frac{M_\infty}{\sigma\,\mathrm{Re}\,0}\,\frac{\mu}{\rho}\sqrt{\frac{T_\infty}{T}}\left(\frac{\partial T}{\partial r}\right)\Bigg|_{r=r_B} \tag{2.8}$$

where

$$A=\sqrt{\frac{\pi\gamma}{2}}\cdot\frac{2-\alpha}{\alpha}$$
$$B=\sqrt{\frac{\pi\gamma}{2}}\cdot\frac{2-\theta}{\theta}\cdot\frac{2\gamma}{\gamma+1}$$

Here α and θ are the momentum and thermal accommodation coefficients. In the computations, $\alpha = 1$ and $\theta = 1$ are taken. (r, θ) represent the coordinates of a point, "r" being the radial distance, and "θ" the vectorial angle. The symbols "u" and "v" represent the velocity components in θ- and r-increasing directions, respectively. Other symbols have their usual meanings. An independent variable appearing as a subscript to a quantity represents the derivative of the quantity with respect to the independent variable.

In the expression for slip velocity, Eq. (2.7), an additional term called the creeping term is taken.

Variables are non-dimensionalized as follows:

$$u=\frac{\bar{u}}{\bar{u}_\infty}, \quad v=\frac{\bar{v}}{\bar{u}_\infty}, \quad p=\frac{\bar{p}}{\bar{\rho}_\infty \bar{u}_\infty^2}, \quad \rho=\frac{\bar{\rho}}{\bar{\rho}_\infty},$$
$$T=\frac{\bar{T}}{\bar{T}_{0\infty}}, \quad \mu=\frac{\bar{\mu}}{\bar{\mu}(\bar{T}_{0\infty})}, \quad r=\frac{\bar{r}}{\bar{r}_N}, \quad \mathrm{Re}_0=\frac{\bar{\rho}_\infty \bar{u}_\infty \bar{r}_N}{\bar{\mu}(T_{0\infty})} \tag{2.9}$$
$$\Lambda=\frac{1}{2}+\frac{1}{(\gamma-1)M_\infty^2}$$

where a bar over a variable represents its dimensional value and $\bar{r}_N$ is the nose radius of curvature of the body.

The curved boundaries formed by the body surface and the outer edge of the merged layer are transformed to straight boundaries by the following transformation:

$$\eta=\frac{r-r_B(\theta)}{r_e(\theta)-r_B(\theta)} \qquad (0\le\eta\le 1), \tag{2.10}$$
$$\theta=\theta$$

The governing equations (2.1) to (2.5) in (η, θ)-plane become the following:

Continuity Equation

$$R_1\frac{\partial\rho}{\partial\eta}+R_2\frac{\partial\rho}{\partial\theta}+R_3\rho=0 \tag{2.11}$$

where

$$R_1=\left(v-\frac{c'}{c}u\right)\frac{1}{ne}$$
$$R_2=\frac{u}{c}$$
$$R_3=\left(\frac{1}{ne}\frac{\partial v}{\partial\eta}+\frac{2v}{c}+\frac{1}{c}\frac{\partial u}{\partial\theta}-\frac{c'}{nec}\frac{\partial u}{\partial\eta}+\frac{1}{c}u\cot\theta\right)$$

where

$$ne = r_B - r_e$$
$$c = r_B + \eta ne$$
$$c' = r_B' + \eta ne'$$
$$c'' = r_B'' + \eta ne''$$

and

$$' = \frac{\partial}{\partial \theta}$$

Normal Momentum Equation

$$A_1 \frac{\partial^2 v}{\partial \eta^2} + A_2 \frac{\partial^2 v}{\partial \eta \partial \theta} + A_3 \frac{\partial^2 v}{\partial \theta^2} + A_4 \frac{\partial v}{\partial \eta} + A_5 \frac{\partial v}{\partial \theta} + A_6 v + A_7 = 0 \qquad (2.12)$$

where

$$A_1 = \frac{\mu}{\mathrm{Re}\,0} \cdot \frac{1}{ne^2}\left[\frac{4}{3} + \left(\frac{c'}{c}\right)^2\right]$$

$$A_2 = -\frac{2\mu}{\mathrm{Re}\,0} \cdot \frac{c'}{ne\,c^2}$$

$$A_3 = \frac{\mu}{\mathrm{Re}\,0} \cdot \frac{1}{c^2}$$

$$A_4 = \frac{\mu}{\mathrm{Re}\,0} \cdot \frac{1}{ne}\left\{\frac{4}{3} \cdot \frac{1}{ne} \cdot \left(\frac{1}{\mu}\frac{\partial \mu}{\partial \eta} + \frac{2ne}{c}\right) + \frac{c'}{c^2}\left(\frac{c'}{ne}\frac{1}{\mu} \cdot \frac{\partial \mu}{\partial \eta} - \frac{1}{\mu} \cdot \frac{\partial \mu}{\partial \theta} - \cot\theta - \frac{c''}{c'} + \frac{2ne'}{ne}\right)\right\}$$
$$- \rho\left(\frac{v}{ne} - \frac{u}{ne} \cdot \frac{c'}{c}\right)$$

$$A_5 = \frac{\mu}{\mathrm{Re}\,0} \cdot \frac{1}{c^2} \cdot \left(\cot\theta + \frac{1}{\mu} \cdot \frac{\partial \mu}{\partial \theta} - \frac{c'}{ne} \cdot \frac{1}{\mu} \cdot \frac{\partial \mu}{\partial \eta}\right) - \frac{\rho u}{c}$$

$$A_6 = -\frac{\mu}{\mathrm{Re}\,0}\frac{4}{3} \cdot \frac{1}{c}\left(\frac{1}{ne} \cdot \frac{1}{\mu} \cdot \frac{\partial \mu}{\partial \eta} + \frac{2}{c}\right)$$

$$A_7 = \frac{1}{3}\frac{\mu}{\mathrm{Re}\,0}\cdot\frac{1}{c}\left\{-\frac{c'}{ne^2}\frac{\partial^2 u}{\partial\eta^2}+\frac{1}{ne}\frac{\partial^2 u}{\partial\eta\theta}+\frac{1}{ne}\left[-\frac{c'}{ne}\cdot\frac{1}{\mu}\cdot\frac{\partial\mu}{\partial\eta}+7\frac{c'}{c}+3\frac{1}{\mu}\frac{\partial\mu}{\partial\theta}+\cot\theta-\frac{ne'}{ne}\right]\frac{\partial u}{\partial\eta}\right.$$
$$\left.-\left[\frac{2}{ne}\frac{1}{\mu}\cdot\frac{\partial\mu}{\partial\eta}+\frac{7}{c}\right]\cdot\left(\frac{\partial u}{\partial\theta}\right)+\left[\frac{1}{ne}\cdot\frac{1}{\mu}\cdot\frac{\partial\mu}{\partial\eta}\left(-2\cot\theta+3\frac{c'}{c}\right)-7\frac{\cot\theta}{c}-3\frac{1}{\mu}\cdot\frac{\partial\mu}{\partial\theta}\cdot\frac{1}{c}\right]u\right\}$$
$$+\left(\frac{\rho u^2}{c}-\frac{1}{ne}\frac{\partial p}{\partial\eta}\right)$$

Tangential Momentum Equation

$$B_1\frac{\partial^2 u}{\partial\eta^2}+B_2\frac{\partial^2 u}{\partial\eta\partial\theta}+B_3\frac{\partial^2 u}{\partial\theta^2}+B_4\frac{\partial u}{\partial\eta}+B_5\frac{\partial u}{\partial\theta}+B_6 u+B_7=0 \qquad (2.13)$$

where

$$B_1=\frac{\mu}{\mathrm{Re}\,0}\cdot\frac{1}{ne^2}\cdot\left[1+\frac{4}{3}\left(\frac{c'}{c}\right)^2\right]$$

$$B_2=-\frac{8}{3}\cdot\frac{\mu}{\mathrm{Re}\,0}\cdot\frac{c'}{c^2}\cdot\frac{1}{ne}$$

$$B_3=\frac{4}{3}\cdot\frac{\mu}{\mathrm{Re}\,0}\cdot\frac{1}{c^2}$$

$$B_4=\frac{\mu}{\mathrm{Re}\,0}\left\{-\frac{4}{3}\cdot\frac{c'}{ne\,c^2}\left[\frac{1}{\mu}\cdot\frac{\partial\mu}{\partial\theta}+\frac{c''}{c'}-\frac{2ne'}{ne}+\cot\theta\right]+\frac{1}{ne^2}\left[1+\frac{4}{3}\left(\frac{c'}{c}\right)^2\right]\frac{1}{\mu}\frac{\partial\mu}{\partial\eta}+\frac{2}{ne\cdot c}\right\}$$
$$-\rho\left[\frac{v}{ne}-\frac{uc'}{ne\cdot c}\right]$$

$$B_5=-\frac{\mu}{\mathrm{Re}\,0}\cdot\frac{4}{3}\cdot\frac{1}{c^2}\left[\frac{1}{\mu}\frac{\partial\mu}{\partial\theta}-\frac{c'}{ne}\frac{1}{\mu}\frac{\partial\mu}{\partial\eta}+\cot\theta\right]-\frac{\rho u}{c}$$

$$B_6=\frac{\mu}{\mathrm{Re}\,0}\left\{-\frac{2}{3}\cdot\frac{1}{c^2}\left[\left(\frac{1}{\mu}\frac{\partial\mu}{\partial\theta}-\frac{c'}{ne}\cdot\frac{1}{\mu}\frac{\partial\mu}{\partial\eta}\right)\cot\theta+2\,\mathrm{cosec}^2\theta\right]\right.$$
$$\left.-\frac{1}{ne}\cdot\frac{1}{c}\cdot\frac{1}{\mu}\cdot\frac{\partial\mu}{\partial\eta}\right\}-\frac{\partial v}{c}$$

$$B_7 = \frac{\mu}{\mathrm{Re}\,0}\left\{-\frac{1}{3}\cdot\frac{1}{ne^2}\frac{c'}{c}\frac{\partial^2 v}{\partial\eta^2}+\frac{1}{3}\cdot\frac{1}{ne}\cdot\frac{1}{c}\cdot\frac{\partial^2 v}{\partial\eta\,\partial\theta}+\frac{1}{ne}\cdot\frac{1}{c}\left(\frac{8}{3}\cdot\frac{ne}{c}+\frac{1}{\mu}\cdot\frac{\partial\mu}{\partial\eta}\right)\frac{\partial v}{\partial\theta}\right.$$
$$-\frac{1}{ne^2}\left[\frac{1}{3}\cdot\frac{c'}{c}\cdot\frac{1}{\mu}\frac{\partial\mu}{\partial\eta}+\frac{2}{3}\cdot\frac{ne}{c}\cdot\frac{1}{\mu}\cdot\frac{\partial\mu}{\partial\theta}+\frac{1}{3}(ne'\cdot c+8ne\cdot c')\right]\frac{\partial v}{\partial\eta}$$
$$\left.+\frac{2}{3}\cdot\frac{1}{c^2}\left[\frac{1}{\mu}\cdot\frac{\partial\mu}{\partial\theta}-\frac{c'}{ne}\cdot\frac{1}{\mu}\cdot\frac{\partial\mu}{\partial\eta}\right]v\right\}-\frac{1}{c}\left(\frac{\partial p}{\partial\theta}-\frac{c'}{ne}\frac{\partial p}{\partial\eta}\right)$$

Energy Equation

$$C_1\frac{\partial^2 T}{\partial\eta^2}+C_2\frac{\partial^2 T}{\partial\eta\,\partial\theta}+C_3\frac{\partial^2 T}{\partial\theta^2}+C_4\frac{\partial T}{\partial\eta}+C_5\frac{\partial T}{\partial\theta}+C_6T+C_7=0 \qquad (2.14)$$

where

$$C_1=\frac{\Lambda}{\mathrm{Re}\,0}\cdot\frac{\mu}{\sigma}\cdot\frac{1}{ne^2}\cdot\left[1+\left(\frac{c'}{c}\right)^2\right]$$

$$C_2=-2\cdot\frac{\Lambda}{\mathrm{Re}\,0}\cdot\frac{\mu}{\sigma}\cdot\frac{1}{ne}\cdot\frac{c'}{c^2}$$

$$C_3=\frac{\Lambda}{\mathrm{Re}\,0}\cdot\frac{\mu}{\sigma}\cdot\frac{1}{c^2}$$

$$C_4=\frac{\Lambda}{\mathrm{Re}\,0}\cdot\frac{\mu}{\sigma}\cdot\frac{1}{ne}\cdot\frac{1}{c}\cdot\left\{2+\frac{1}{\mu}\cdot\frac{\partial\mu}{\partial\eta}\cdot\frac{c}{ne}\left[1+\left(\frac{c'}{c}\right)^2\right]-\frac{c''}{c}+\frac{c'}{c}\left(-\frac{1}{\mu}\cdot\frac{\partial\mu}{\partial\theta}+\frac{2ne'}{ne}-\cot\theta\right)\right\}-\frac{\Lambda\rho}{ne}\left(v-u\frac{c'}{c}\right)$$

$$C_5=\frac{\Lambda}{\mathrm{Re}\,0}\cdot\frac{1}{\sigma}\cdot\frac{1}{c^2}\left[\frac{1}{\mu}\cdot\frac{\partial\mu}{\partial\theta}-\frac{c'}{ne}\frac{1}{\mu}\cdot\frac{\partial\mu}{\partial\eta}+\cot\theta\right]-\Lambda\rho\frac{u}{c}$$

$$C_6=0.0$$

$$C_7=\frac{\mu}{\mathrm{Re}\,0}\left\{\frac{2}{ne^2}\left(\frac{\partial v}{\partial\eta}\right)^2+\frac{2}{c^2}\left[\left(\frac{\partial v}{\partial\theta}-\frac{c'}{ne}\frac{\partial\mu}{\partial\eta}\right)+v\right]^2+\frac{2}{c^2}(v+u\cot\theta)^2\right.$$
$$+\left[\frac{1}{ne}\frac{\partial u}{\partial\eta}-\frac{u}{c}+\frac{1}{c}\left(\frac{\partial v}{\partial\theta}-\frac{c'}{ne}\frac{\partial v}{\partial\eta}\right)\right]^2-\frac{2}{3}\cdot\frac{1}{c^2}\left[\frac{c}{ne}\frac{\partial v}{\partial\eta}+2v+u\cot\theta+\left(\frac{\partial u}{\partial\theta}-\frac{c'}{ne}\frac{\partial u}{\partial\eta}\right)\right]^2\Bigg\}$$
$$+\left[\left(v-\frac{c'}{c}u\right)\frac{\partial p}{\partial\eta}+\frac{u}{c}\frac{\partial p}{\partial\theta}\right]$$

Equation of State

$$p=\frac{\gamma-1}{\gamma}\Lambda\rho T \qquad (2.15)$$

For ease of computation, the governing equations (2.11) to (2.15) are transformed from (η, θ)-plane to the computational (ζ, ϕ)-plane by the following relations:

$$\zeta = \zeta(\eta, \theta)$$
$$\phi = \phi(\eta, \theta) \tag{2.16}$$

For the general case, equivalent derivatives in (η, θ)-plane and (ζ, ϕ)-plane are the following:

First Order Derivatives

$$\frac{\partial f}{\partial \eta} = \zeta_\eta \frac{\partial f}{\partial \zeta} + \phi_\eta \frac{\partial f}{\partial \phi} \tag{2.17a}$$

$$\frac{\partial f}{\partial \theta} = \zeta_\theta \frac{\partial f}{\partial \zeta} + \phi_\theta \frac{\partial f}{\partial \phi} \tag{2.17b}$$

where the metric coefficients are given by

$$\zeta_\eta = \frac{\theta_\phi}{J}, \quad \zeta_\theta = -\frac{\eta_\phi}{J}$$
$$\phi_\eta = -\frac{\theta_\zeta}{J}, \quad \phi_\theta = \frac{\eta_\zeta}{J}$$
$$J = \left(\eta_\zeta \theta_\phi - \eta_\phi \theta_\zeta\right)$$

Second Order Derivatives

$$\frac{\partial^2 f}{\partial \eta^2} = \zeta_\eta^2 \frac{\partial^2 f}{\partial \zeta^2} + 2\zeta_\eta \phi_\eta \frac{\partial^2 f}{\partial \phi \partial \zeta} + \phi_\eta^2 \frac{\partial^2 f}{\partial \phi^2} + \zeta_{\eta\eta} \frac{\partial f}{\partial \zeta} + \phi_{\eta\eta} \frac{\partial f}{\partial \phi} \tag{2.18a}$$

$$\frac{\partial^2 f}{\partial \theta^2} = \zeta_\theta^2 \frac{\partial^2 f}{\partial \zeta^2} + 2\zeta_\theta \phi_\theta \frac{\partial^2 f}{\partial \zeta \partial \phi} + \phi_\theta^2 \frac{\partial^2 f}{\partial \phi^2} + \zeta_{\theta\theta} \frac{\partial f}{\partial \zeta} + \phi_{\eta\eta} \frac{\partial f}{\partial \phi} \tag{2.18b}$$

$$\frac{\partial^2 f}{\partial \eta \partial \theta} = \zeta_\eta \zeta_\theta \frac{\partial^2 f}{\partial \zeta^2} + \left(\zeta_\eta \phi_\theta + \zeta_\theta \phi_\eta\right) \frac{\partial^2 f}{\partial \zeta \partial \phi} + \phi_\eta \phi_\theta \frac{\partial^2 f}{\partial \phi^2} + \zeta_{\eta\theta} \frac{\partial f}{\partial \zeta} + \phi_{\eta\theta} \frac{\partial f}{\partial \phi} \tag{2.18c}$$

Here, the second order metric coefficients in (η, θ)-plane are related to the metric coefficients in (ζ, ϕ)-plane by the following relations:

$$
\begin{aligned}
\zeta_{\eta\eta} &= \frac{1}{J^3}\left\{\theta_\phi^2\left(\theta_{\zeta\zeta}\,\eta_\phi - \theta_\phi\,\eta_{\zeta\zeta}\right) + \theta_\zeta^2\left(\theta_{\phi\phi}\,\eta_\phi - \theta_\phi\,\eta_{\phi\phi}\right) + 2\theta_\phi\,\theta_\zeta\left(\theta_\phi\,\eta_{\zeta\phi} - \theta_{\zeta\phi}\,\eta_\phi\right)\right\} \\
\phi_{\eta\eta} &= -\frac{1}{J^3}\left\{\theta_\phi^2\left(\theta_{\zeta\zeta}\,\eta_\zeta - \theta_\zeta\,\eta_{\zeta\zeta}\right) + \theta_\zeta^2\left(\theta_{\phi\phi}\,\eta_\zeta - \theta_\zeta\,\eta_{\phi\phi}\right) + 2\theta_\zeta\,\theta_\phi\left(\theta_\zeta\,\eta_{\zeta\phi} - \theta_{\zeta\phi}\,\eta_\zeta\right)\right\} \\
\zeta_{\theta\theta} &= \frac{1}{J^3}\left\{\eta_\phi^2\left(\theta_{\zeta\zeta}\,\eta_\phi - \theta_\phi\,\eta_{\zeta\zeta}\right) + \eta_\zeta^2\left(\theta_{\phi\phi}\,\eta_\phi - \theta_\phi\,\eta_{\phi\phi}\right) + 2\eta_\zeta\,\eta_\phi\left(\theta_\phi\,\eta_{\zeta\phi} - \theta_{\zeta\phi}\,\eta_\phi\right)\right\} \\
\phi_{\theta\theta} &= -\frac{1}{J^3}\left\{\eta_\phi^2\left(\theta_{\zeta\zeta}\,\eta_\zeta - \theta_\zeta\,\eta_{\zeta\zeta}\right) + \eta_\zeta^2\left(\theta_{\phi\phi}\,\eta_\zeta - \theta_\zeta\,\eta_{\phi\phi}\right) + 2\eta_\zeta\,\eta_\phi\left(\theta_\zeta\,\eta_{\zeta\phi} - \theta_{\zeta\phi}\,\eta_\zeta\right)\right\} \\
\zeta_{\eta\phi} &= -\frac{1}{J^3}\left\{\eta_\phi\theta_\phi\left(\theta_{\zeta\zeta}\,\eta_\phi - \theta_\phi\,\eta_{\zeta\zeta}\right) + \theta_\zeta\eta_\zeta\left(\theta_{\phi\phi}\,\eta_\phi - \theta_\phi\,\eta_{\phi\phi}\right) + \left(\theta_\zeta\,\eta_\phi + \theta_\phi\,\eta_\zeta\right)\left(\eta_{\zeta\phi}\,\theta_\phi - \eta_\phi\,\theta_{\zeta\phi}\right)\right\} \\
\phi_{\eta\theta} &= \frac{1}{J^3}\left\{\eta_\phi\theta_\phi\left(\theta_{\zeta\zeta}\,\eta_\zeta - \theta_\zeta\,\eta_{\zeta\zeta}\right) + \eta_\zeta\theta_\zeta\left(\theta_{\phi\phi}\,\eta_\zeta - \theta_\zeta\,\eta_{\phi\phi}\right) + \left(\eta_\zeta\,\theta_\phi + \eta_\phi\,\theta_\zeta\right)\left(\theta_\zeta\,\eta_{\zeta\phi} - \theta_{\zeta\phi}\,\eta_\zeta\right)\right\}
\end{aligned}
\tag{2.19}
$$

These expressions help us express the derivatives of a function with respect to η and θ in terms of the derivatives of the function with respect to ζ and ϕ.

The governing equations (2.11) to (2.15) in the computational plane defined by equations (2.16) are the following:

Continuity Equation

$$P_1\frac{\partial\rho}{\partial\zeta} + P_2\frac{\partial\rho}{\partial\phi} + P_3\,\rho = 0 \tag{2.20}$$

where

$$P_1 = R_1\,\zeta_\eta + R_2\,\zeta_\theta$$
$$P_2 = R_1\,\phi_\eta + R_2\,\phi_\theta$$

and

$$P_3 = R_3$$

Normal Momentum Equation

$$\alpha_1\frac{\partial^2 v}{\partial\zeta^2} + \alpha_2\frac{\partial^2 v}{\partial\zeta\partial\phi} + \alpha_3\frac{\partial^2 v}{\partial\phi^2} + \alpha_4\frac{\partial v}{\partial\zeta} + \alpha_5\frac{\partial v}{\partial\phi} + \alpha_6 v + \alpha_7 = 0 \tag{2.21}$$

where

$$\alpha_1 = A_1\zeta_\eta^2 + A_2\zeta_\eta\zeta_\theta + A_3\zeta_\theta^2$$
$$\alpha_2 = 2A_1\zeta_\eta\zeta_\theta + A_2\left(\zeta_\eta\phi_\theta + \zeta_\theta\phi_\eta\right) + 2A_3\zeta_\theta\phi_\theta$$
$$\alpha_3 = A_1\phi_\eta^2 + A_2\phi_\eta\phi_\theta + A_3\phi_\theta^2$$
$$\alpha_4 = A_1\zeta_{\eta\eta} + A_2\zeta_{\eta\theta} + A_3\zeta_{\theta\theta} + A_4\zeta_\eta + A_5\zeta_\theta$$
$$\alpha_5 = A_1\phi_{\eta\eta} + A_2\phi_{\eta\theta} + A_3\phi_{\theta\theta} + A_4\phi_\eta + A_5\phi_\theta$$
$$\alpha_6 = A_6$$
$$\alpha_7 = A_7$$

Tangential Momentum Equation:

$$\beta_1\frac{\partial^2 u}{\partial\zeta^2} + \beta_2\frac{\partial^2 u}{\partial\zeta\partial\phi} + \beta_3\frac{\partial^2 u}{\partial\phi^2} + \beta_4\frac{\partial u}{\partial\zeta} + \beta_5\frac{\partial u}{\partial\phi} + \beta_{6u} + \beta_7 = 0 \qquad (2.22)$$

where

$$\beta_1 = B_1\zeta_\eta^2 + B_2\zeta_\eta\zeta_\theta + B_3\zeta_\theta^2$$
$$\beta_2 = 2B_1\zeta_\eta\phi_\eta + B_2\left(\zeta_\eta\phi_\theta + \zeta_\theta\phi_\eta\right) + 2B_3\,\zeta_\theta\phi_\theta$$
$$\beta_3 = B_1\phi_\eta^2 + B_2\phi_\eta\phi_\theta + B_3\phi_\theta^2$$
$$\beta_4 = B_1\zeta_{\eta\eta} + B_2\zeta_{\eta\theta} + B_3\zeta_{\theta\theta} + B_4\zeta_\eta + B_5\zeta_\theta$$
$$\beta_5 = B_1\phi_{\eta\eta} + B_2\phi_{\eta\theta} + B_3\phi_{\theta\theta} + B_4\phi_\eta + B_5\phi_\theta$$
$$\beta_6 = B_6$$
$$\beta_7 = B_7$$

Energy Equation:

$$\gamma_1\frac{\partial^2 T}{\partial\zeta^2} + \gamma_2\frac{\partial^2 T}{\partial\zeta\partial\phi} + \gamma_3\frac{\partial^2 T}{\partial\phi^2} + \gamma_4\frac{\partial T}{\partial\zeta} + \gamma_5\frac{\partial T}{\partial\phi} + \gamma_6 T + \gamma_7 = 0 \qquad (2.23)$$

where

$$\gamma_1 = C_1\zeta_\eta^2 + C_2\zeta_\eta\zeta_\theta + C_3\zeta_\theta^2$$

$$\gamma_2 = 2C_1\zeta_\eta\phi_\eta + C_2\left(\zeta_\eta\phi_\theta + \zeta_\theta\phi_\eta\right) + 2C_3\zeta_\theta\phi_\theta$$

$$\gamma_3 = C_1\phi_\eta^2 + C_2\phi_\eta\phi_\theta + C_3\phi_\theta^2$$

$$\gamma_4 = C_1\zeta_{\eta\eta} + C_2\zeta_{\eta\theta} + C_3\zeta_{\theta\theta} + C_4\zeta_\eta + C_5\zeta_\theta$$

$$\gamma_5 = C_1\phi_{\eta\eta} + C_2\phi_{\eta\theta} + C_3\phi_{\theta\theta} + C_4\phi_\eta + C_5\phi_\theta$$

$$\gamma_6 = C_6$$

$$\gamma_7 = C_7$$

Equation of State:

$$p = \Lambda\left(\frac{\gamma-1}{\gamma}\right)\rho T \tag{2.24}$$

The boundary conditions become:

1. At the edge of the domain of interaction, $\zeta = 1$, viz.,

$$u = \sin\phi, \qquad v = -\cos\phi$$

$$\rho = 1, \qquad T = 1 - \frac{1}{2\Lambda} \tag{2.25}$$

$$p = \frac{1}{\gamma M_\infty^2}$$

2. At the surface, $\zeta = 0$

$$u_s = \sqrt{\frac{\pi y}{2}}\cdot\frac{2-\alpha}{\alpha}\cdot\frac{M_\infty}{\mathrm{Re}\,0}\cdot\frac{\mu}{\rho}\cdot\sqrt{\frac{T_\infty}{T}}\left(\frac{1}{ne}\frac{\partial u}{\partial\eta} - \frac{u}{c}\right) + \frac{1}{5}\cdot\frac{\gamma}{\gamma-1}\cdot\frac{1}{\sigma} - \frac{1}{\mathrm{Re}\,0}\cdot\frac{\mu}{\rho T}\left(\frac{\partial u}{\partial\theta} - \frac{c'}{ne}\frac{\partial u}{\partial\eta}\right) \tag{2.26a}$$

and

$$T_s = T_w + \sqrt{\frac{\pi\gamma}{2}}\cdot\frac{2-\theta}{\theta}\cdot\frac{2\gamma}{\gamma+1}\cdot\frac{1}{\sigma}\cdot\frac{M_\infty}{\mathrm{Re}\,0}\cdot\frac{\mu}{\rho}\sqrt{\frac{T_\infty}{T}}\left(\frac{1}{ne}\cdot\frac{\partial T}{\partial\eta}\right) \tag{2.26b}$$

The first order derivatives in the normal and tangential directions in (η,θ)-plane are converted to the computational (ζ, ϕ)-plane from the relationships defined in Eq. (2.17).

Calculations have been carried out to accommodate situations where grid distribution in η-direction on each radial line differs from the other. In other words, the grids along each radial line do not depend upon θ-direction. In this case, the following simplified transformation from (η, θ)-plane to the computational (ζ, ϕ)-plane is adequate:

$$\zeta = \zeta(\eta) \tag{2.27a}$$

$$\phi = \phi(\theta) \tag{2.27b}$$

Under such conditions,

$$\phi_\eta = 0,\ \zeta_\theta = 0,\ \zeta_{\eta\theta} = 0,\ \phi_{\eta\theta} = 0$$

and

$$\begin{aligned} \zeta_\eta &= \frac{1}{\eta_\zeta}, & \phi_\theta &= \frac{1}{\theta_\phi} \\ \zeta_{\eta\eta} &= -\frac{\eta_{\zeta\zeta}}{\eta_\zeta^3}, & \phi_{\theta\theta} &= -\frac{\theta_{\phi\phi}}{\theta_\phi^3} \\ \zeta_{\eta\theta} &= 0, & \phi_{\eta\theta} &= 0 \end{aligned} \tag{2.28}$$

Here,

$$\begin{aligned} \frac{\partial f}{\partial \eta} &= \frac{1}{\eta_\zeta}\frac{\partial f}{\partial \zeta} \\ \frac{\partial f}{\partial \theta} &= \frac{1}{\theta\phi}\frac{\partial f}{\partial \phi} \\ \frac{\partial f}{\partial \eta^2} &= \frac{1}{\eta_\zeta^2}\frac{\partial f}{\partial \zeta^2} - \frac{\eta_{\zeta\zeta}}{\eta_\zeta^3}\frac{\partial f}{\partial \zeta} \\ \frac{\partial^2 f}{\partial \theta^2} &= \frac{1}{\theta_\phi^2}\frac{\partial f}{\partial \phi^2} - \frac{\theta_{\phi\phi}}{\theta_\phi^3}\frac{\partial f}{\partial \phi} \\ \frac{\partial^2 f}{\partial \eta \partial \theta} &= \frac{1}{\eta_\zeta \theta_\phi}\frac{\partial^2 f}{\partial \zeta \partial \phi} \end{aligned} \tag{2.29}$$

and the governing equations are reduced to the following form:

Continuity Equation:

$$P_1\frac{\partial \rho}{\partial \zeta} + P_2\frac{\partial \rho}{\partial \phi} + P_3\,\rho = 0 \tag{2.30}$$

where

$$\begin{aligned} P_1 &= \frac{1}{\eta_\zeta}R_1 \\ P_2 &= \frac{1}{\theta_\phi}R_2 \\ P_3 &= R_3 \end{aligned}$$

Radial Momentum Equation:

$$\alpha_1 = \frac{1}{\eta_\zeta^2} A_1, \qquad \alpha_2 = \frac{A_2}{\eta_\zeta \theta_\phi}, \qquad \alpha_3 = \frac{A_3}{\theta_\phi^2}$$

$$\alpha_4 = \frac{A_4}{\eta_\zeta} - \frac{\eta_{\zeta\zeta} A_1}{\eta_\zeta^3}, \quad \alpha_5 = \frac{A_5}{\theta_\phi} - \frac{\theta_{\phi\phi} A_3}{\theta_\phi^3}, \tag{2.31}$$

$$\alpha_6 = A_6, \qquad \alpha_7 = A_7$$

Tangential Momentum Equation:

$$\beta_1 \frac{\partial^2 u}{\partial \zeta^2} + \beta_2 \frac{\partial^2 u}{\partial \zeta \partial \phi} + \beta_3 \frac{\partial^2 u}{\partial \theta^2} + \beta_4 \frac{\partial u}{\partial \zeta} + \beta_5 \frac{\partial u}{\partial \phi} + \beta_6 u + \beta_7 = 0 \tag{2.32}$$

where

$$\beta_1 = \frac{1}{\eta_\zeta^2} B_1, \qquad \beta_2 = \frac{B_2}{\eta_\zeta \theta_\phi}, \qquad \beta_3 = \frac{B_3}{\theta_\phi^2}$$

$$\beta_4 = \frac{B_6}{\eta_\zeta} - \frac{\eta_{\zeta\zeta}}{\eta_\zeta^3} B_1, \quad \beta_5 = \frac{B_5}{\theta_\phi} - \frac{\theta_{\phi\phi}}{\theta_\phi^3} B_3$$

$$\beta_6 = B_6, \qquad \beta_7 = B_7$$

Energy Equation:

$$\gamma_1 \frac{\partial^2 T}{\partial \zeta^2} + \gamma_2 \frac{\partial^2 T}{\partial \zeta \partial \phi} + \gamma_3 \frac{\partial^2 T}{\partial \phi^2} + \gamma_4 \frac{\partial T}{\partial \zeta} + \gamma_5 \frac{\partial T}{\partial \phi} + \gamma_6 T + \gamma_7 = 0 \tag{2.33}$$

where

$$\gamma_1 = \frac{C_1}{\eta_\zeta^2}, \qquad \gamma_2 = \frac{C_2}{\eta_\zeta \theta_\phi}, \qquad \gamma_3 = \frac{C_3}{\theta_\phi^2}$$

$$\gamma_4 = \frac{C_4}{\eta_\zeta} - \frac{\eta_{\zeta\zeta}}{\eta_\zeta^3} C_1, \quad \gamma_5 = \frac{C_5}{\theta_\phi} - \frac{\theta_{\phi\phi}}{\theta_\phi^3} C_1$$

$$\gamma_6 = C_6, \qquad \gamma_7 = C_7$$

Equation of State:

$$p = \frac{\gamma - 1}{\gamma} \Lambda \rho T \tag{2.34}$$

Boundary Conditions:

1. At the outer edge of the ML, $\zeta = 1$

$$u=\sin\theta, \qquad v=-\cos\phi \qquad \rho=1,$$
$$T=1-\frac{1}{2\Lambda}, \quad p=\frac{1}{\gamma M_\infty^2}. \tag{2.35}$$

2. At the surface, $\zeta = 0$.

$$u_s=\sqrt{\frac{\pi\gamma}{2}}\cdot\frac{2-\alpha}{\alpha}\cdot\frac{M_\infty}{\mathrm{Re}0}\cdot\frac{\mu}{\rho}\cdot\sqrt{\frac{T_\infty}{T}}\left(\frac{1}{ne}\cdot\frac{\partial u}{\partial\zeta}-\frac{u}{c}\right)_{\eta=0}$$
$$\underbrace{+\frac{1}{5}\cdot\frac{\gamma}{\gamma-1}\cdot\frac{1}{\sigma}\cdot\frac{1}{\mathrm{Re}0}\cdot\frac{\mu}{\rho T}\left(\frac{1}{\theta_\phi}\frac{\partial T}{\partial\phi}-\frac{c'}{ne}\cdot\frac{1}{\eta_\zeta}\frac{\partial T}{\partial\zeta}\right)}_{Creeping\ Term} \tag{2.36}$$

$$T=T_w+\sqrt{\frac{\pi\gamma}{2}}\cdot\frac{2-\theta}{\theta}\cdot\frac{2\gamma}{\gamma+1}\cdot\frac{1}{\sigma}\cdot\frac{M_\infty}{\mathrm{Re}0}\cdot\frac{\mu}{\rho}\sqrt{\frac{T_\infty}{T}}\left(\frac{1}{ne}\cdot\frac{1}{\eta_\zeta}\frac{\partial T}{\partial\zeta}\right) \tag{2.37}$$

We notice that for a monoatomic gas, $\gamma = 1.67$, $\sigma = .67$, the coefficient in the creeping term, $\frac{1}{5}\cdot\frac{\gamma}{\gamma-1}\cdot\frac{1}{\sigma}\approx\frac{3}{4}$, the same as derived by Maxwell.

Section 3
STAGNATION LINE SOLUTION

Stagnation line solution provides one of the boundary conditions to solve numerically the full steady-state Navier-Stokes equations for predicting flowfield on a body surface. They also provide an accurate description of the flowfield and surface quantities in the stagnation region of the body.

Here, calculations have been carried out for a general body of revolution described below.

Let the body surface be represented by revolving the conic section

$$\bar{r}_B = \frac{a}{1+e\cos\theta} \tag{3.1}$$

about its major axis. Here, $\bar{r}_B$ is the radius vector of any point on the body from the focus of the conic section; θ is the angle that the radius vector makes with the incoming stream; a is the radius of curvature at the nose ($\theta = 0$) of the body and e is the eccentricity of the conic section.

In the non-dimensional form, the Eq. (3.1) can be written as

$$r_B = \frac{\bar{r}_B}{a} = \frac{1}{1+e\cos\theta} \tag{3.2}$$

e = 0, for a sphere.
< 1, for an ellipse.
= 1, for a parabola.
> 1, for a hyperbola.

Equation (3.1) is expanded in ascending power of θ as follows:

$$r_B = \underbrace{\frac{1}{1+e}}_{0\ order} + \underbrace{\frac{e}{2(1+e)^2}\theta^2}_{first\ order} + \underbrace{\frac{e}{4(1+e)^2}\left[\frac{e}{1+e}-\frac{1}{6}\right]\theta^4}_{second\ order} + \cdots \tag{3.3}$$

which is valid for all values of 'e' in the neighborhood of the stagnation line. It has been found that even the first order approximation with terms up to 0 (θ^2) approximates reasonably well the body surface near the stagnation line.

Let the body surface be represented as:

$$r_B(\theta) = \frac{a_1}{1+e_1\cos\theta}, \tag{3.4}$$

and the outer edge of the merged layer (ML) as:

$$r_e(\theta) = \frac{a_2}{1+e_2\cos\theta}. \tag{3.5}$$

Then, the ML thickness is:

$$\begin{aligned} n_e(\theta) &= r_e(\theta) - r_B(\theta) \\ &= \alpha_1 + \alpha_2\theta^2 + \cdots, \end{aligned} \tag{3.6}$$

where

$$\alpha_1 = \frac{a_2}{1+e_2} - \frac{a_1}{1+e_1},$$

$$\alpha_2 = \frac{1}{2}\left[\frac{a_2 e_2}{(1+e_2)^2} - \frac{a_1 e_1}{(1+e_1)^2}\right],$$

Using the transformation,

$$\begin{aligned} \eta &= \frac{r - r_{B(\theta)}}{r_{e(\theta)} - r_{B(\theta)}} \\ &= \frac{r - r_{B(\theta)}}{ne(\theta)}, \end{aligned}$$

the radial distance of any point in the ML from the focus of the conic section is:

$$\begin{aligned} r &= r_B(\theta) + \eta\, ne(\theta) \qquad (0 \le \eta \le 1) \\ &= \beta_1 + \beta_2\,\theta^2 + \beta_4\,\theta^4 + \cdots, \end{aligned} \tag{3.7}$$

where

$$\beta_1 = \frac{a_1}{1+e_1} + \eta\left(\frac{a_2}{1+e_2} - \frac{a_1}{1+e_1}\right),$$

$$\beta_2 = \frac{1}{2}\left[\frac{a_1 e_1}{(1+e_1)^2} + \eta\left(\frac{a_2 e_2}{(1+e_2)^2} - \frac{a_1 e_1}{(1+e_1)^2}\right)\right],$$

$$\beta_4 = \frac{1}{4}\left\{\frac{a_1 e_1}{(1+e_1)^2}\left(\frac{e_1}{1+e_1} - \frac{1}{6}\right) + \eta\left[\frac{a_2 e_2}{(1+e_2)^2}\left(\frac{e_2}{1+e_2} - \frac{1}{6}\right) - \frac{a_1 e_1}{(1+e_1)^2}\left(\frac{e_1}{1+e_1} - \frac{1}{6}\right)\right]\right\}.$$

Local similar solutions of the NS equations are obtained by assuming the following form of the primitive variables:

$$\begin{aligned} &u = u_o(\eta)\sin\theta, \qquad && v = v_o(\eta)\cos\theta, \\ &\rho = \rho_o(\eta), && T = T_o(\eta), \\ &p = p_o(\eta) + p_2(\eta)\sin^2\theta \end{aligned} \tag{3.8}$$

Substituting Eq. (3.8) in the governing equations and boundary conditions and collecting various order terms, we get the set of equations, valid in the stagnation region of the body. Using the transformation given in Eq. (2.16), we get the following set of equations for the stagnation region flow:

Continuity Equation

$$\frac{1}{\alpha_1}\frac{1}{\eta_\zeta}\frac{d}{d\zeta}(\rho_o v_o)+\frac{2\rho_o(u_o+v_o)}{\beta_1}=0\,. \tag{3.9}$$

Tangential Momentum Equation

$$\begin{aligned}\frac{1}{\alpha_1^2}\left[\frac{1}{\eta_\zeta^2}\frac{d^2u_o}{d\zeta^2}-\frac{\eta_{\zeta\zeta}}{\eta_\zeta^3}\frac{du_o}{d\zeta}\right]=\frac{\mathrm{Re}\,0}{\mu_o}\Bigg\{&\frac{\rho_o v_o}{\alpha_1}\cdot\frac{1}{\eta_\zeta}\frac{du_o}{d\zeta}+\frac{\rho_o u_o(u_o+v_o)}{\beta_1}+\frac{2}{\beta_1}\left[p_2(\zeta)-\frac{\beta_2}{\alpha_1\eta_\zeta}\frac{dp_o}{d\zeta}\right]\Bigg\}\\&+\left[\frac{32}{3}\frac{\beta_2}{\beta_1^2}-\frac{2}{\beta_1}-\frac{1}{\alpha_1}\cdot\frac{1}{\mu_o}\cdot\frac{1}{\eta_\zeta}\frac{d\mu_o}{d\zeta}\right]\frac{1}{\alpha_1}\cdot\frac{1}{\eta_\zeta}\frac{du_o}{d\zeta}\\&+\frac{1}{3}\cdot\frac{1}{\beta_1}\left[\left(3+4\frac{\beta_2}{\beta_1}\right)\frac{1}{\alpha_1}\cdot\frac{1}{\eta_\zeta}\frac{1}{\mu_o}\cdot\frac{d\mu_o}{d\zeta}+\frac{8}{\beta_1}\right](u_o+v_o)\\&+\frac{1}{3}\cdot\frac{1}{\alpha_1\beta_1}\Bigg\{\frac{2\beta_2}{\alpha_1}\left(\frac{1}{\eta_\zeta^2}\frac{d^2v_o}{d\zeta^2}-\frac{\eta_{\zeta\zeta}}{\eta_\zeta^3}\frac{dv_o}{d\zeta}\right)\\&+\left(1+\frac{2\alpha_2}{\alpha_1}+16\frac{\beta_2}{\beta_1}+2\frac{\beta_2}{\alpha_1}\frac{1}{\mu_o}\frac{1}{\eta_\zeta}\frac{d\mu_o}{d\zeta}\right)\frac{1}{\eta_\zeta}\frac{dv_o}{d\zeta}\Bigg\}.\end{aligned} \tag{3.10}$$

Normal Momentum Equation for $p_o(\zeta)$:

$$\begin{aligned}\frac{1}{\alpha_1^2}\left[\frac{1}{\eta_\zeta^2}\frac{d^2v_o}{d\zeta^2}-\frac{\eta_{\zeta\zeta}}{\eta_\zeta^3}\frac{dv_o}{d\zeta}\right]=\frac{3}{4}\frac{\mathrm{Re}\,0}{\mu_o}&\left[\frac{\rho_o v_o}{\alpha_1}\cdot\frac{1}{\eta_\zeta}\frac{dv_o}{d\zeta}+\frac{1}{\alpha_1}\cdot\frac{1}{\eta_\zeta}\cdot\frac{dp_o}{d\zeta}\right]\\&-\left[\frac{1}{\alpha_1}\cdot\frac{1}{\mu_o}\cdot\frac{1}{\eta_\zeta}\frac{d\mu_o}{d\zeta}+\frac{2}{\beta_1}-\frac{3\beta_2}{\beta_1^2}\right]\frac{1}{\alpha_1}\cdot\frac{1}{\eta_\zeta}\frac{dv_o}{d\zeta}\\&+\left[\frac{7}{2}\cdot\frac{1}{\beta_1}+\frac{1}{\alpha_1}\cdot\frac{1}{\mu_o}\cdot\frac{1}{\eta_\zeta}\frac{d\mu_o}{d\zeta}\right]\frac{u_o+v_o}{\beta_1}\\&-\frac{1}{2}\cdot\frac{1}{\alpha_1\beta_1}\cdot\frac{1}{\eta_\zeta}\cdot\frac{du_o}{d\zeta}\,.\end{aligned} \tag{3.11}$$

Energy Equation

$$\frac{\Lambda}{\sigma}\cdot\frac{\mu_o}{\mathrm{Re}\,0}\left\{\frac{\beta_1^2}{\alpha_1^2}\left(\frac{1}{\eta_\zeta^2}\frac{d^2T_o}{d\zeta^2}-\frac{\eta_{\zeta\zeta}}{\eta_\zeta^3}\frac{dT_o}{d\zeta}\right)\right.$$
$$\left.+\frac{\beta_1}{\alpha_1}\left[2+\frac{\beta_1}{\alpha_1}\cdot\frac{1}{\mu_o}\cdot\frac{1}{\eta_\zeta}\cdot\frac{d\mu_o}{d\zeta}-4\frac{\beta_2}{\beta_1}\right]\frac{1}{\eta_\zeta}\cdot\frac{dT}{d\zeta}\right\}$$
$$-\frac{\Lambda\beta_1^2}{\alpha_1}\cdot\frac{\rho_o v_o}{\eta_\zeta}\cdot\frac{dT}{d\zeta}+\frac{\beta_1^2}{\alpha_1}\cdot\frac{v_o}{\eta_\zeta}\frac{dp_o}{d\zeta} \qquad (3.12)$$
$$+\frac{\mu_o}{\mathrm{Re}\,0}\left\{\frac{2\beta_1^2}{\alpha_1^2}\left(\frac{1}{\eta_\zeta}\frac{dv_o}{d\zeta}\right)^2+4(u_o+v_o)^2-\frac{2}{3}\left[\frac{\beta_1}{\alpha_1}\cdot\frac{1}{\eta_\zeta}\cdot\frac{dv_o}{d\zeta}+2(u_o+v_o)\right]^2\right\}$$
$$=0\,.$$

Equation Determining $p_2(\zeta)$:

$$\frac{3}{4}\cdot\frac{\mathrm{Re}\,0}{\mu_o}\left\{\left[\frac{\alpha_2}{\alpha_1}\rho_o v_o+\frac{2\beta_2}{\beta_1}u_o\right]\frac{1}{\alpha_1}\cdot\frac{1}{\eta_\zeta}\cdot\frac{dv_o}{d\zeta}+\frac{\rho_o u_o(v_o+u_o)}{\beta_1}\right.$$
$$\left.+\frac{1}{\alpha_1}\cdot\frac{1}{\eta_\zeta}\left(\frac{\alpha_2}{\alpha_1}\cdot\frac{dp_o}{d\zeta}-\frac{dp_2}{d\zeta}\right)+\frac{1}{2}\frac{1}{\alpha_1\eta_\zeta}\left(\rho_o v_o\frac{dv_o}{d\zeta}-\frac{dp_o}{d\zeta}\right)\right\}$$
$$+\frac{1}{\alpha_1^2\eta_\zeta^2}\left(3\frac{\beta_2^2}{\beta_1^2}-2\frac{\alpha_2}{\alpha_1}\right)\left(\frac{d^2v_o}{d\zeta^2}-\frac{\eta_{\zeta\zeta}}{\eta_\zeta}\frac{dv_o}{d_\zeta}\right)$$
$$-\left[\frac{1}{\alpha_1\eta_\zeta}\left(2\frac{\alpha_2}{\alpha_1}-3\frac{\beta_2^2}{\beta_1^2}\right)\frac{1}{\mu_o}\frac{1}{\eta_\zeta}\cdot\frac{d\mu_o}{d\zeta}+\frac{1}{\beta_1}\left(2\frac{\alpha_2}{\alpha_1}-\frac{\beta_2}{\beta_1}\right)\right.$$
$$\left.-\frac{3}{\beta_1}\left(2\frac{\beta_2^2}{\beta_1^2}-u\frac{\beta_4}{\beta_1}+3\frac{\alpha_2\beta_2}{\alpha_1\beta_1}\right)\right]\frac{1}{\alpha_1\eta_\zeta}\frac{dv_o}{d\zeta}$$
$$+\frac{1}{\beta_1}\left[\frac{1}{\alpha_1\eta_\zeta}\left(\frac{\alpha_2}{\alpha_1}+\frac{5}{2}\frac{\beta_2}{\beta_1}\right)\frac{1}{\mu_o}\frac{d\mu_o}{d\zeta}+7\frac{\beta_2}{\beta_1^2}\right](u_o+v_o) \qquad (3.13)$$

(Continued on next page)

Equation Determining $p_2(\zeta)$ (Concluded)

$$-\frac{1}{2}\left[\frac{\beta_2}{\alpha_1^2\beta_1}\cdot\frac{1}{\eta_\zeta^2}\left(\frac{d^2u_o}{d\zeta^2}-\frac{\eta_{\zeta\zeta}}{\eta_\zeta}\frac{du_o}{d_\zeta}\right)\right.$$

$$\left.+\frac{1}{\alpha_1\beta_1}\cdot\frac{1}{\eta_\zeta}\left(2\frac{\alpha_2}{\alpha_1}-6\frac{\beta_2}{\beta_1}+\frac{\beta_2}{\alpha_1}\frac{1}{\mu_o}\cdot\frac{1}{\eta_\zeta}\frac{d\mu_o}{d\zeta}\right)\cdot\left(\frac{du_o}{d\zeta}\right)\right]$$

$$=0\,.$$

Equation of State

$$p_o=\frac{\gamma-1}{\gamma}\cdot\Lambda\rho_oT_o\,. \tag{3.14}$$

Boundary Conditions

1. At the outer edge, $\zeta = \zeta_e$

$$u_o(\zeta_e)=1, \qquad v_o(\zeta_e)=-1, \qquad \rho_o(\zeta_e)=1, \tag{3.15}$$

$$T_o(\zeta_e)=1-\frac{1}{2\Lambda} \qquad p_o(\zeta_e)=\frac{1}{\gamma M_\infty^2}, \qquad p_2(\zeta_e)=0. \tag{3.16}$$

2. On the surface, $\zeta = 0$

$$u_s=\sqrt{\frac{\pi\gamma}{2}}\cdot\frac{2-\alpha}{\alpha}\frac{M_\infty}{\mathrm{Re}\,0}\frac{\mu_o}{\rho_o}\sqrt{\frac{T_\infty}{T_o}}\left(\frac{1}{\alpha_1}\frac{1}{\eta_\zeta}\frac{du_o}{d\zeta}-\frac{u_o}{\beta_1}\right)_{\zeta=0} \tag{3.17}$$

$$v_s=0 \tag{3.18}$$

$$T_s=T_w+\sqrt{\frac{\pi\gamma}{2}}\cdot\frac{2-\theta}{\theta}\cdot\frac{2\gamma}{\gamma+1}\frac{M_\infty}{\mathrm{Re}\,0\cdot\sigma}\frac{\mu_o}{\rho_o}\sqrt{\frac{T_\infty}{T_o}}\left(\frac{1}{\alpha_1}\frac{1}{\eta_\zeta}\frac{\partial T_o}{\partial_\zeta}\right)_{\zeta=0} \tag{3.19}$$

The equations (3.9) to (3.14) along with the boundary conditions (3.15) to (3.19) are integrated by the Successive Accelerated Replacement (SAR) method of numerical integration, under a wide variety of prescribed conditions and on bodies of different geometrical shapes. The findings of this investigation are reported in Refs. [1,2].

Section 4
GOVERNING EQUATIONS OF MOTION IN CYLINDRICAL COORDINATE SYSTEM

The non-dimensional form of the Navier-Stokes equations in cylindrical coordinates with axial symmetry are the following:

Continuity Equation

$$\frac{\partial}{\partial r}(\rho v)+\frac{\partial}{\partial z}(\rho u)=0 \tag{4.1}$$

Radial Momentum Equation

$$\rho\left(v\frac{\partial v}{\partial r}+u\frac{\partial v}{\partial z}\right)=-\frac{\partial p}{\partial r}+\frac{1}{\mathrm{Re}_0}\left\{\frac{\partial}{\partial r}\left[\frac{2}{3}\mu\left(2\frac{\partial v}{\partial r}-\frac{\partial u}{\partial z}-\frac{v}{r}\right)\right]+\frac{\partial}{\partial z}\left[\mu\left(\frac{\partial v}{\partial z}+\frac{\partial u}{\partial r}\right)\right]+\frac{2\mu}{r}\left[\frac{\partial v}{\partial r}-\frac{v}{r}\right]\right\} \tag{4.2}$$

Axial Momentum Equation

$$\rho\left(v\frac{\partial u}{\partial r}+u\frac{\partial u}{\partial z}\right)=-\frac{\partial p}{\partial z}+\frac{1}{\mathrm{Re}_0}\left\{\frac{\partial}{\partial z}\left[\frac{2}{3}\mu\left(2\frac{\partial u}{\partial z}-\frac{\partial v}{\partial r}-\frac{v}{r}\right)\right]+\frac{1}{r}\frac{\partial}{\partial r}\left[\mu r\left(\frac{\partial v}{\partial z}+\frac{\partial u}{\partial r}\right)\right]\right\} \tag{4.3}$$

Energy Equation

$$\rho\, c_p\left(v\frac{\partial T}{\partial r}+u\frac{\partial T}{\partial z}\right)=-\frac{1}{\Lambda}\left[v\frac{\partial p}{\partial r}+u\frac{\partial p}{\partial z}\right]+\frac{1}{\mathrm{Re}_0}\cdot\frac{1}{\sigma}\cdot\left\{\frac{1}{r}\frac{\partial}{\partial r}\left(r\mu c_p\frac{\partial T}{\partial r}\right)+\frac{\partial}{\partial z}\left(\mu c_p\frac{\partial T}{\partial z}\right)\right\}+\frac{1}{\Lambda}\cdot\frac{\mu}{\mathrm{Re}_0}\cdot\Phi \tag{4.4}$$

where

$$\Phi=2\left[\left(\frac{\partial v}{\partial r}\right)^2+\left(\frac{v}{r}\right)^2+\left(\frac{\partial u}{\partial z}\right)^2\right]+\left[\left(\frac{\partial v}{\partial z}+\frac{\partial u}{\partial r}\right)^2-\frac{2}{3}\left(\frac{\partial v}{\partial r}+\frac{v}{r}+\frac{\partial u}{\partial z}\right)^2\right]$$

Equation of State

$$p=\frac{\gamma-1}{\gamma}\Lambda\rho T \tag{4.5}$$

Here

$$\Lambda = \frac{1}{2} + \frac{1}{(\gamma - 1)} \cdot \frac{1}{M_\infty^2}$$

and the variables are non-dimensionalized as follows:

$$\begin{aligned} r &= \frac{\bar{r}}{\bar{r}_N}, & z &= \frac{\bar{z}}{\bar{r}_N} \\ v &= \frac{\bar{v}}{\bar{u}_\infty}, & u &= \frac{\bar{u}}{\bar{u}_\infty} \\ p &= \frac{\bar{p}}{\bar{\rho}_\infty \bar{u}_\infty^2}, & \rho &= \frac{\bar{\rho}}{\bar{\rho}_\infty} \\ T &= \frac{\bar{T}}{\bar{T}_{o\infty}}, & \mu &= \frac{\bar{\mu}}{\bar{\mu}(\bar{T}_{o\infty})} \\ c_p &= \frac{\bar{c}_p}{\bar{c}_{p_\infty}} \end{aligned} \tag{4.6}$$

where a bar over a variable denotes its non-dimensional value; subscript ∞ denotes free-stream quantity, and subscript o ∞ denotes free-stream stagnation conditions. Other variables are defined in the list of nomenclature.

The non-dimensional numbers are defined as follows:

$$\textit{Stagnation Reynolds number} = \frac{\bar{\rho}_\infty \bar{u}_\infty \bar{r}_N}{\bar{\mu}(\bar{T}_{o\infty})}$$

$$\textit{Prandtl number} = \frac{\bar{\mu}_\infty \bar{c}_{p_\infty}}{\bar{k}_\infty}$$

Boundary Conditions

1. At the outer edge of the domain of integration:

$$\begin{aligned} u &= 1.0 \\ v &= 0.0 \\ p &= \frac{1}{\gamma M_\infty^2} \\ \rho &= 1.0 \\ T &= 1 - \frac{1}{2\Lambda} \end{aligned} \tag{4.7}$$

2. On the cylindrical portion of the body, surface slip and temperature jump conditions are:

$$u_s = \sqrt{\frac{\pi\gamma}{2}} \cdot \frac{2-\alpha}{\alpha} \cdot \frac{M_\infty}{\mathrm{Re}_0} \cdot \frac{\mu}{\rho} \cdot \sqrt{\frac{T_\infty}{T}} \cdot \frac{\partial u}{\partial r} + \underbrace{\left(\frac{1}{5} \cdot \frac{\gamma}{\gamma-1} \cdot \frac{1}{\sigma}\right) \cdot \frac{1}{\mathrm{Re}_0} \cdot \frac{\mu}{\rho T} \cdot \frac{\partial T}{\partial z}}_{\textit{creeping term}} \tag{4.8a}$$

$$T_s = Tw + \sqrt{\frac{\pi\gamma}{2}} \cdot \frac{2-\theta}{\theta} \cdot \frac{2\gamma}{\gamma+1} \cdot \frac{1}{\sigma} \cdot \frac{M_\infty}{\mathrm{Re}_0} \cdot \frac{\mu}{\rho} \cdot \sqrt{\frac{T_\infty}{T}} \cdot \left(\frac{\partial T}{\partial r}\right) \tag{4.8b}$$

3. On the base of hemisphere, the slip and temperature jump conditions are:

$$u_s = \sqrt{\frac{\pi\gamma}{2}} \cdot \frac{2-\alpha}{\alpha} \cdot \frac{M_\infty}{\mathrm{Re}_0} \cdot \frac{\mu}{\rho} \cdot \sqrt{\frac{T_\infty}{T}} \cdot \frac{\partial v}{\partial z} + \underbrace{\left(\frac{1}{5} \cdot \frac{\gamma}{\gamma-1} \cdot \frac{1}{\sigma}\right) \frac{1}{\mathrm{Re}_0} \cdot \frac{\mu}{\rho T} \cdot \frac{\partial T}{\partial r}}_{\textit{creeping term}} \tag{4.9a}$$

$$T_s = Tw + \sqrt{\frac{\pi\gamma}{2}} \cdot \frac{2-\theta}{\theta} \cdot \frac{2\gamma}{\gamma+1} \cdot \frac{1}{\sigma} \cdot \frac{M_\infty}{\mathrm{Re}_0} \cdot \frac{\mu}{\rho} \cdot \sqrt{\frac{T_\infty}{T}} \cdot \frac{\partial T}{\partial z} \tag{4.9b}$$

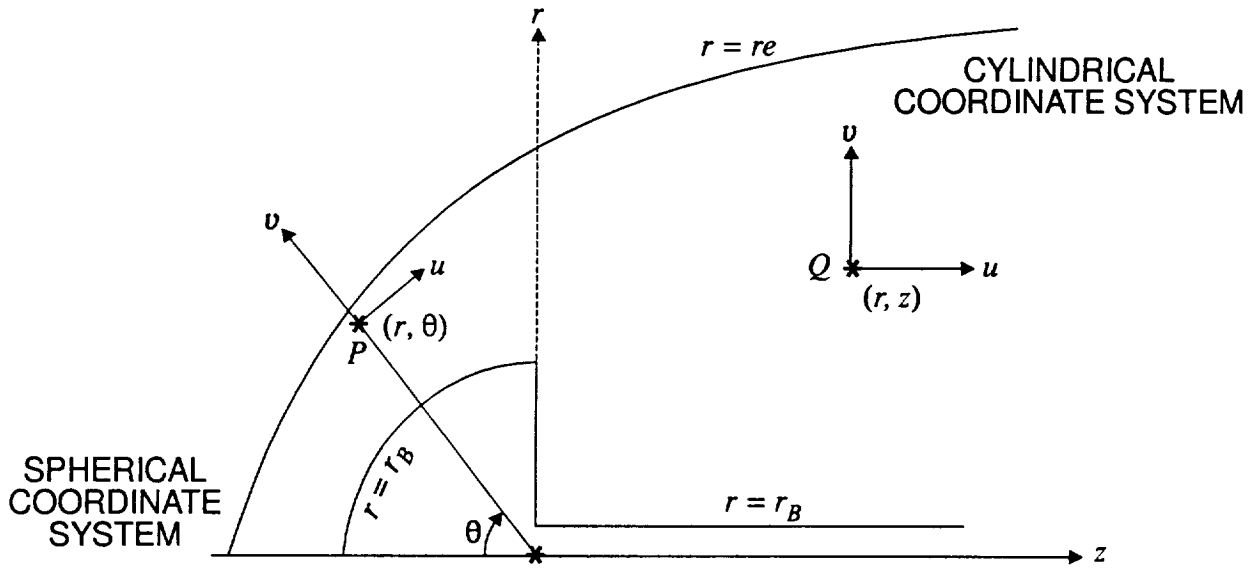

Figure 4.1a: Physical Plane

Physical domain bounded by $r = r_B$ and $r = r_e$ with unequal grids is transformed to a rectangular domain with unequal grids through the transformation

$$\eta = \frac{r - r_e}{r_e - r_B}, \quad 0 \le \eta \le 1 \tag{4.10}$$

$$\zeta = z$$

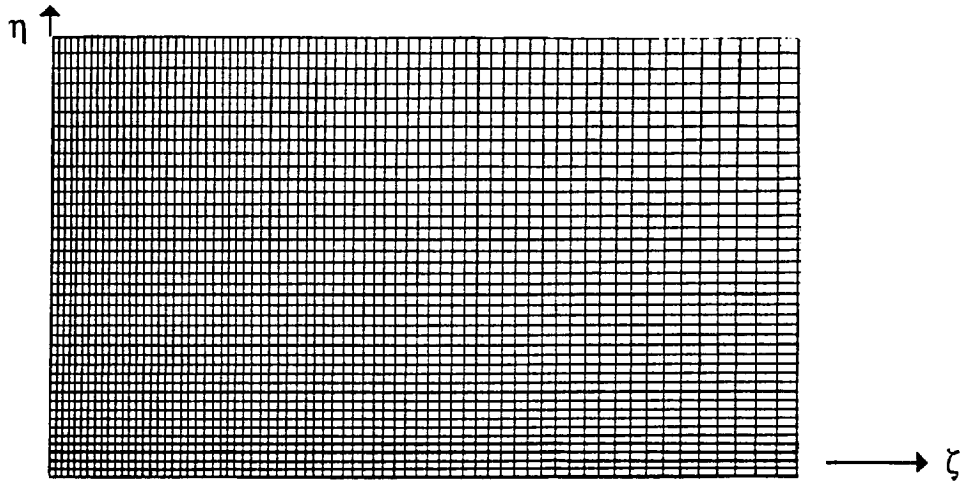

Figure 4.1b: Computational Plane in (η, ζ) Coordinate System

We notice from Eq. (4.10) that the grid points are allowed to change along the radial lines only. This approach minimizes the numerical error as the grid points are orderly placed. Distribution of grids in the radial direction is provided by algebraic, elliptic and/or adaptive grid generation procedures.

Using the transformation of independent variables in Eq. (4.10), from *(r, z)* to *(η, ζ)* and the following relationships between the derivatives in the two planes, the governing equations (4.1) to (4.5) are transformed from *(r, z)* to *(η, ζ)*-plane.

Let

$$\begin{aligned} ne(z) &= r_B(z) - re(z) \\ ne' &= r'_B - r'e \end{aligned} \tag{4.11}$$

where

$$' = \frac{\partial}{\partial z}$$

$$r = r_B + \eta \cdot ne$$

$$\frac{\partial}{\partial r} = \frac{1}{ne}\frac{\partial}{\partial \eta}$$

$$\frac{\partial}{\partial z} = \frac{\partial}{\partial \zeta} - \frac{r'_B + \eta \cdot ne'}{ne} \cdot \frac{\partial}{\partial \eta}$$

$$\frac{\partial^2}{\partial r^2} = \frac{1}{ne^2}\frac{\partial}{\partial \eta^2}$$

$$\frac{\partial^2}{\partial z^2} = \frac{\partial^2}{\partial \zeta^2} - \left(\frac{r_B' + \eta \cdot ne'}{ne}\right)^2 \cdot \frac{\partial^2}{\partial \eta^2} - 2\frac{r_B' + \eta \cdot ne'}{ne}\frac{\partial^2}{\partial \eta \partial \zeta}$$

$$\frac{\partial^2}{\partial z \partial r} = -\left[\frac{r_B' + \eta \cdot ne'}{ne^2}\frac{\partial^2}{\partial \eta^2} - \frac{1}{ne}\frac{\partial^2}{\partial \eta \partial \zeta} + \frac{ne'}{ne^2}\frac{\partial}{\partial \eta}\right]$$

The governing equations (4.1) to (4.5) in (η, ζ)-plane become the following:

Continuity Equation

$$R_1 \frac{\partial \rho}{\partial \eta} + R_2 \frac{\partial \rho}{\partial \zeta} + R_3 \rho = 0 \tag{4.12}$$

where we represent

$$c = r_B + \eta \cdot ne$$
$$c' = r_B' + \eta \cdot ne'$$
$$c'' = r_B'' + \eta \cdot ne''$$

and

$$R_1 = \frac{v}{ne} - \frac{c'}{ne} u$$
$$R_2 = u$$

and

$$R_3 = \frac{1}{ne}\frac{\partial v}{\partial \eta} + \frac{v}{c} + \left(\frac{\partial u}{\partial \zeta} - \frac{c'}{ne}\frac{\partial u}{\partial \eta}\right)$$

Radial Momentum Equation

$$A_1 \frac{\partial^2 v}{\partial \eta^2} + A_2 \frac{\partial^2 v}{\partial \eta \partial \zeta} + A_3 \frac{\partial^2 v}{\partial \zeta^2} + A_4 \frac{\partial v}{\partial \eta} + A_5 \frac{\partial v}{\partial \zeta} + A_6 v + A_7 = 0 \tag{4.13}$$

where

$$A_1 = \frac{\mu}{\mathrm{Re}\,0}\left(\frac{4}{3} + c'^2\right) \cdot \frac{1}{ne^2}$$

$$A_2 = -\frac{2\mu}{\mathrm{Re}\,0} \cdot \frac{c'}{ne}$$

$$A_3 = \frac{\mu}{\mathrm{Re}\,0}$$

$$A_4 = \frac{1}{ne}\left\{\rho(uc' - v) + \frac{1}{\mathrm{Re}\,0}\left[\mu\left(\frac{2c'ne'}{ne} - c'' + \frac{1}{3}c\right) + \left(\frac{4}{3} + c'^2\right) \cdot \frac{1}{ne} \cdot \frac{\partial \mu}{\partial \eta} - c'\frac{\partial \mu}{\partial \zeta}\right]\right\}$$

$$A_5 = -\rho u + \frac{1}{\mathrm{Re}_0}\left(\frac{\partial \mu}{\partial \zeta} - \frac{c'}{ne}\frac{\partial \mu}{\partial \eta}\right)$$

$$A_6 = -\frac{1}{c}\left[\frac{2}{3}\cdot\frac{1}{\mathrm{Re}_0}\right]\left[\frac{1}{ne}\frac{\partial \mu}{\partial \eta} + \frac{2}{c}\mu\right]$$

$$A_7 = -\frac{1}{ne}\frac{\partial p}{\partial \eta} + \frac{1}{3}\frac{1}{\mathrm{Re}_0}\left[-\frac{\mu c'}{ne^2}\frac{\partial^2 u}{\partial \eta^2} + \frac{\mu}{ne}\frac{\partial^2 u}{\partial \eta \partial \zeta} + \left(3\frac{\partial \mu}{\partial \zeta} - \frac{c'}{ne}\frac{\partial \mu}{\partial \eta} - \frac{ne'}{ne}\mu\right)\cdot\frac{1}{ne}\frac{\partial u}{\partial \eta} - 2\frac{1}{ne}\frac{\partial \mu}{\partial \eta}\frac{\partial u}{\partial \zeta}\right]$$

Tangential Momentum Equation

$$B_1\frac{\partial^2 u}{\partial \eta^2} + B_2\frac{\partial^2 u}{\partial \eta \partial \zeta} + B_3\frac{\partial^2 u}{\partial \zeta^2} + B_4\frac{\partial u}{\partial \eta} + B_5\frac{\partial u}{\partial \zeta} + B_6 u + B_7 = 0 \qquad (4.14)$$

where

$$B_1 = \frac{1}{ne^2}\cdot\frac{\mu}{\mathrm{Re}_0}\cdot\left(\frac{4}{3}c'^2 + 1\right)$$

$$B_2 = -\frac{2}{3}\cdot\frac{\mu}{\mathrm{Re}_0}\cdot\frac{c'}{ne}$$

$$B_3 = \frac{4}{3}\cdot\frac{\mu}{\mathrm{Re}_0}$$

$$B_4 = \frac{1}{ne}\left\{\rho(c'u - v) + \frac{1}{\mathrm{Re}_0}\left[\mu\cdot\frac{4}{3}\left(\frac{2c'ne'}{ne} - c''\right) + \left(\frac{\mu}{c} - \frac{4}{3}c'\frac{\partial \mu}{\partial \zeta}\right) + \left(\frac{4}{3}c'^2 + 1\right)\cdot\frac{1}{ne}\cdot\frac{\partial \mu}{\partial \eta}\right]\right\}$$

$$B_5 = -\rho u + \frac{4}{3}\cdot\frac{1}{\mathrm{Re}_0}\left(\frac{\partial \mu}{\partial \zeta} - \frac{c'}{ne}\frac{\partial \mu}{\partial \eta}\right)$$

$$B_6 = 0$$

$$B_7 = \frac{1}{3}\cdot\frac{1}{\mathrm{Re}_0}\left\{-\frac{\mu c'}{ne^2}\frac{\partial^2 v}{\partial \eta^2} + \frac{\mu}{ne}\frac{\partial^2 v}{\partial \eta \partial \zeta} + \left(\frac{3}{ne}\frac{\partial \mu}{\partial \eta} + \frac{\mu}{c}\right)\frac{\partial v}{\partial \zeta}\right.$$
$$\left. -\frac{1}{ne}\left[\mu\left(\frac{ne'}{ne} + \frac{c'}{c}\right) + \frac{c'}{ne}\frac{\partial \mu}{\partial \eta} + 2\frac{\partial \mu}{\partial \zeta}\right]\frac{\partial v}{\partial \eta} - 2\left(\frac{\partial \mu}{\partial \zeta} - \frac{c'}{ne}\cdot\frac{\partial \mu}{\partial \eta}\right)\frac{v}{c}\right\}$$
$$-\left(\frac{\partial p}{\partial \zeta} - \frac{c'}{ne}\frac{\partial p}{\partial \eta}\right)$$

Energy Equation

$$C_1\frac{\partial^2 T}{\partial \eta^2} + C_2\frac{\partial^2 T}{\partial \eta \partial \zeta} + C_3\frac{\partial^2 T}{\partial \zeta^2} + C_4\frac{\partial T}{\partial \eta} + C_5\frac{\partial T}{\partial \zeta} + C_6 T + C_7 = 0 \qquad (4.15)$$

where

$$C_1 = \frac{\Lambda}{\mathrm{Re}_0}\cdot\frac{1}{\sigma}\cdot\frac{\mu c_p\left(1+c'^2\right)}{ne^2}$$

$$C_2 = -\frac{2\Lambda}{\mathrm{Re}_0}\cdot\frac{1}{\sigma}\cdot\frac{\mu c_p c'}{ne}$$

$$C_3 = \frac{\Lambda}{\mathrm{Re}_0}\cdot\frac{1}{\sigma}\cdot\mu c_p$$

$$C_4 = \frac{1}{ne}\left\{\frac{\Lambda}{\mathrm{Re}_0}\cdot\frac{1}{\sigma}\cdot\left[\mu c_p\left(\frac{1}{c}+\frac{2c'ne'}{ne}-c''\right)+\left(1+c'^2\right)\cdot\frac{1}{ne}\cdot\frac{\partial}{\partial\eta}\left(\mu c_p\right)-c'\frac{\partial}{\partial\zeta}\left(\mu c_p\right)\right]\right.$$

$$\left.-\Lambda\rho c_p(v-c'u)\right\}$$

$$C_5 = -\frac{\Lambda}{\mathrm{Re}_0}\cdot\frac{1}{\sigma}\cdot\left[\frac{\partial}{\partial\zeta}\left(\mu c_p\right)-\frac{c'}{ne}\frac{\partial}{\partial\eta}\left(\mu c_p\right)\right]-\Lambda\rho c_p u$$

$$C_6 = 0.0$$

$$C_7 = \frac{\mu}{\mathrm{Re}_0}\Phi+(v-c'u)\cdot\frac{1}{ne}\frac{\partial p}{\partial\eta}+u\frac{\partial p}{\partial\zeta}$$

and

$$\Phi = 2\left[\left(\frac{1}{ne}\frac{\partial v}{\partial\eta}\right)^2+\left(\frac{v}{c}\right)^2+\left(\frac{\partial u}{\partial\zeta}-\frac{c'}{ne}\frac{\partial u}{\partial\eta}\right)^2\right]$$

$$+\left[\frac{\partial v}{\partial\zeta}-\frac{C'}{ne}\frac{\partial v}{\partial\eta}+\frac{1}{ne}\frac{\partial u}{\partial\eta}\right]^2$$

$$-\frac{2}{3}\left[\frac{1}{ne}\frac{\partial v}{\partial\eta}+\frac{v}{C}+\left(\frac{\partial u}{\partial\zeta}-\frac{c'}{ne}\frac{\partial u}{\partial\eta}\right)\right]^2$$

Equation of State

$$p = \frac{\gamma-1}{\gamma}\Lambda\rho T \tag{4.16}$$

For ease of computation, the governing equations (4.12) to (4.16) in (η, z)-plane with unequal grids are transformed to the computational (y,x)-plane with equal grids through the use of the following transformation:

$$\begin{aligned} y &= y(\eta,\zeta) \\ x &= x(\eta,\zeta) \end{aligned} \tag{4.17}$$

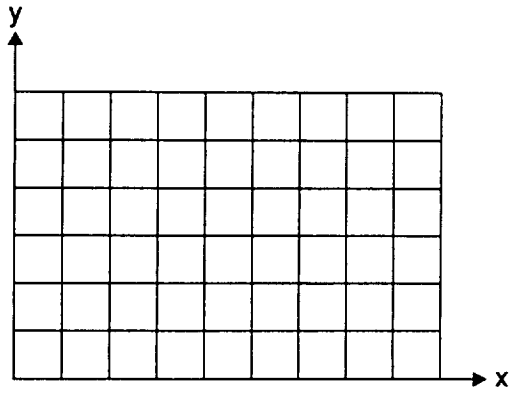

Figure 4.1c: (y,x)-Plane with Equal Grids

Final form of the Navier-Stokes equations and slip and temperature jump boundary conditions in the computational (y,x)-plane are exactly the same as given by equations (2.20) to (2.24). However, using a particular form of the transformation given in Eq. (2.27), we get the following set of equations. The continuity equation (4.12) becomes:

$$p_1 \frac{\partial \rho}{\partial y} + p_2 \frac{\partial \rho}{\partial x} + p_3 \rho = 0 \tag{4.18}$$

where

$$p_1 = \frac{1}{\eta_y} \cdot R_1$$

$$p_2 = \frac{1}{\zeta_x} \cdot R_2$$

$$p_3 = R_3$$

Radial momentum equation (4.13) becomes:

$$\alpha_1 \frac{\partial^2 v}{\partial y^2} + \alpha_2 \frac{\partial^2 v}{\partial y \partial x} + \alpha_3 \frac{\partial^2 v}{\partial x^2} + \alpha_4 \frac{\partial v}{\partial y} + \alpha_5 \frac{\partial v}{\partial x} + \alpha_6 v + \alpha_7 = 0 \tag{4.19}$$

where

$$\alpha_1 = \frac{A_1}{\eta_y^2}, \qquad \alpha_2 = \frac{A_2}{\eta_y \zeta_x}, \qquad \alpha_3 = \frac{A_3}{\zeta_x^2}$$

$$\alpha_4 = \frac{A_4}{\eta_y} - \frac{\eta_{yy} A_1}{\eta_y^3}, \qquad \alpha_5 = \frac{A_5}{\zeta_x} - \frac{\zeta_{xx} A_3}{\zeta_x^3},$$

$$\alpha_6 = A_6, \qquad \alpha_7 = A_7$$

Axial momentum equation (4.14) becomes:

$$\beta_1 \frac{\partial^2 u}{\partial y^2} + \beta_2 \frac{\partial^2 u}{\partial y \partial x} + \beta_3 \frac{\partial^2 u}{\partial x^2} + \beta_4 \frac{\partial u}{\partial y} + \beta_5 \frac{\partial u}{\partial x} + \beta_6 u + \beta_7 = 0$$

where

$$\beta_1 = \frac{B_1}{\eta_y^2}, \qquad \beta_2 = \frac{B_2}{\eta_y \zeta_x}, \qquad \beta_3 = \frac{B_3}{\zeta_x^2}$$

$$\beta_4 = \frac{B_4}{\eta_y} - \frac{\eta_{yy} B_1}{\eta_y^3}, \qquad \beta_5 = \frac{B_5}{\zeta_x} - \frac{\zeta_{xx} B_3}{\zeta_x^3},$$

$$\beta_6 = B_6, \qquad \beta_7 = B_7$$

The energy equation (4.15) becomes:

$$\gamma_1 \frac{\partial^2 T}{\partial y^2} + \gamma_2 \frac{\partial^2 T}{\partial y \partial x} + \gamma_3 \frac{\partial^2 T}{\partial x^2} + \gamma_4 \frac{\partial T}{\partial y} + \gamma_5 \frac{\partial T}{\partial x} + \gamma_6 T + \gamma_7 = 0 \qquad (4.20)$$

where

$$\gamma_1 = \frac{C_1}{\eta_y^2}, \qquad \gamma_2 = \frac{C_2}{\zeta_x \eta_y}, \qquad \gamma_3 = \frac{C_3}{\zeta_x^2}$$

$$\gamma_4 = \frac{C_4}{\eta_y} - \frac{\eta_{yy}}{\eta_y^3} C_1, \qquad \gamma_5 = \frac{C_5}{\zeta_x} - \frac{\zeta_{xx} C_3}{\zeta_x^3}$$

$$\gamma_6 = C_6, \qquad \gamma_7 = C_7$$

Surface slip and temperature jump boundary conditions in (y, x)-plane assume the following form:

1. On the cargo bay

$$u_{slip} = \sqrt{\frac{\pi \gamma}{2}} \frac{2-\alpha}{\alpha} \frac{M_\infty}{\mathrm{Re}_0} \frac{\mu}{\rho} \sqrt{\frac{T_\infty}{T}} \cdot \frac{1}{ne} \frac{1}{\eta_y} \frac{\partial u}{\partial y} + \frac{1}{5} \frac{\gamma}{\gamma - 1} \cdot \frac{1}{\sigma} \cdot \frac{1}{\mathrm{Re}_0} \cdot \frac{\mu}{\rho T} \cdot \left(\frac{1}{\zeta_x} \frac{\partial T}{\partial x} - \frac{c'}{ne} \cdot \frac{1}{\eta_y} \cdot \frac{\partial T}{\partial y} \right) \qquad (4.21a)$$

$$T_{slip} = Tw + \sqrt{\frac{\pi \gamma}{2}} \cdot \frac{2-\theta}{\theta} \cdot \left(\frac{2\gamma}{\gamma + 1} \cdot \frac{1}{\sigma} \right) \cdot \frac{M_\infty}{\mathrm{Re}_0} \cdot \frac{\mu}{\rho} \cdot \sqrt{\frac{T_\infty}{T}} \cdot \frac{1}{ne \eta_y} \frac{\partial T}{\partial y} \qquad (4.21b)$$

2. On the base of hemispherical surface:

$$u_{slip} = \sqrt{\frac{\pi\gamma}{2}}\frac{2-\alpha}{\alpha}\frac{M_\infty}{\mathrm{Re}_0}\frac{\mu}{\rho}\sqrt{\frac{T_\infty}{T}}\cdot\left(\frac{1}{\zeta_x}\frac{\partial v}{\partial x}-\frac{c'}{ne\eta_y}\cdot\frac{\partial v}{\partial y}\right)+ \frac{1}{5}\cdot\frac{\gamma}{\gamma-1}\cdot\frac{1}{\sigma}\cdot\frac{1}{\mathrm{Re}_0}\cdot\frac{\mu}{\rho T}\cdot\frac{1}{ne}\cdot\frac{1}{\eta_y}\frac{\partial T}{\partial y} \quad (4.22a)$$

$$T_{slip} = Tw+\sqrt{\frac{\pi\gamma}{2}}\cdot\frac{2-\theta}{\theta}\cdot\frac{2\gamma}{\gamma+1}\cdot\frac{1}{\sigma}\cdot\frac{M_\infty}{\mathrm{Re}_0}\cdot\frac{\mu}{\rho}\cdot\sqrt{\frac{T_\infty}{T}}\cdot\frac{1}{\zeta_x}\frac{\partial T}{\partial x} \quad (4.22b)$$

Section 5
DESCRIPTION OF NUMERICAL METHOD OF INTEGRATION

Here, a third-order accurate upwind biased scheme of numerical integration with the provision to use a second-order accurate central-difference scheme at the grid points adjoining the boundary is used. In the upwind-biased numerical scheme, the first-order derivatives in the convective terms are differenced as follows:

$$q\left(\frac{\partial f}{\partial y}\right)_{i,j} = \frac{1}{6\Delta y}\{2f(i,j+1)+3f(i,j)-6f(i,j-1)+f(i,j-2)\} \; if \; q>0 \qquad (5.1a)$$

$$q\left(\frac{\partial f}{\partial y}\right)_{i,j} = \frac{(-1)}{6\Delta y}\{2f(i,j-1)+3f(i,j)-6f(i,j+1)+f(i,j+2)\} \; if \; q<0 \qquad (5.1b)$$

First order and second-order derivatives appearing in the viscous and heat conduction terms of the governing equations (4.20) to (4.22) and the metric coefficients appearing in the equations are differenced with a second-order accurate central-difference approximation. At every grid point, information about the velocity component with regard to its sign is evaluated and, depending on the sign, finite-difference approximation (5.1a) or (5.1b) is used. We notice that the stencil in (5.1a, b) involves information at four grid points. For $q > 0$, we use formula (5.1a). To use this result we need information at one grid point at $(i, j+1)$ ahead and two grid points at $(i, j-1)$ and $(i, j-2)$ behind the grid point at (i, j) under consideration. Thus, in case $q > 0$ at a grid point adjacent to the solid boundary, viz., $j = 2$, we need information at the grid points $j = 1$ and $j = 0$. Information at $j = 0$, inside the solid boundary is not available. Hence, under the conditions described above, the upwind biased scheme fails to compute the flow near the solid boundary. We used the central-difference scheme to compute the flow at the grid point under consideration.

In the following, we have identified the conditions and the areas in the domain of integration where computation of the flow by the upwind biased numerical scheme is not possible. In the strips in Figs. 5.1a–5.1d marked with dotted lines in the domain of integration, we have computed the flow by a second-order accurate central-difference scheme of numerical integration, while the flow inside the rectangle formed by solid lines is computed by the third-order accurate upwind biased numerical scheme of integration.

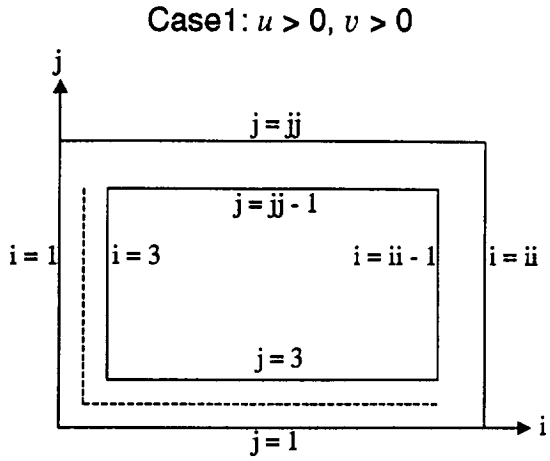

Figure 5.1a: Domain of Integration with Upwind Biased Scheme for Case $u > 0$, $v > 0$

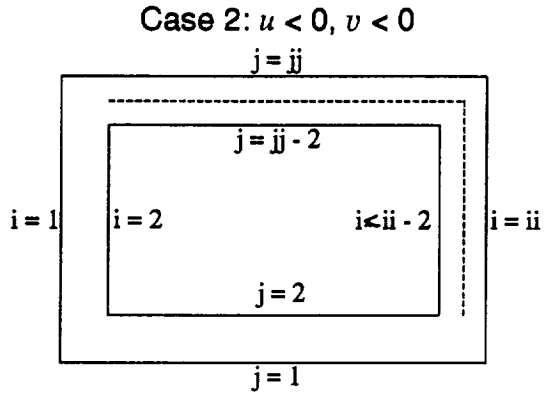

Figure 5.1b: Domain of Integration with Upwind Biased Scheme for Case $u < 0$, $v < 0$

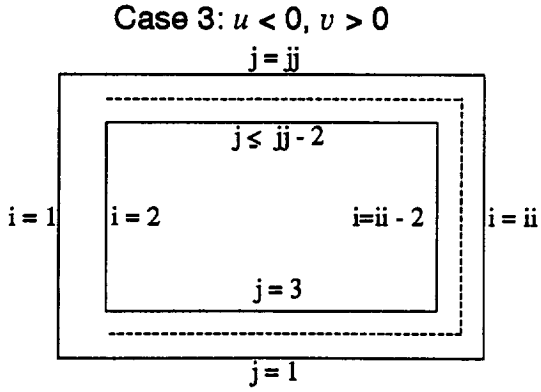

Figure 5.1c: Domain of Integration with Upwind Biased Scheme for Case $u < 0$, $v > 0$

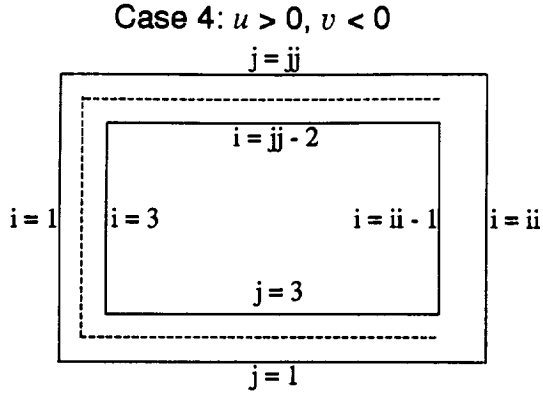

Figure 5.1d: Domain of Integration with Upwind Biased Scheme for Case $u > 0$, $v < 0$

Pressure gradient terms in the governing equations are differenced in the manner convective terms are differenced.

In the normal momentum equation, pressure gradient term appears as $\left(\frac{1}{ne}\cdot\frac{1}{\eta_y}\cdot\frac{\partial p}{\partial y}\right)$ while in the tangential momentum equation, pressure gradient term appears as $\left(\frac{1}{\zeta_x}\frac{\partial p}{\partial x}-\frac{c'}{ne}\cdot\frac{1}{\eta_y}\frac{\partial p}{\partial y}\right)$. In the energy equation, work done by pressure forces is represented by $\left[(v-c'u)\cdot\frac{1}{ne}\cdot\frac{1}{\eta_y}\cdot\frac{\partial p}{\partial y}+u\frac{1}{\zeta_x}\frac{\partial p}{\partial x}\right]$.

In the central-difference scheme, pressure gradient terms are represented by

$$\frac{\partial p}{\partial y}=\frac{p(i,j+1)-p(i,j-1)}{2\Delta y}$$

$$\frac{\partial p}{\partial x}=\frac{p(i+1,j)-p(i-1,j)}{2\Delta x}$$

In the upwind biased scheme, $\frac{\partial p}{\partial y}$ in the normal momentum equation at a particular grid point (i, j) is differenced as per the sign of normal component of velocity (v) while $\frac{\partial p}{\partial x}$ and $\frac{\partial p}{\partial y}$ appearing in the tangential momentum equation are differenced as per sign of the tangential component of velocity (u). In the energy equation, $\frac{\partial p}{\partial y}$ and $\frac{\partial p}{\partial x}$ are associated with the velocity components u or v. Hence, they are differenced as per sign of (u) and (v). Thus, the contribution to the energy by the pressure forces is evaluated in the following four cases:

Case 1: $u > 1$, $v > 0$

Case 2: $u < 1$, $v < 0$

Case 3: $u < 1, \quad v > 0$

Case 4: $u > 1, \quad v < 0$

and the analysis is incorporated in the main program.

Derivatives in the normal direction appearing in the surface slip and temperature jump boundary conditions are replaced by the second-order accurate one-sided finite-difference approximation:

$$\frac{\partial f}{\partial y} = \frac{4f(i,j+1) - f(i,j+2) - 3f(i,j)}{2\Delta y}$$

while the derivative in the tangential direction appearing in the creeping term is replaced by

$$\frac{\partial f}{\partial x} = \frac{f(i+1,j) - f(i-1,j)}{2\Delta x}$$

The computer code is so written that we can compute the entire flow in the wake region by the second-order accurate central-difference scheme of numerical integration, or use a third order accurate upwind biased scheme in the rectangles bounded by solid lines in Figs. 5.1a to 5.1d and a second order accurate central-difference scheme along the dotted strips in Figs. 5.1a to 5.1d.

Section 6
GENERATION OF GRIDS ON THE AFTBODY

Aftbody may consist of sphere-cylinder (Fig. 6.1a) or a hemisphere, with a cylindrical bay (Fig. 6.1b) (an AFE-type configuration).

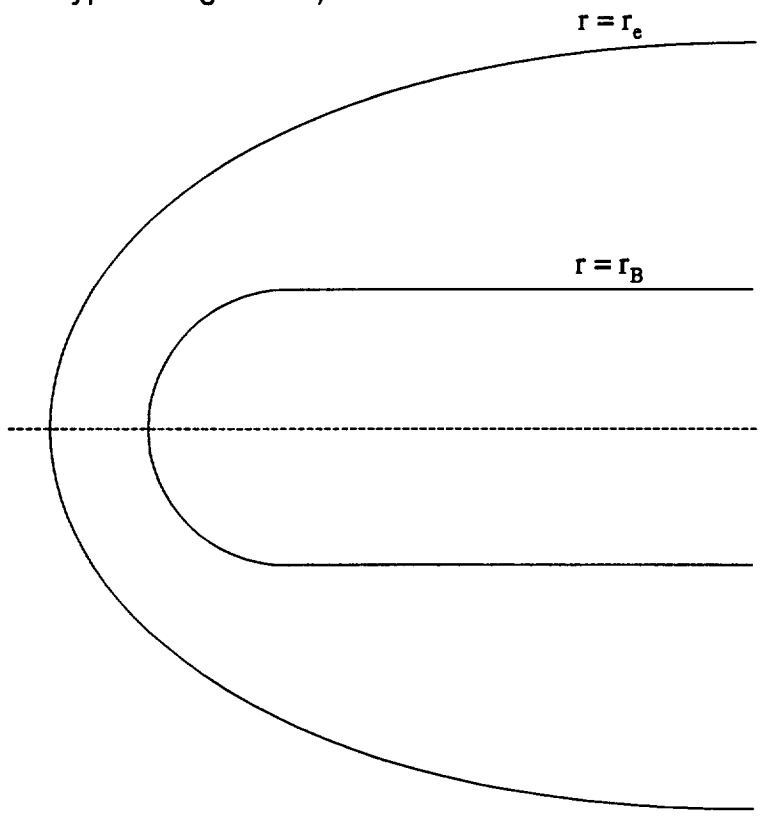

Figure 6.1a: Sphere-Cylinder Configuration

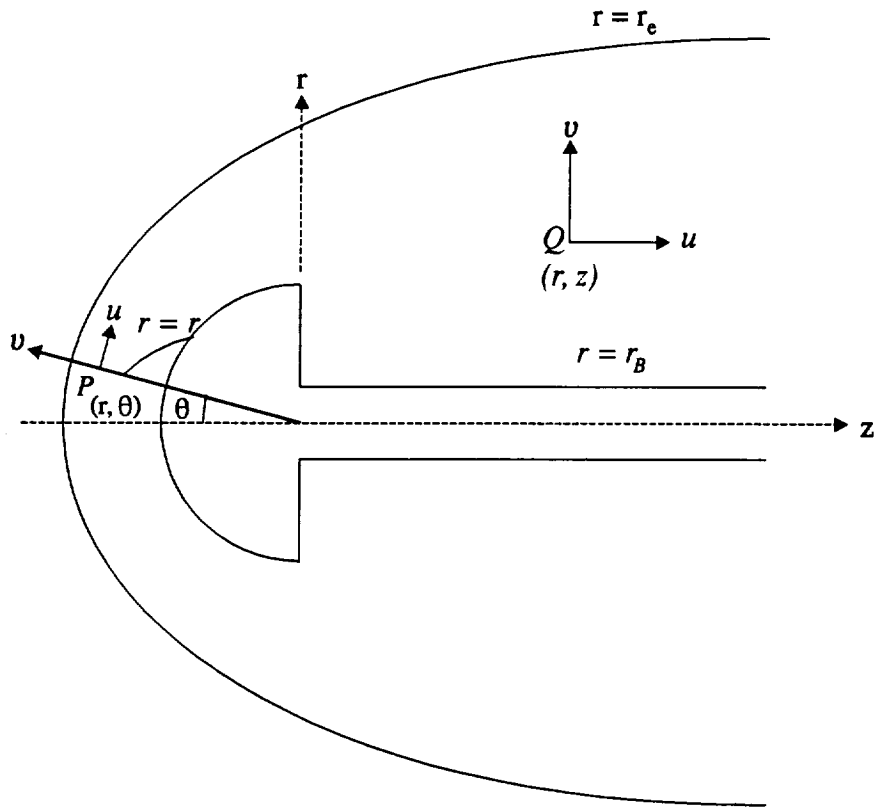

Figure 6.1b: Hemisphere with a Cylindrical Bay Configuration

In spherical coordinate system, the outer domain of integration is represented by

$$\bar{r}_e = \frac{a_2}{1 + e_2 \cos\theta} \tag{6.1}$$

where

a_2 = Nose radius of curvature

= $\frac{b^2}{a}$, b and a being the semi-minor and semi-major axis of the conic section

e_2 = $\frac{c}{a}$, c being the focus of the conic section

Similarly, we can in general represent a body by the equation

$$\bar{r}_B = \frac{a_1}{1 + e_1 \cos\theta} \tag{6.2}$$

where

e_1 = 0 gives sphere

< 1 gives ellipse

= 1 gives parabola

> 1 gives hyperbola

In the present computations, $r_B = \frac{\bar{r}_B}{\bar{r}_N} = 1$ and $e_1 = 0$. Thus, the body is a sphere or hemisphere.

In cylindrical coordinates,

$$\bar{r}_e = \sqrt{a_2^2 + 2a_2 e_2 z - \left(1 - e_2^2\right) * z^2} \tag{6.3}$$

and

$$\bar{r}_B = \sqrt{a_1^2 + 2a_1 e_1 z - \left(1 - e_1^2\right) * z^2} \tag{6.4}$$

The surface of a cylinder is represented by $\bar{r}_B$ = constant = radius of the cylinder.

Several schemes of grid generation have been incorporated into the code. Provision is made to generate uniformly spaced grids, reading grids from a file generated by some other code and stretching grids as per the following logarithmic function:

$$\eta = \frac{1}{1+2\alpha}\left[1 + \beta\frac{1-y}{1+y}\right] \tag{6.5}$$

where

$$y = \left(\frac{\beta+1}{\beta-1}\right)$$

where

α = 0 clusters the grids near the surface

α = 0.5 clusters the grids at either end of the radial line

$\beta \rightarrow 0$ reduces the size of the grid

The grid stretching function in Eq. (6.5) correlates the uniform grids in the computational (y, x)-plane with the nonuniform grids in the (η, ζ)-plane. The grids in the (η, ζ)-plane are correlated with the grids in the physical (r, z)-plane through the following relation:

$$\begin{aligned} r &= r_B + \eta(re - r_B) \\ z &= \zeta \end{aligned} \tag{6.6}$$

This subroutine has the capability to stretch grids algebraically according to the law similar to Eq. (6.5), in the tangential direction.

Vigorous attempts have been made to develop grids that contain the salient features of the flowfield on the fore spherical portion and the aft cylindrical portion of the flowfield. In the denser portion of the transitional regime, we expect a bow shock and a shear layer near the surface on the forepart of the body and a bow shock diffusing in

the wake, and a shear layer detaching from the corner of the hemispherical surface and reattaching on the cylindrical surface, thus, entrapping a recirculating flow between the body and shear layer. In order to resolve the flowfield adequately, we need to cluster grids around the bow shock, shear layer, near the reattachment point and all around the body surface (hemisphere, base and the cylindrical portion of the body).

A specially designed mathematical procedure based upon the logarithmic grid stretching function and division of the flowfield into various segments has been developed to achieve the objectives stated above. A separate computer code for grid generation purposes has been developed. In Figs. 6.2 – 6.4, grid patterns are shown that illustrate the capability of the code to cluster grids at the desired locations.

Salient features of the grid generation code are the following:

1. The domain of integration can be divided into any number of segments. In Fig. 6-4, the forepart domain of integration is divided into two segments, separated by the bow shock while the rearpart domain is divided into three segments, which are separated by the bow shock and shear layer.
2. In order to avoid excessive variation in cell areas (Jacobian $J \neq 0$ anywhere in the flowfield) and to keep simplicity, grid points are allowed to move along the radial lines only (not sideways).
3. The grids cluster around the shear layer which bends toward the cylindrical afterbody.
4. To avoid excessive clustering of grids in the first segment and sparseness of grids in the second segment in the spherical portion of the body, a procedure is developed that allows us to change the total number of nodal points along a radial line in each segment. Care is taken to see that the total number of grid points along each radial line remains unchanged. Thus, in the first segment between the shock and the body, the nodal points vary from 31 at $\theta = 0$ to 24 at $\theta = 90$ deg, eliminating one grid point on the alternate radial line.
5. In the aft part of the body, the grid points in segment one between the shear layer and the body are reduced from 16 at the base to 8 near the reattachment point, eliminating one grid point on the successive radial lines and the grid points in segment two between the shock wave and shear layer are correspondingly increased. Grid points in segment three between the outer edge of the domain of integration and the bow shock wave remain constant at the value given at the shoulder.
6. The mathematical procedure is so developed that the grid points from the forepart and aft part merge smoothly at the radial line at the corner of the hemisphere, thus avoiding the need of interpolating the values of the flow variables.

The computer code for generating grid points with the salient features stated above enables us to generate grids that cluster around the important features of the flowfield. Besides, we have capability to change the location of the shock and shear layer and if need be, cluster grids around wake shocks that may possibly develop in the dense portion of the atmosphere.

The computed results on the grid system developed above will give us the flowfield for adaptive gridding. In adaptive gridding, after extensive numerical computations, we developed the following weight function [10]:

$$w_i = 1 + A\left(\frac{ds}{dr}\right)_{i,j} + B\left(1/k_{i,j}\right)$$

where (ds) is the arc length of the profile of the flow variable, given by $\left(\frac{ds}{dr}\right)_{i,j} = \sqrt{1+\left(\frac{\partial f}{\partial r}\right)^2_{i,j}}$, f being the flow variable and $k_{i,j}$ the curvature of the profile at the grid point (i, j) under consideration.

$$k_{i,j} = \frac{\frac{\partial^2 f}{\partial r^2}}{\left[1+\left(\frac{\partial f}{\partial r}\right)^2\right]^{3/2}}$$

then

$$A = 0.3$$
$$B = 0.3$$

Computations have been carried out for the case $M_\infty = 10$, $\gamma = 1.4$, $\sigma = .71$, $Tw = 0.2$ and for Reynolds number up to $Re0$ = zero. Results of computations with adaptive gridding and comparison of the results with the results of another independently developed code, called Hypersonic Viscous Shock Layer (HVSL), are presented in Figs. 6.5, 6.6 and 6.7. It is seen that adaptive gridding increases the capability of the present procedure to predict sharp shocks up to reasonably high Reynolds numbers.

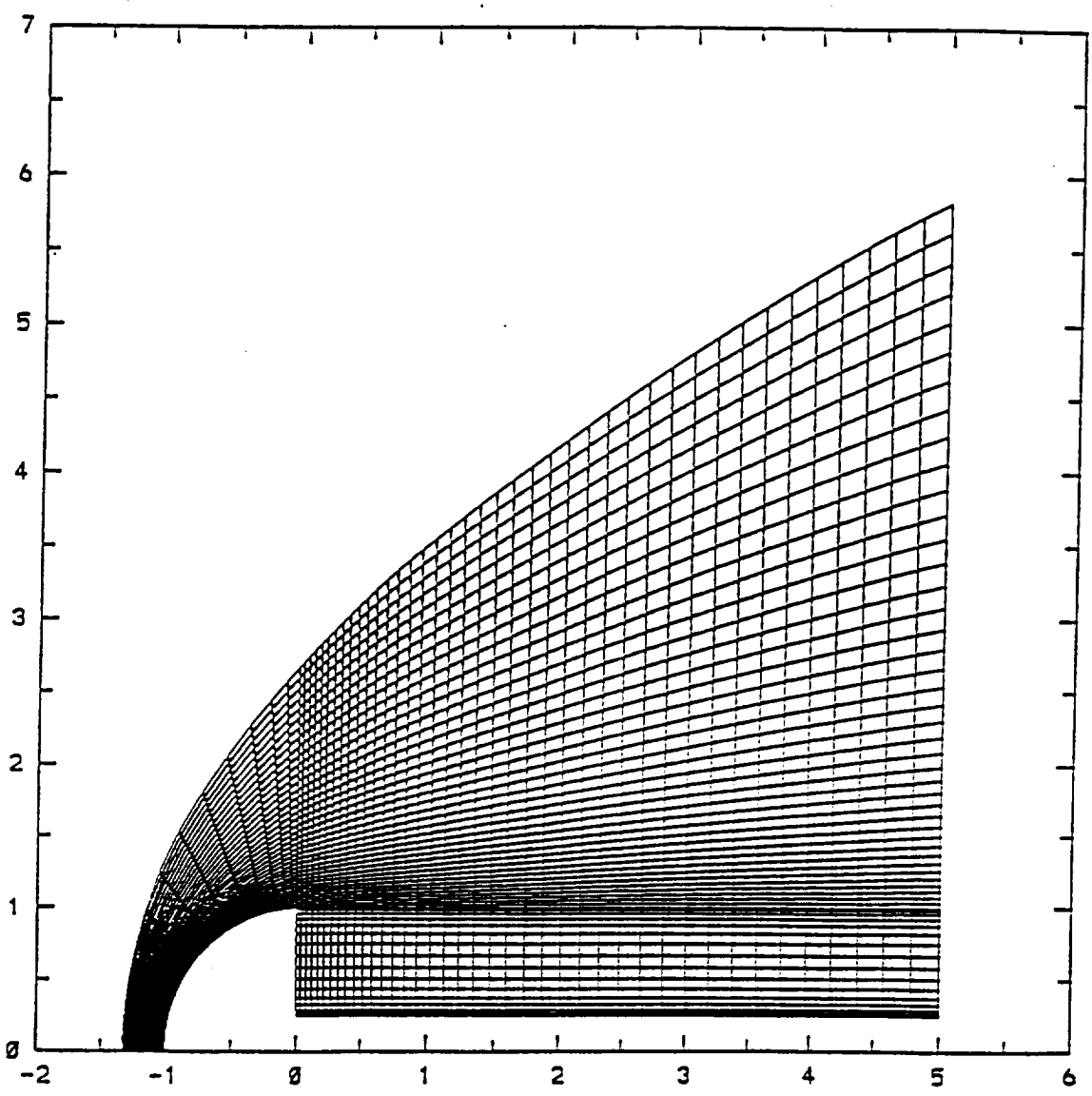

Figure 6.2: Grid Pattern on a Hemisphere with Cylindrical Afterbody: Clustering of Grids Near the Body Surface and Near Shear Layer in the Wake

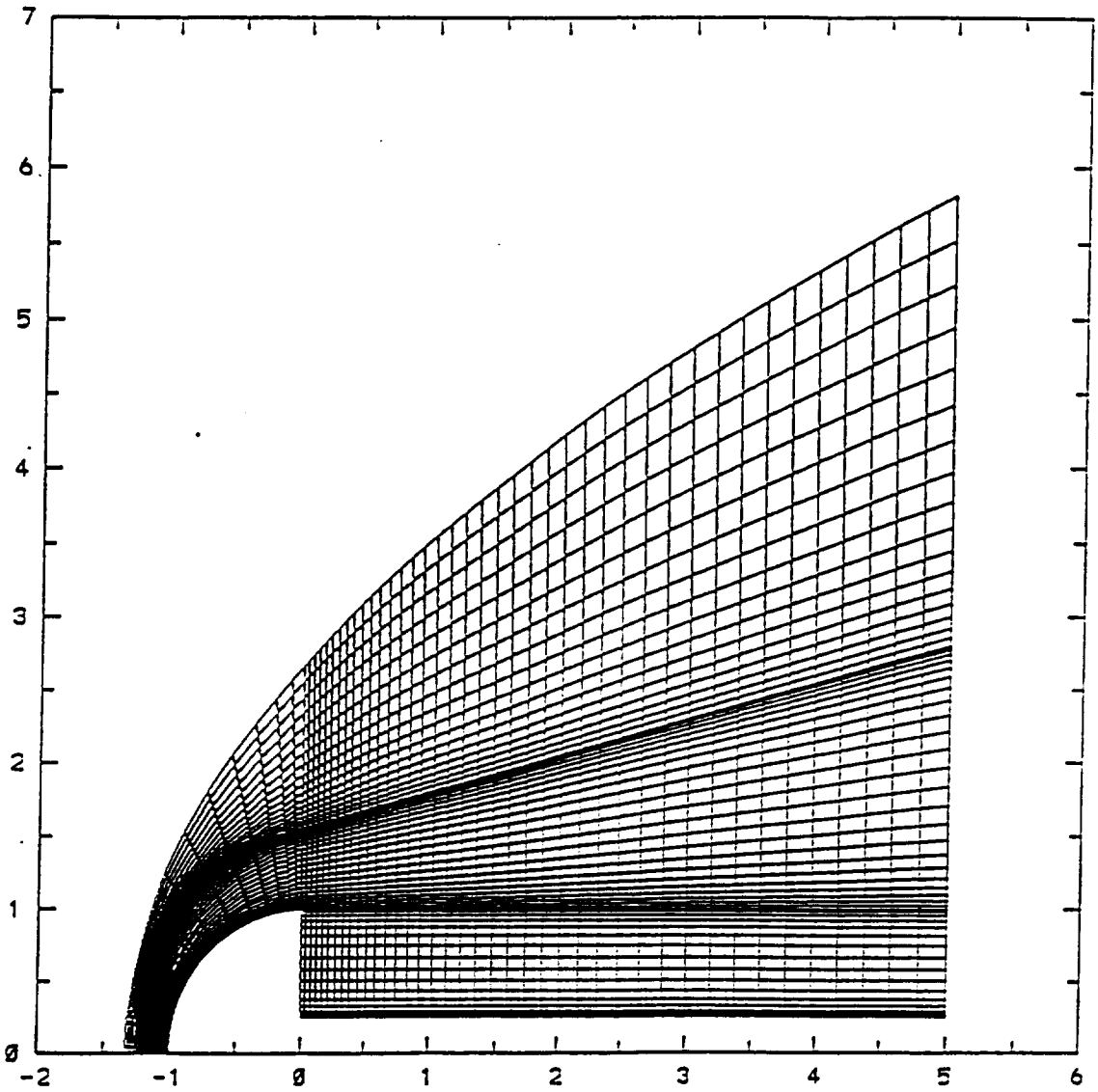

Figure 6.3: Grid Pattern on a Hemisphere with Cylindrical Afterbody: Grids Cluster around the Body Surface, Shear Layer and Bow Shock

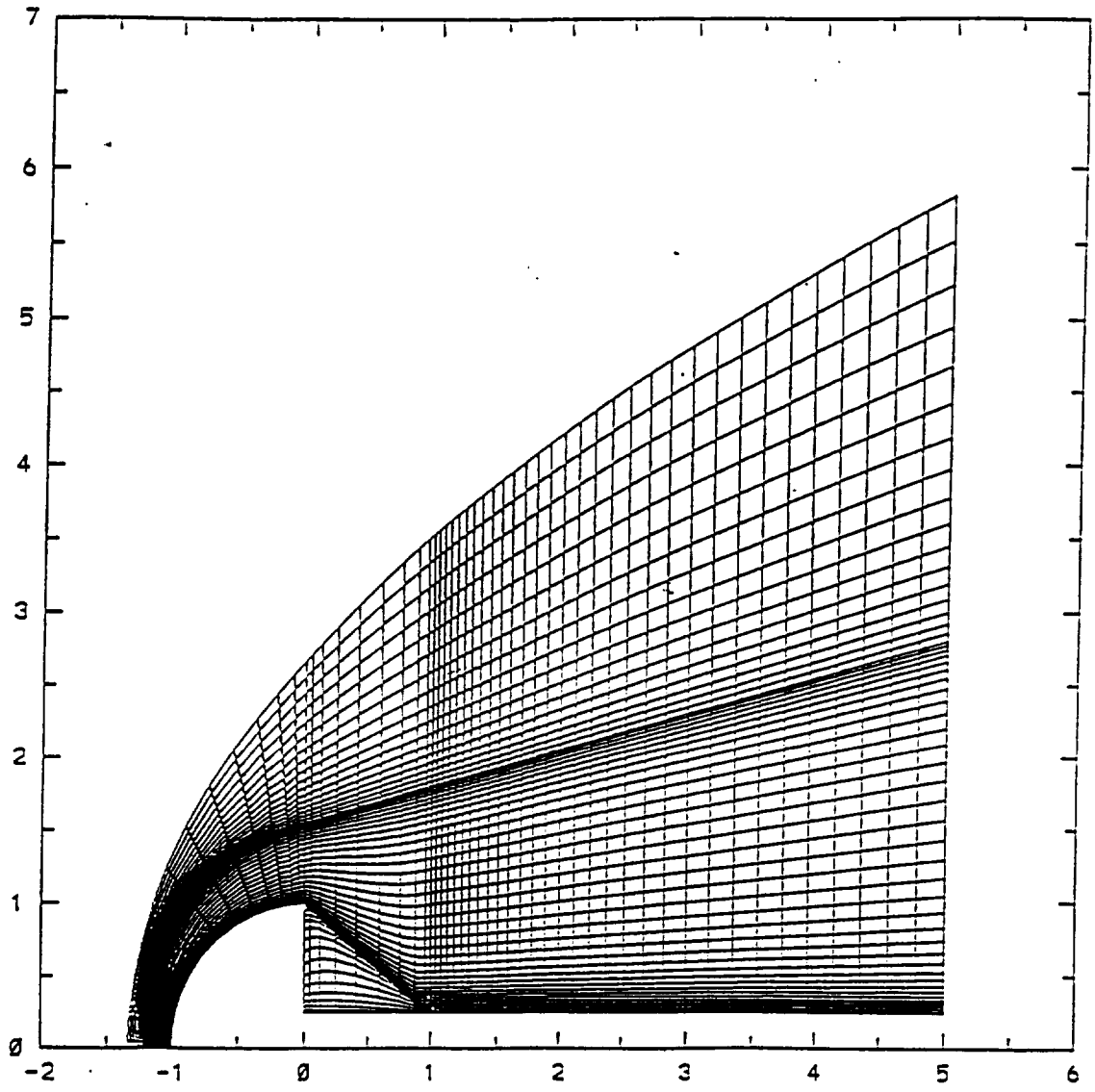

Figure 6.4: Grid Pattern on a Hemisphere with a Cylindrical Afterbody: Grids Cluster around the Body Surface, Shear Layer and at the Reattachment Point on the Afterbody and Bow Shock

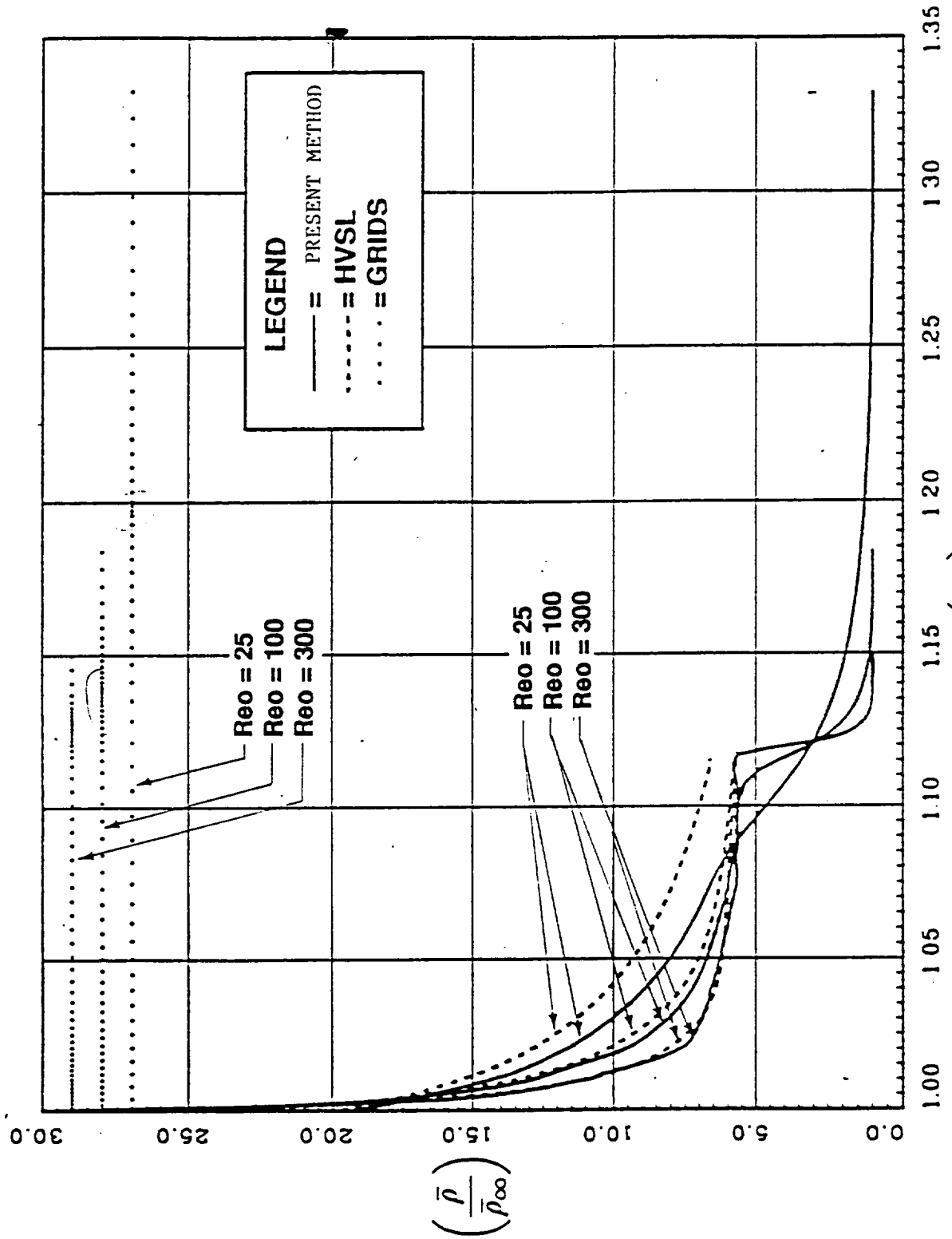

Figure 6.5: Comparison of Density Profiles from the Present Method and HVSL Computer Codes for M_∞ =10, γ = 1.4, Pr. No. = 0.7, Tw = 0.2

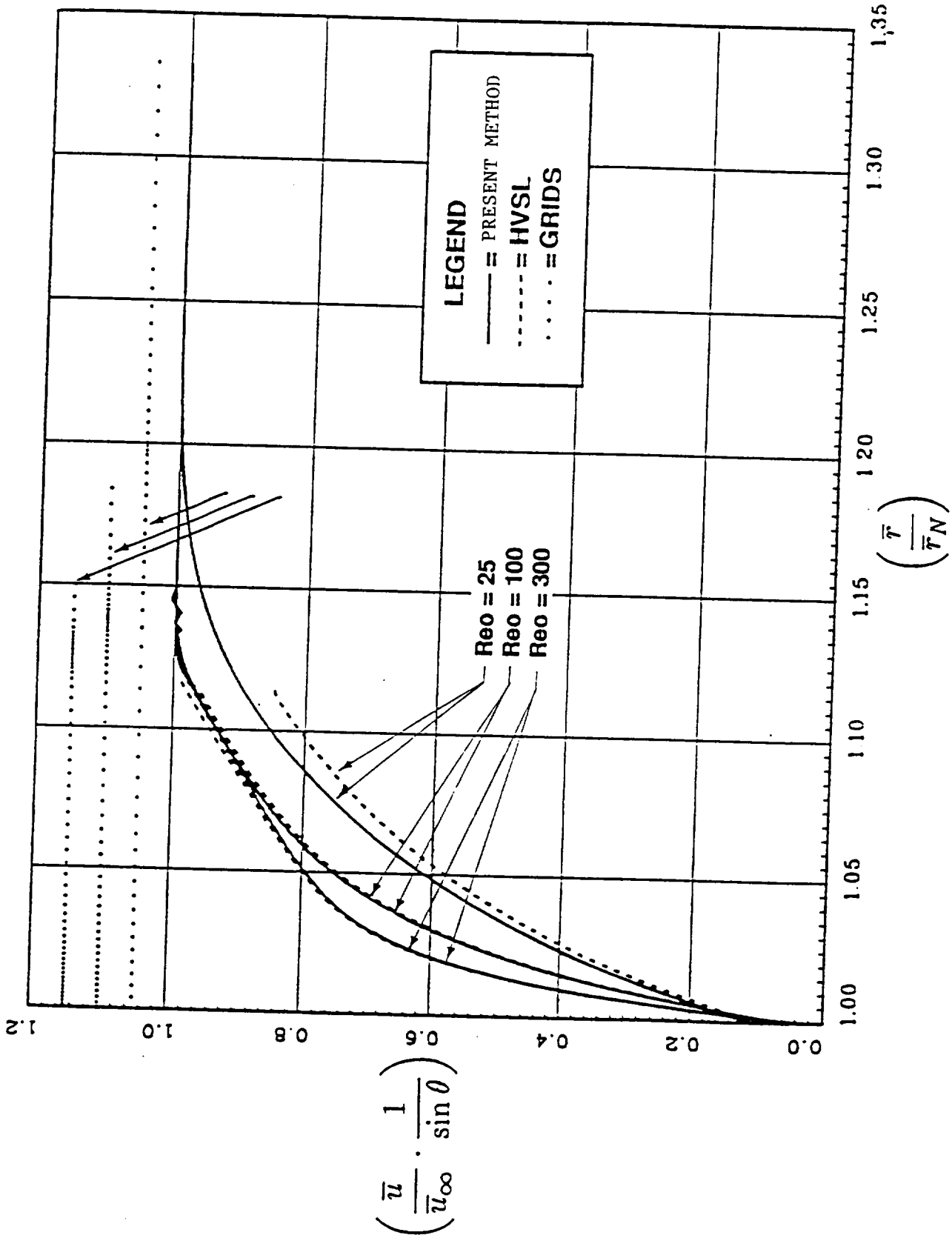

Figure 6.6: Comparison of Tangential Component of Velocity Profiles from the Present Method and HVSL Computer Codes for M_∞ =10, γ = 1.4, Pr. No. = 0.7, T_W = 0.2

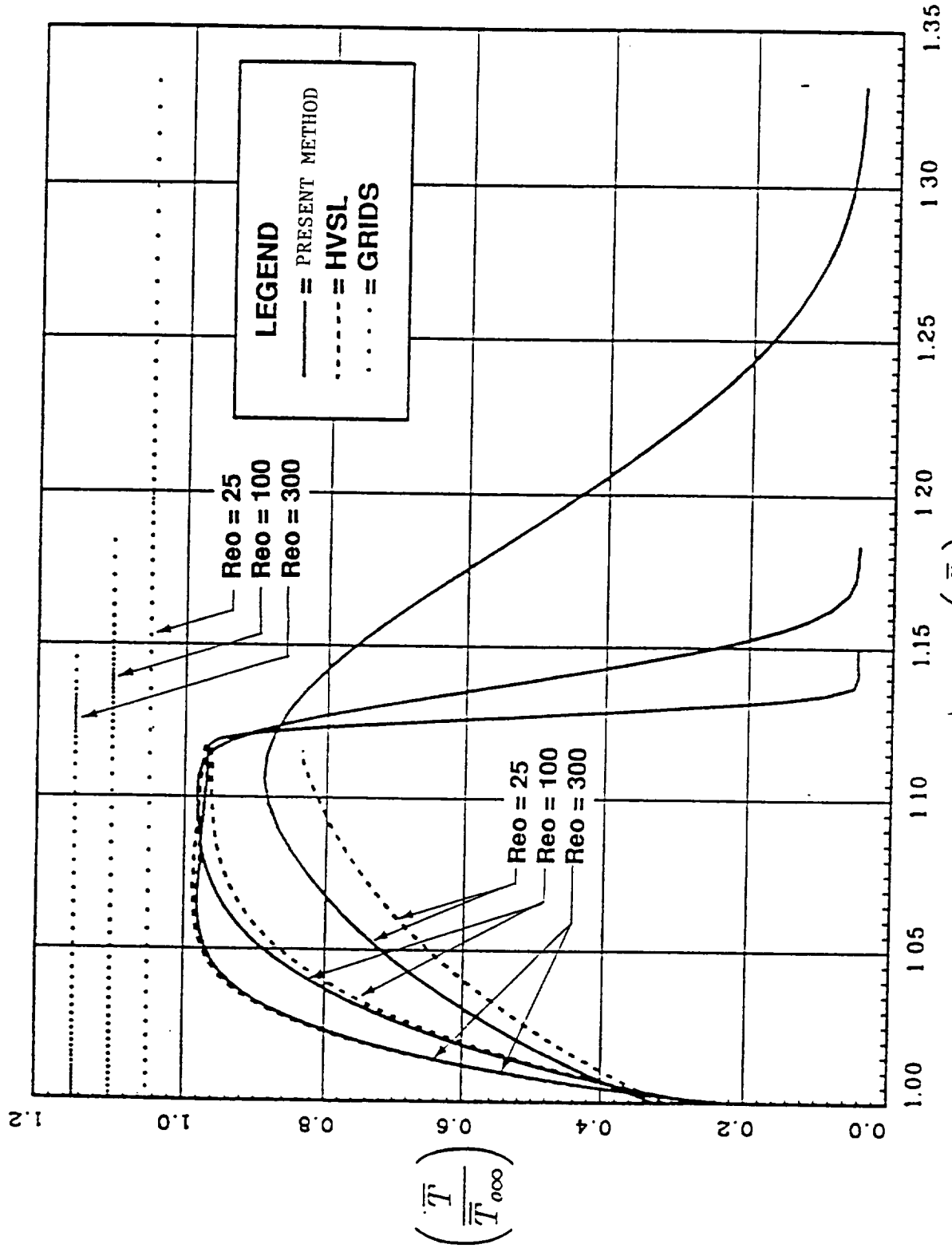

Figure 6.7: Comparison of Temperature Profiles from the Present Method and HVSL Computer Codes for M_∞ =10, γ = 1.4, Pr. No. = 0.7, T_W = 0.2

Section 7
DEVELOPMENT OF INITIAL CONDITIONS

For a given prescribed condition, converged solutions for the stagnation line flowfield are obtained. Then, the stagnation line solution at $\theta = 0$ is extended up to approximately $\theta = 48$ deg by using the relations:

$$\begin{aligned} u(\eta,\theta) &= u_o(\eta)\sin\theta \\ v(\eta,\theta) &= v_o(v)\cos\theta \\ T(\eta,\theta) &= T_o(\eta) \\ \rho(\eta,\theta) &= \rho_o(\eta) \\ p(\eta,\theta) &= p_1(\eta) + p_2(\eta)\sin^2\theta \end{aligned} \tag{7.1}$$

With the initial conditions in Eq. (7.1), the governing equations are iterated up to 250 iterations to give a semi-convergent solution on sphere up to $\theta = 48$ deg. The semi-converged solution at the last but one radial line, viz., at $\theta = 42$ deg is extended up to $\theta = 84$ deg by considering the distribution of the flow variables at the grid points on each radial line lying between $\theta = 42$ deg and $\theta = 84$ deg. With these initial conditions, a semi-converged solution between $\theta = 0$ deg and $\theta = 84$ deg is obtained with an additional 200 iterations. Then, the solution at $\theta = 78$ deg is extended up to $\theta = 108$ deg and a converged solution between $\theta = 0$ deg and $\theta = 108$ deg is obtained.

On the cylindrical portion with a sphere cylinder configuration, the distribution of the flow variables at $\theta = 90$ deg is extended up to $z = 10\ \Delta z$ and a semi-convergent solution between $z = 0$ and $z = 10\ \Delta z$ with the wake part code is obtained. Similar process is repeated for every 10 steps in z-direction until a convergent solution on the cylindrical part of the body is obtained.

With the hemisphere and a sting configuration for a generic AFE shape, solution at the shoulder of hemisphere, viz., $\theta = 90$ deg, is extended between the shear layer and outer edge of the domain of integration. Profiles of the flow variables between the shear layer and the sting are represented by linear or quadratic expressions.

Section 8
COMPUTATION PROCEDURE

8.1 Description of ASR Method

In the present investigation, Accelerated Successive Replacement (ASR) method as suggested by Liberstein [11] has been used. It solves linear or nonlinear algebraic equations arising in the finite difference approximation of the governing equations. The method is good to solve elliptic partial differential equations or ordinary differential equations with split boundary conditions. It has at least a quadratic convergence.

The Liberstein ASR method is a combination of Newton's method and Young's method of Accelerated Successive Convergence.

Newton Method

Let

$$f(x) = 0 \tag{8.1}$$

be the algebraic equation in the variable, x. Let x^k be close to the root of Eq. (8.1).

$$\therefore \qquad f\left(x^{k+1}\right) = f\left(x^k\right) + \left(x^{k+1} - x^k\right)\frac{df}{dx} \approx 0 \tag{8.2}$$

The right-hand side of Eq. (8.2) is approximately equivalent to the given equation, (8.1.) Eq. (8.2) can be written as

$$x^{k+1} = x^k - \frac{f\left(x^k\right)}{f'\left(x^k\right)} \tag{8.3}$$

where

$$f' \equiv \frac{df}{dx}$$

It is clear that for fast convergence, the initial guess should be reasonably good.

For functions of several variables, viz.,

$$f_i\left(x_1, x_2, \cdots x_n\right) = 0, i = 1,2, \cdots n \tag{8.4}$$

and using Taylor's series expansion, we get

$$fi\left(x_1^k, x_2^k, \cdots x_n^k\right) + \sum_{j=1}^{n} f_{ij}\left(x_1^k, x_2^k, \cdots x_n^k\right) \cdot \left(x_j^{k+1} - x_j^k\right) = 0, i = 1,2, \cdots n \tag{8.5}$$

where

$$f_{ij} = \frac{\partial fi}{\partial xj}$$

The set of equations (8.5) can be solved by the inversion of the determinant procedure which is impractical when the number of variables is large or by successive iteration procedure which is inefficient. Thus, Newton's method is practical only when the number of variables is small. However, it is applicable for linear and nonlinear algebraic equations.

Young's Accelerated Successive Replacement Method

Let

$$\sum_{j=1}^{n} a_{ij} x_j = b_i, i = 1,2,\cdots,n \tag{8.6}$$

be the set of equations.

Then,

$$x_i^{k+1} = (1-\omega)x_i^k + \frac{\omega}{a_{ii}}\left[b_i - \sum_{j=1}^{i-1} a_{ij}\, x_j^{k+1} - \sum_{j=i+1}^{n} a_{ij}\, x_j^k \right], i = 1,2,\cdots n \tag{8.7}$$

represents *(k+1)*-th approximation of the roots of the Eq. (8.6). Here, ω is called the acceleration or deceleration factor. Also, $0 < \omega < 2$ and

$\omega > 1$, acceleration factor

$\omega < 1$, deceleration factor

It is evident that Young's method is good for linear equations only.

Equation (8.7) can be written as

$$x_i^{k+1} = x_i^k + \frac{\omega}{a_{ii}}\left[b_i - \sum_{j=1}^{i-1} a_{ij}\, x_j^{k+1} - \sum_{j=i}^{n} a_i\, x_j^k \right], i = 1,2,\cdots n \tag{8.8}$$

Liberstein [11] generalized it to a form where it can be used for nonlinear equations, viz.,

$$x_i^{k+1} = x_i^k - \omega + \frac{f_i\left(x_1^{k+1}, x_2^{k+1}, \cdots x_{i-1}^{k+1}, x_i^k, \cdots x_n^k\right)}{f_{ii}\left(x_1^{k+1}, \cdots x_{i-1}^{k+1}, x_i^k, \cdots x_n^k\right)}, i = 1,2,\cdots n \tag{8.9}$$

when

$0 < \omega < 2$

and

$$f_{ii} = \left(\frac{\partial f_i}{\partial x_i} \right)$$

We have chosen the value of the acceleration factor, ω, such that the percentage change in the flow variable at every grid point is less than a prescribed number, ε, viz.,

$$\left| \frac{x_i^{k+1} - x_i^k}{x_i^k} \right| = \sigma_i \left| \frac{f_i}{x_i^k f_{ii}} \right| < \varepsilon \tag{8.10}$$

or

$$\sigma_i < \varepsilon \left| x_i^k \frac{f_{ii}}{f_i} \right| < \varepsilon.$$

If

$$\sigma_i < 1$$

then

$$\omega = \sigma_i.$$

If

$$\sigma_i \geq 1$$

then

$$\omega = 1.$$

8.2 Special Features of the Method

1. In developing the flow from some arbitrarily prescribed conditions, sometimes the changes in the flow variables become large, which leads to a divergent solution. The present method helps greatly to control these changes.
2. In each iteration, changes in each of the flow variables at each grid point are controlled in such a way that all parts of the flowfield converge simultaneously. In other words, it accelerates the convergent process of slowly converging fluid and decelerates that of fastly converging fluid.
3. In certain cases, the control exercised by this procedure fails to bring the desired changes. In such cases, we had to resort temporarily to manual changes in the value of the acceleration factor.
4. Once the converged solution for one set of prescribed parameters is obtained, the solution for another set of parameters is obtained through a series of computations involving small changes in the prescribed conditions.

5. At each stage of the computation, boundary conditions are satisfied. The successive iteration improves upon the flow structure at the inner grid points.
6. In view of the inherent characteristics of the method, it should work reasonably well with the stiff equations which arise in fluid flow problems capturing shocks and flows with chemical reactions.
7. The numerical accuracy of a solution depends upon the extent it satisfies the governing equations. The magnitude of the residue gives an estimation of the error. In the present method, the calculation of residue is carried out at each grid point in the iteration as part of the solution procedure.
8. During the process of convergence, sometimes it was found that the error oscillated about some mean value. The situation can be rectified by slightly changing either one or all of the following:
   a. Initial conditions
   b. Outer domain of integration
   c. Prescribed conditions

Main code is divided into the following three subroutines:

1. Stagpt
2. Forepart
3. Aftpart

Stagpt subroutine solves the local similar solutions of the Navier-Stokes equations and gives the flowfield in the stagnation region.

Forepart subroutine solves the full Navier-Stokes equations in spherical coordinate system and calculates the flow on the spherical portion of the body. Aftpart subroutine solves the Navier-Stokes equations in cylindrical coordinate system and provides flowfield on the cylindrical portion of the body. Each of the subroutines converges to the desired level of accuracy before the computations on the next subroutine are initiated. In the code, there is provision for overlaid grids where the information from spherical system is passed to the cylindrical system.

The computer code so developed has the following salient features:

1. We can compute the flow up to any part of the body and automatically store the information in a restart file for further use in the computation of the flowfield on the remaining part of the body. For example, we can store the converged solution on the forepart of the body and use it to make extensive numerical experiments for computing the flow on the aftpart of the body.
2. Solution for the successive values of the prescribed conditions can be obtained by using the converged results from the previous set of prescribed conditions as initial conditions.
3. Besides solving the problem on sphere-cylinder and hemisphere with a sting, the present code in spherical cylindrical coordinate system enables us to solve the

flowfield on a variety of configurations, viz., cone with a blunt nose with or without a sting, biconic sections, etc.

In each of the subroutines various flow quantities are evaluated in the sequential order stated below:

1. Normal component of velocity from the normal momentum equation. It is observed that this equation converges slowly. In each global iteration, this equation is iterated twice.
2. Tangential component of velocity from the tangential momentum equation.
3. Temperature from the energy equation.
4. Density from the continuity equation. Continuity equation becomes singular at the surface. Density at the surface is evaluated in the following manner:

   "Pressure gradient in the radial direction, viz., $(\partial p / \partial r)$, at the surface is evaluated from the normal momentum equation, then the pressure at the wall is obtained as follows:

   $$p_{wall} = p_{(M,1)} = \frac{1}{3}\left[4p(M,2) - p(M,3) - 2\Lambda r\left(\frac{\partial p}{\partial r}\right)_{wall}\right]$$

   and the density at the wall from the equation of state.

   In some cases, we had to resort to linear extrapolation of density to the wall and then evaluate wall pressure from the equation of state.
5. Pressure at the inner grid points is evaluated from the equation of state.

8.3 Criterion for Convergence

The following five types of error estimates were made at every 50th iteration:

1. Mean square root of the tangential component of velocity
2. Mean square root of normal component of velocity.
3. Mean square root of temperature
4. Mean square root of pressure
5. Maximum of the difference of the values of the tangential component of velocity and temperature at every grid point in the flowfield at every 50 iterations.

The most stringent of the five criteria stated above was accepted as the criterion of convergence. Besides, the residues of each of the governing equations at each grid point were printed along with the converged results. By visual inspection, we satisfied ourselves that these residues are reasonably small at each grid point in the flowfield. This indicates that the computed results of the flow variables satisfy the governing equations and the boundary condition.

Section 9
DISCUSSION OF RESULTS

Extensive numerical computations have been carried out under conditions that can be obtained in SR3 low-density tunnel at the Centre National de la Recherche Scientific (CNRS) in France. The reasons for selecting these conditions for testing our code are that (1) CNRS proposes to conduct experiments to understand the wake structure on a 70 degree blunt cone with a cylindrical bay on its base and (2) theoretical investigations on the blunted cone using DSMC and the Navier-Stokes equations have already appeared in the literature. The configuration of the our body is sphere-cylinder or hemisphere with a cylindrical bay which simulates the generic shape of Aeroassisted Flight Experiment Vehicle (AFE). Although the generic AFE shape is quite different from the 70 degree blunted cone adopted by the previous investigators, yet we found similarities in the prediction of wake structure of AFE and blunted cone. Using the kinetic theory formulation of viscosity, Moss et al. [6] calculated the prescribed conditions in the CNRS tunnel in terms of the following dimensionless parameters:

$$M_\infty = 20.2,\ \mathrm{Re}_\infty = 768,\ \gamma = 1.4,\ \mathrm{Pr.}\ No. = 0.71,\ Tw = .2726$$

Here, the Reynolds number is based on the diameter of the base of the blunted cone.

Using the square-root viscosity law, we calculated the dimensionless parameters for our calculations as follows:

$$M_\infty = 20.19,\ \mathrm{Re}_0 = 84.48,\ \gamma = 1.4,\ \mathrm{Pr.}\ No. = 0.71,\ Tw = .2726$$

Computations have been carried out on sphere-cylinder and on hemisphere with a cylindrical bay with radius equal to a quarter of the radius of the base of the hemisphere. The purpose of computing the flow on sphere-cylinder is to understand the effect of dropping the cylindrical surface to quarter of the radius of base of hemisphere, on the main flowfield. The computations have thus been divided into the following three parts:

1. Computation of the flowfield on sphere-cylinder.
2. Computation of the flowfield on hemisphere with a cylindrical bay.
3. Comparison of the flowfield on sphere-cylinder and hemisphere with a cylindrical bay or generic AFE configuration in the common region of flow.

Computations have been carried out using 16 x 71 grids on the spherical surface and 31 x 71 grids on the cylindrical surface of sphere-cylinder body. For hemisphere with a cylindrical bay or generic AFE configuration, 37 grid points were added along the base of the hemisphere. Thus, for the generic AFE shape, there are 31 x 107 gridpoints in the region over the cylindrical surface. As stated earlier, first the solution for the stagnation region was made to converge and then the solution on the spherical portion was made to converge and finally the solution in the wake region converged. In the present report, only the results of the above mentioned case are presented. Other

cases calculated by the present investigator are not reported mainly because they offered no new insight into the nature of the flow on the spherical surface or in the wake structure.

CASE (A) COMPUTATION OF THE FLOWFIELD ON SPHERE-CYLINDER.

In Figs. 9.1 and 9.2, temperature profiles at various locations on sphere-cylinder configuration are drawn. From these graphs, the following observations can be made:

1. Temperature profiles indicate that a relatively strong shock from the forepart of the body diffuses progressively as it moves downstream of the body.
2. In the present procedure, a specially designed mathematical procedure is applied to obtain numerical solutions of the full Navier-Stokes equations along the stagnation line [1,2]. The solution along the stagnation line so obtained provide one of the boundary conditions to integrate the full Navier-Stokes equations over the surface of the body. Special efforts were made to see that this solution along the stagnation line merges smoothly with the solution over the rest of the surface of sphere.
3. A big advantage of using spherical polar coordinate system is that the junction of the sphere with cylinder viz., $\theta = 90$ degrees or $z = 0.0$ is not a singular point in that the normal at the junction is well defined. It is not so when the body oriented coordinate system is used. In body oriented coordinate system, there are infinite number of normals as we pass over the juncture point from the spherical side to cylindrical side. As such, it becomes reasonably difficult to obtain smoothly varying solution around the junction point. In the present investigation, no such problem is encountered as is evident from the graphs in Figs. 9.1 t0 9.7. Temperature, tangential component of velocity, pressure and density profiles show smooth changes as flow passes over the junction point.
4. Under the prescribed conditions, there does not appear to be any inviscid zone on the spherical surface. A thick viscous layer near the surface merges smoothly with a relatively thick bow shock. In the merged layer, there is almost a continuous increase of temperature from the surface right up to the compressive side of the shockwave. However, from the stagnation point up to the shoulder, the shock strength decreases and consequently the maximum in temperature profile (Figs. 9.;1 and 9.2) decreases continuously.

Beyond the shoulder and on the cylindrical portion, there seems to be significant expansion of the fluid which lowers the temperature level in the main body of the merged layer. There is a slight increase of temperature in the viscous layer near the cylinder body and a sharp drop of temperature across the shock wave. In between the shock wave and viscous layer, there is an inviscid zone whose extent grows with the distance downstream the cylindrical body.

In Figs. 9.3 and 9.4, profiles for tangential component of velocity are drawn at various locations on the spherical surface. We find that as θ varies from 0.0 t0 90 degrees, the tangential component of velocity $\frac{u}{u_\infty}$ changes its values from zero to unity. As

such, the shock strength is not perceptible in the profiles drawn in the fore part of the spherical surface. However, the increment in shock strength is quite evident as we approach the fluid at θ = 90 degrees. Beyond θ = 90 degrees, due to expansion in the main body of the fluid, the fluid velocity decreases, the shock diffuses and the shock strength decreases.

In Figs. 9.5 and 9.6, pressure profiles are drawn at various locations on the sphere-cylinder surface. On the fore part of the spherical surface, there is a significant rise in pressure across the shock followed by a slight compression in the viscous layer underneath the shock wave. As we move downstream, the expansion of flow in the viscous layer reduces the pressure level in the viscous layer and diminishes the shock strength in pressure profiles. We further notice that , on the spherical portion, the pressure continuously rises from the surface up to the shock. As such, the boundary layer approximation, viz., the gradient of pressure normal to the surface is negligible , is not valid under the prescribed rarefied conditions. The pressure levels are reasonably low on the cylindrical portion of the body and as expected the shock strength decreases.

In Figs. 9.7 and 9.8, density profiles at selected locations on the spherical and cylindrical surfaces are drawn. We notice that along the line of symmetry, the fluid suffers compression across the shock as well as in the viscous layer . The density at the stagnation point is much larger than the density across the shock wave. As such, the presence of the shock in the density profile at θ = 0.0 is not so evident. As we move down stream, the shock strength decreases and it moves away from the surface, allowing expansion of the flow to take place in the viscous layer. This process reduces the level of density in the viscous layer, so much so that the density behind the shock wave becomes larger than the density in the viscous layer. Thus, the formation of the shock becomes evident in the density profiles..

In Figs. 9.9 and 9.10, graphs are drawn to show the variation of heat transfer and pressure coefficients on the spherical and cylindrical surfaces of sphere-cylinder configuration . We observe that C_H near θ = 0.0 and at θ = 90 degrees are not smoothly merging with the corresponding values downstream, and there are slight fluctuations in the values of C_H on the cylindrical surface. In our view, these fluctuations are spurious and can be removed by further numerical experimentation with respect to the size of grids. Overall values are not going to change.

CASE (B): COMPUTATION OF THE FLOWFIELD ON HEMISPHERE WITH A CYLINDRICAL BAY OR GENERIC AFE CONFIGURATION

In the wake region, density of the fluid is pretty low, usually less than 10 percent of the free stream density. So, it became quite difficult to estimate the slip velocity on the base of the hemisphere from the computations.

We found from Fig. 13 of Ref. [8] that the slip velocity on the base of the blunted cone and on cylindrical bay is in any case very low probably due to the extremely slow motion of the fluid in the base region. For the time being, slip velocity on the base of the hemisphere is replaced with the no slip velocity. However, the slip velocity on the

spherical portion and on the cylindrical portion of the generic AFE shape is retained without the creeping term.

In Figs. 9.11 to 9.20, a brief description of the nature of the wake is presented. Description of the flow on the spherical surface and in the main body of the flow is not very different from the description of the flow on sphere-cylinder presented in case (A) above.

From Figs. 9.11 and 9.20, we find that there is no separation of the flow in the wake region under the prescribed conditions. Numerous numerical experiments with different grid sizes and initial conditions were carried out to see whether under any other condition separation bubble is possible. None of these efforts succeeded to catch separation bubble in the wake. There is no evidence of a separation shock or a distinct wake shock under these rarefied conditions. Under the same prescribed conditions as stated above, Moss , Mitcheltree , Wilmoth and Dogra [6] also found that there is no separation of the fluid in the wake region of the blunted cone. The results in Ref. [6] confirm our findings.

From Fig. 9.11 and 9.12, we find that the wake region is heated due to the presence of Knudsen layer and the viscous effects near the surface of the cylindrical bay. Figs. 9.13 and 9.14 show that. the fluid is greatly decelerated in the wake region. Figs. 9.15 and 9.16 indicate that the pressure level in the wake region is extremely low. Similar conclusion is derived from Fig. 9.17 where density profiles at selected locations on the cylindrical bay are drawn. Fig. 9.17 clearly indicates that the density in the wake region under the prescribed conditions are very low , generally, less than 10 percent of the free stream value of the density. In Fig. 9.18, surface slip velocity and temperature jump conditions are plotted against the distances on the surface of the generic AFE body. It is found that in the wake region, slip velocity and temperature increase quite significantly. In Figs. 9.19 and 9.20, surface quantities , viz., heat transfer, skin-friction and pressure coefficients, are drawn against the distances on the generic AFE body. It is found that all the surface quantities i.e. C_H, C_f and C_P are reasonably small on the cylindrical cargo bay of the AFE body. We may thus conclude the following :

"UNDER THE PRESCRIBED CONDITIONS, THE WAKE OF A GENERIC AFE BODY CONTAINS A SLOW MOVING, HIGH TEMPERATURE, LOW DENSITY AND CONSEQUENTLY LOW PRESSURE FLUID."

These conclusion are in conformity with the conclusion derived earlier in Ref. [10]

CASE (C) COMPARISON OF THE FLOWFIELD ON SPHERE-CYLINDER AND HEMISPHERE WITH A CYLINDRICAL BAY OR A GENERIC AFE CONFIGURATION IN THE COMMON REGION OF FLOW

In Figs 9.21 to 9.24, comparison of certain flow quantities and surface quantities on sphere-cylinder and on a generic AFE body is made with a view to understand the effect of wake structure on the main flowfield. In Figs. 9.21 and 9.22, temperature and density profiles at certain selected locations on the cylindrical surfaces are compared. From the graphs, we find that the wake cools slightly and reduces the density in the main flowfield. The effect is realized more near the shear layer than near the shock

wave. The location of the shock wave is unaffected. Figs. 9.23 and 9.24 show that the heat transfer and pressure levels on the cylindrical portion of the generic AFE are greatly reduced.

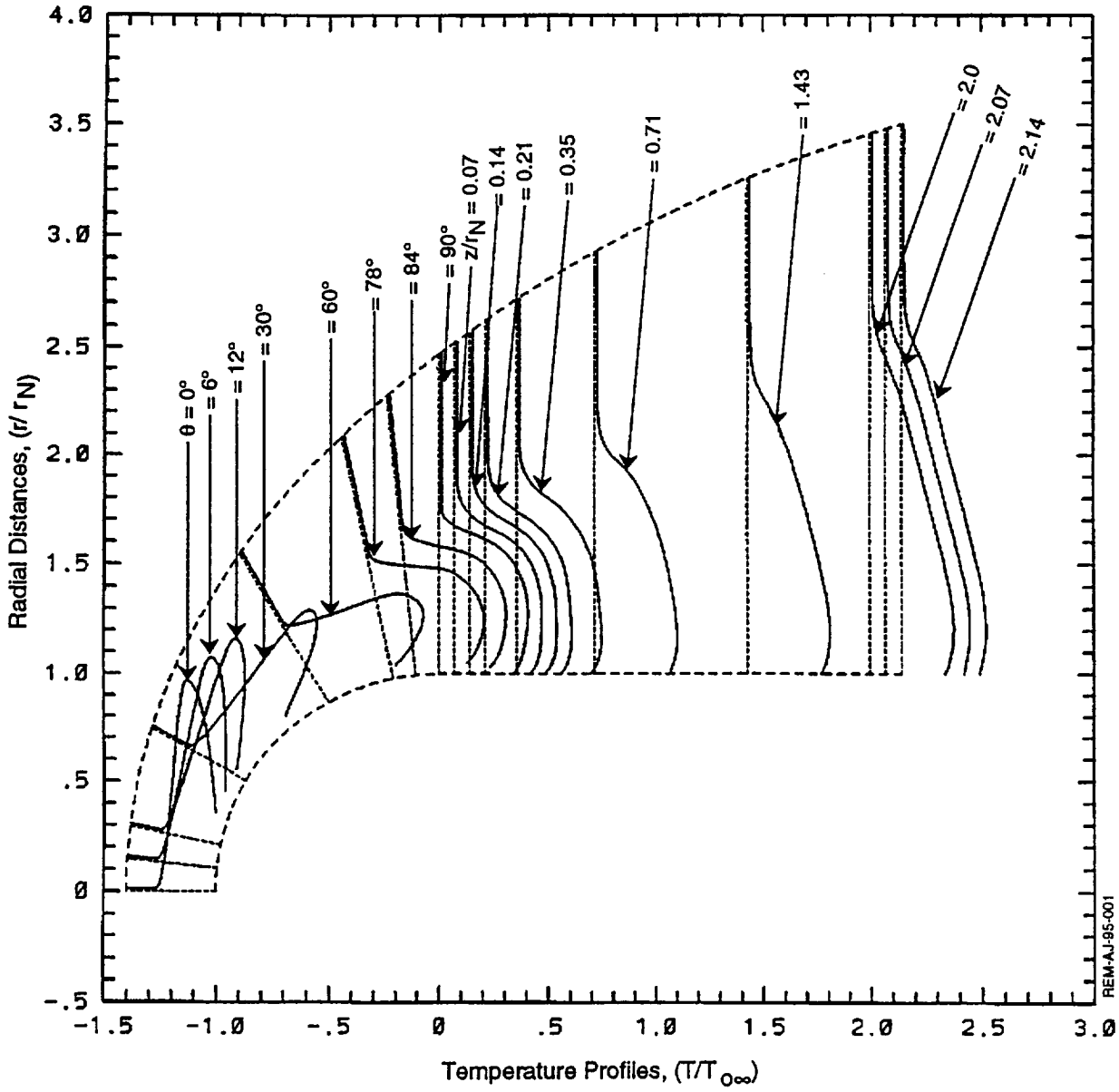

Figure 9.1: Temperature Profiles at Various Locations on Sphere-Cylinder Configuration

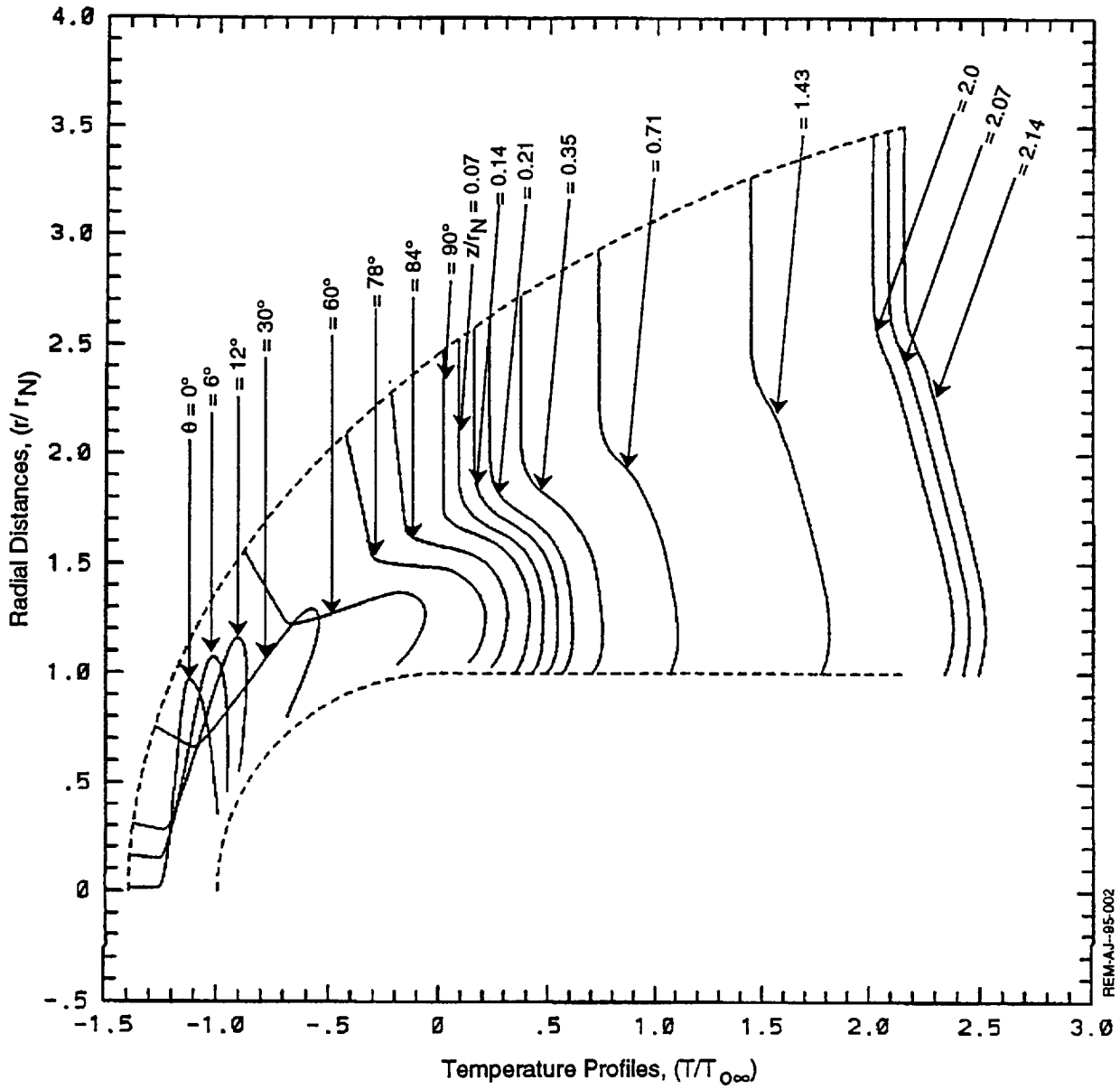

Figure 9.2: Temperature Profiles on Sphere-Cylinder Configurations

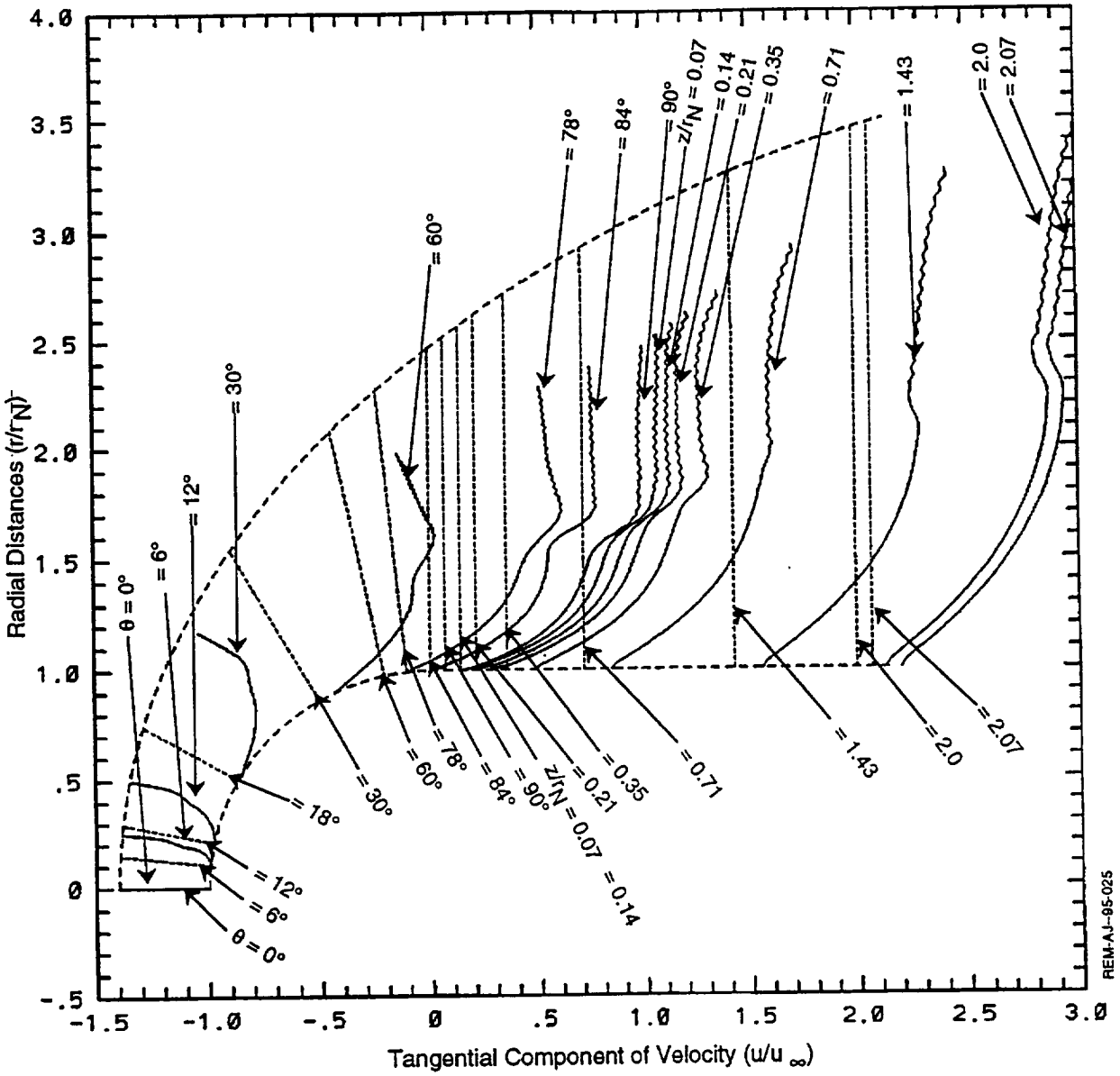

Figure 9.3: Profiles for Tangential Component of Velocity on Sphere-Cylinder Configurations

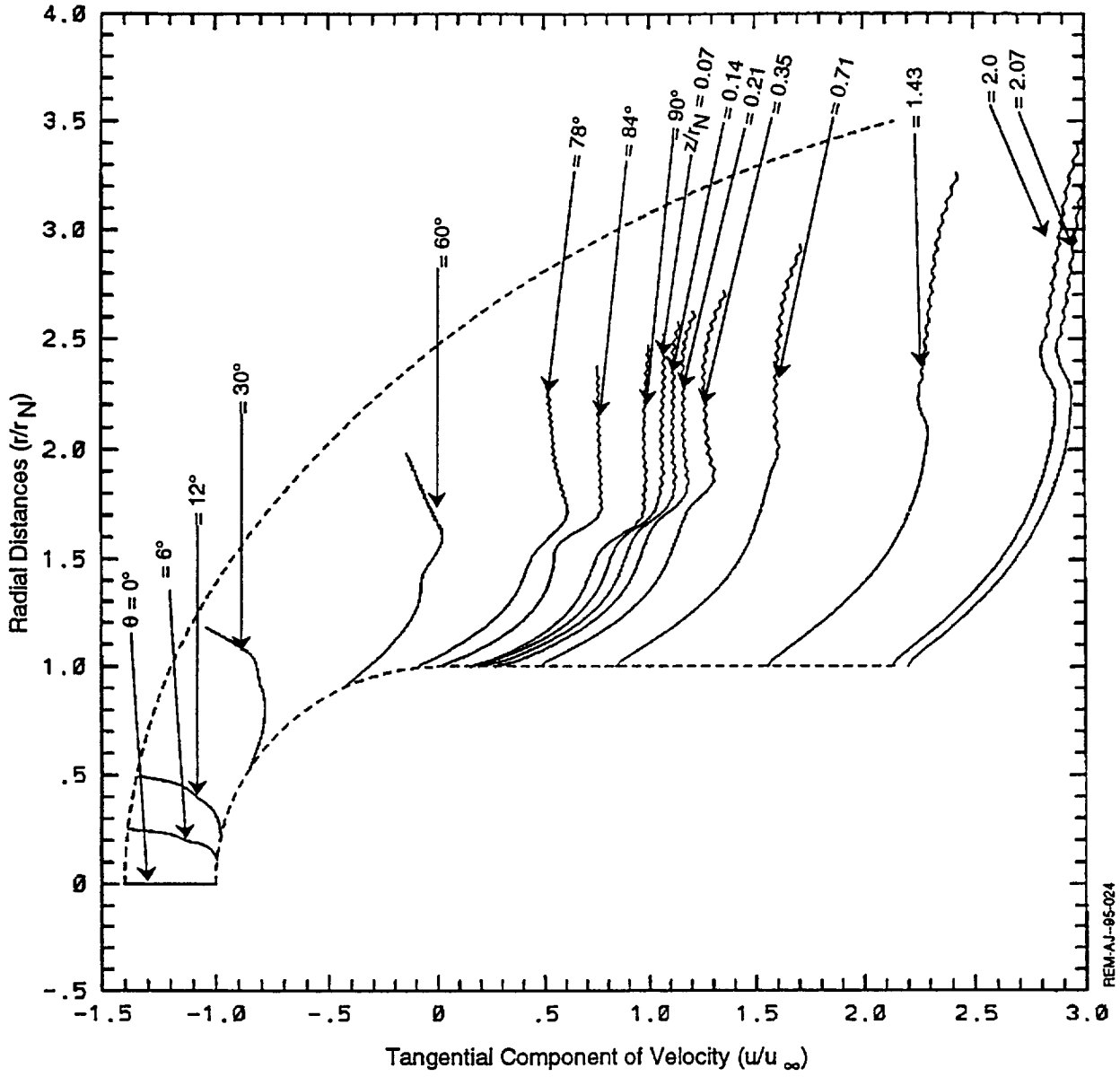

Figure 9.4: Profiles for Tangential Component of Velocity on Sphere-Cylinder Configuration

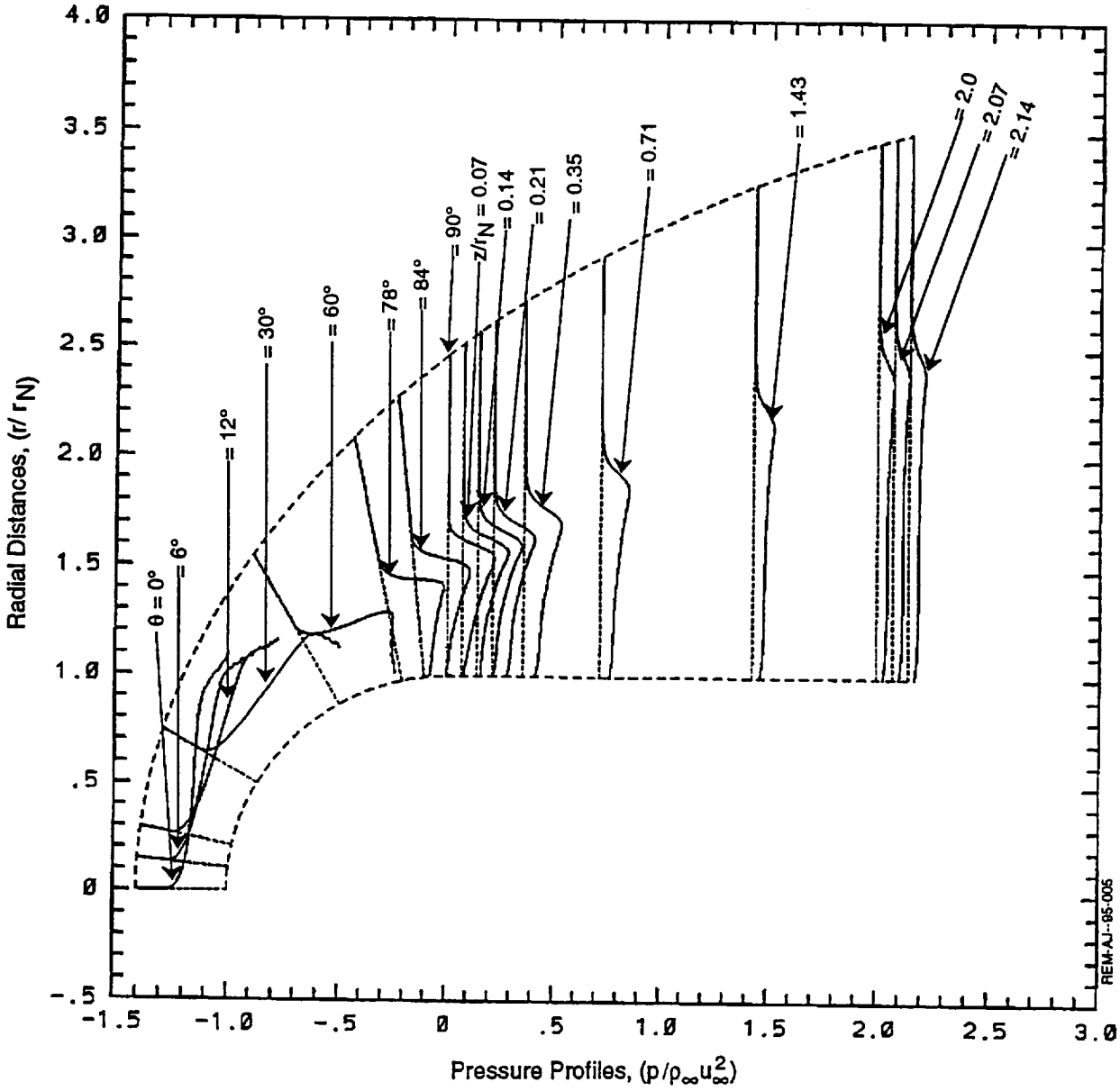

Figure 9.5: Pressure Profiles on Sphere-Cylinder Configuration

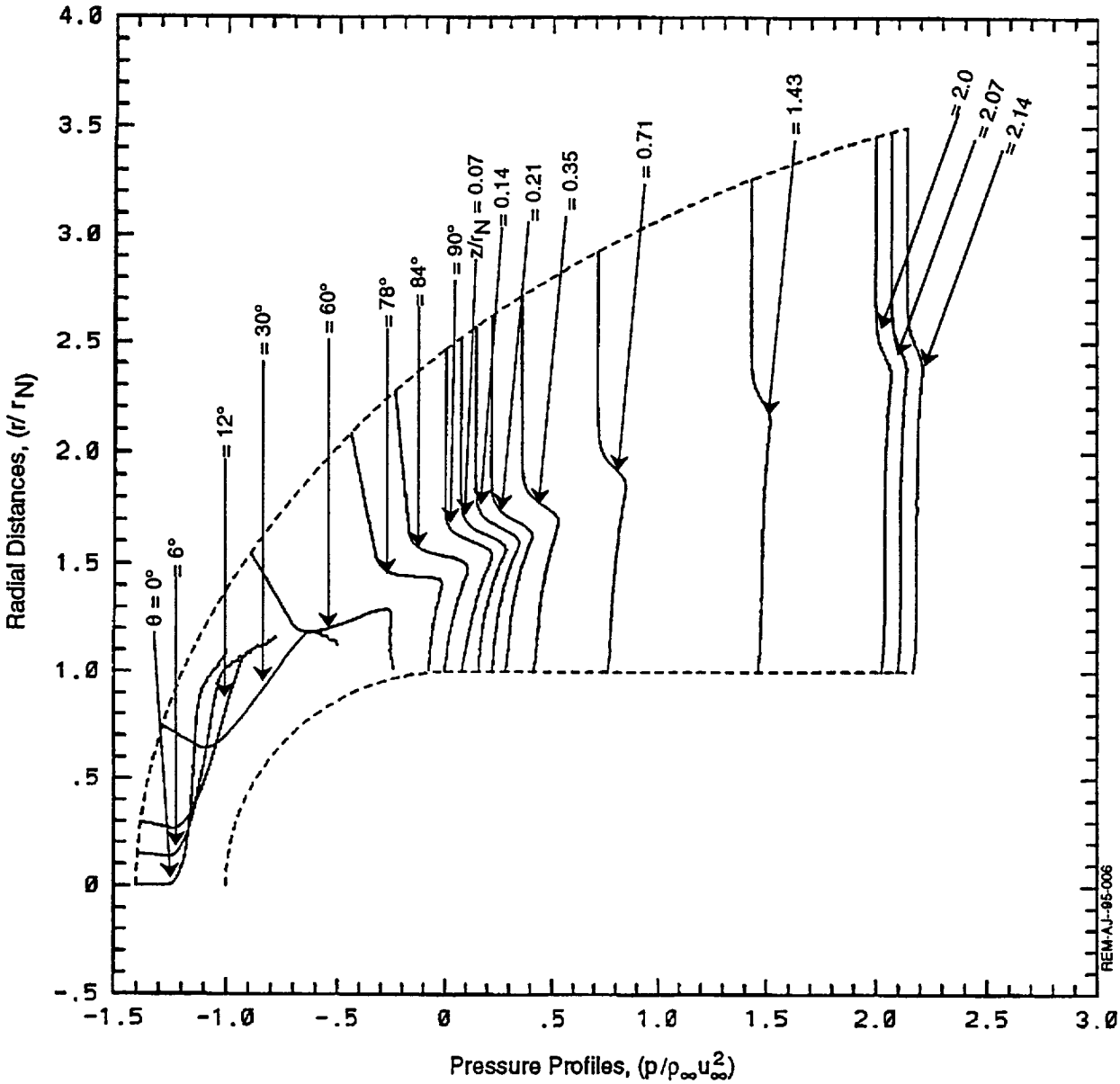

Figure 9.6: Pressure Profiles on Sphere-Cylinder Configuration

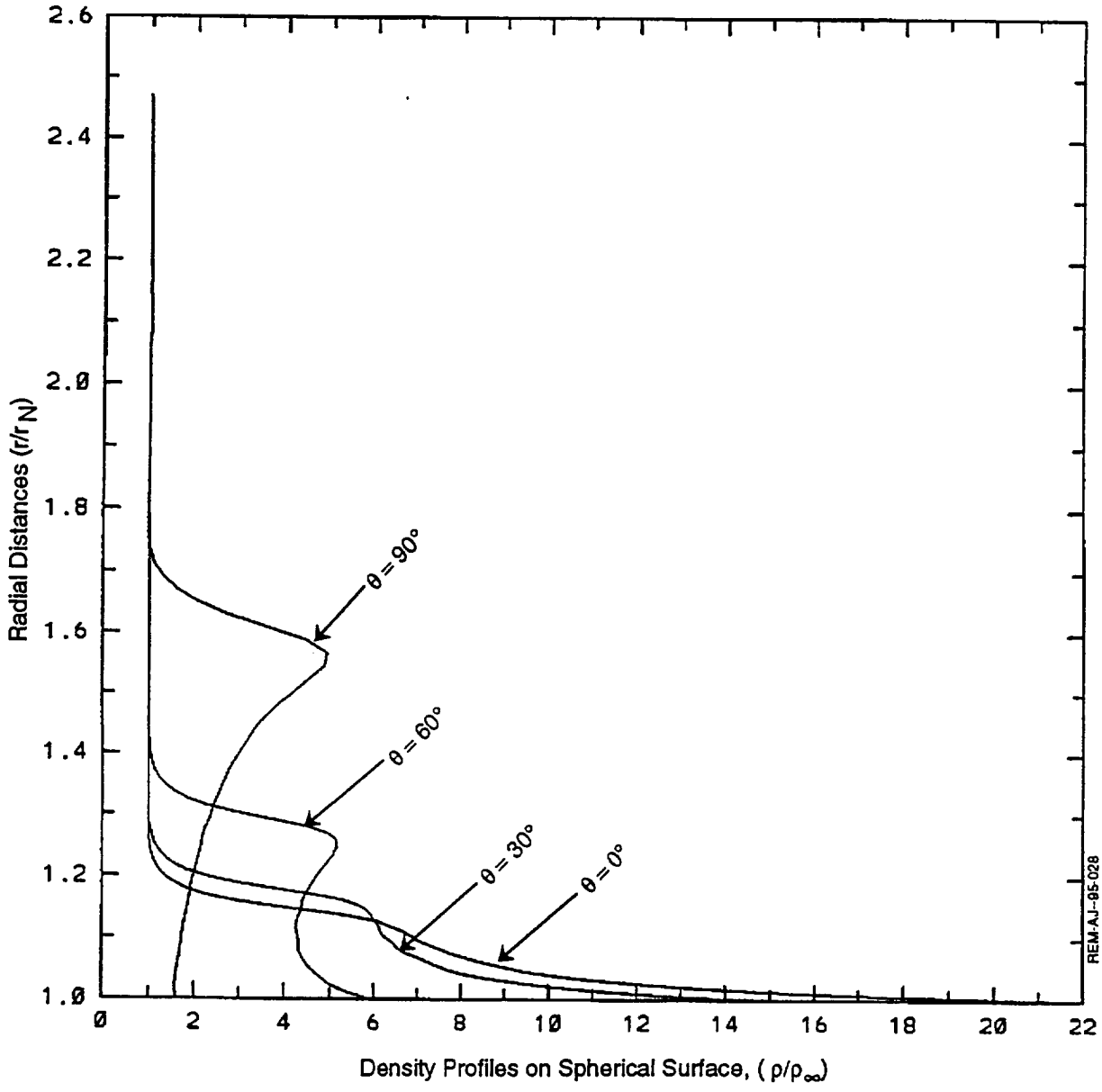

Figure 9.7: Density Profiles on Spherical Position of Sphere-Cylinder Configuration

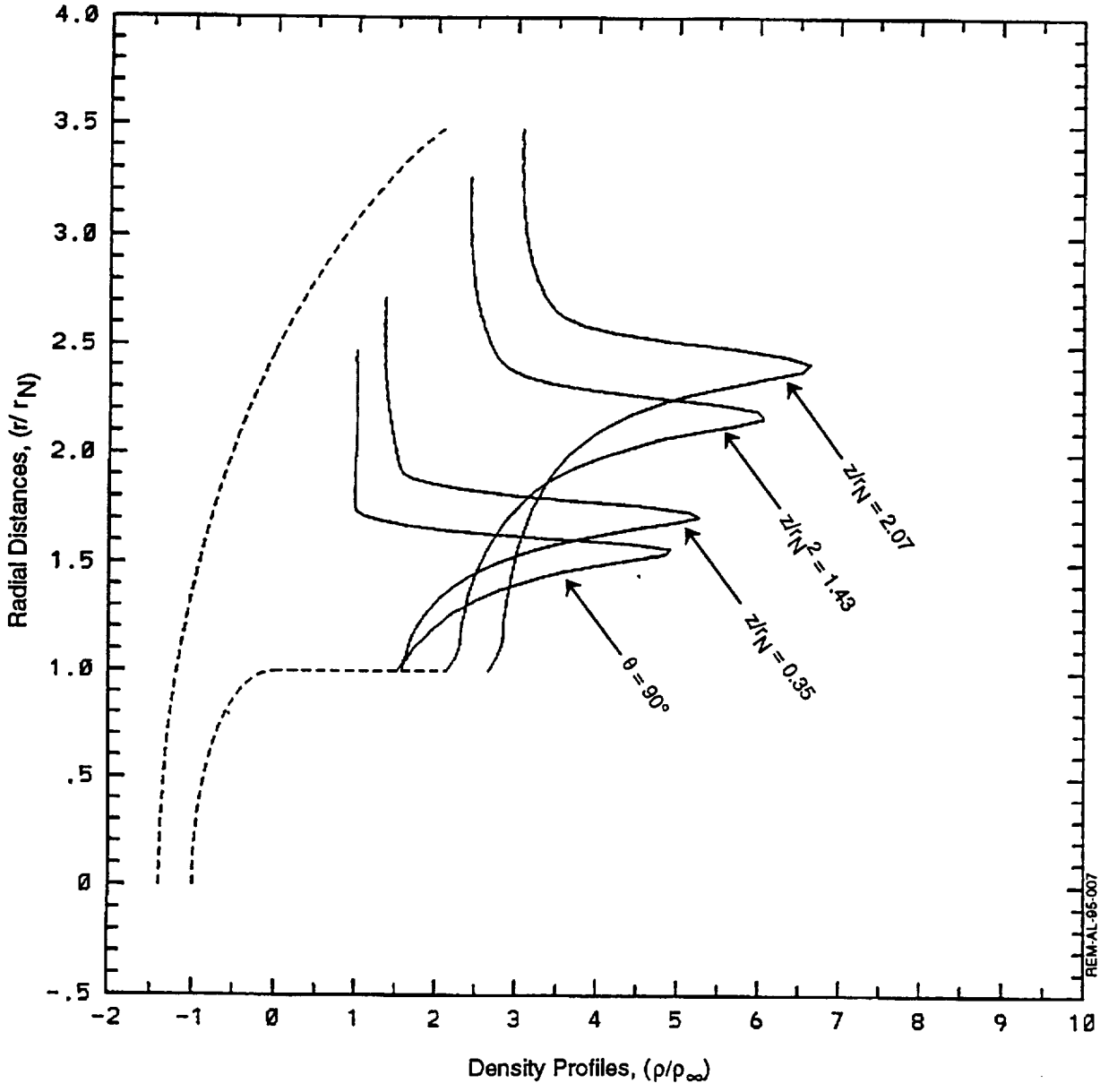

Figure 9.8: Density Profiles on the Cylindrical Portion of Sphere-Cylinder Configuration

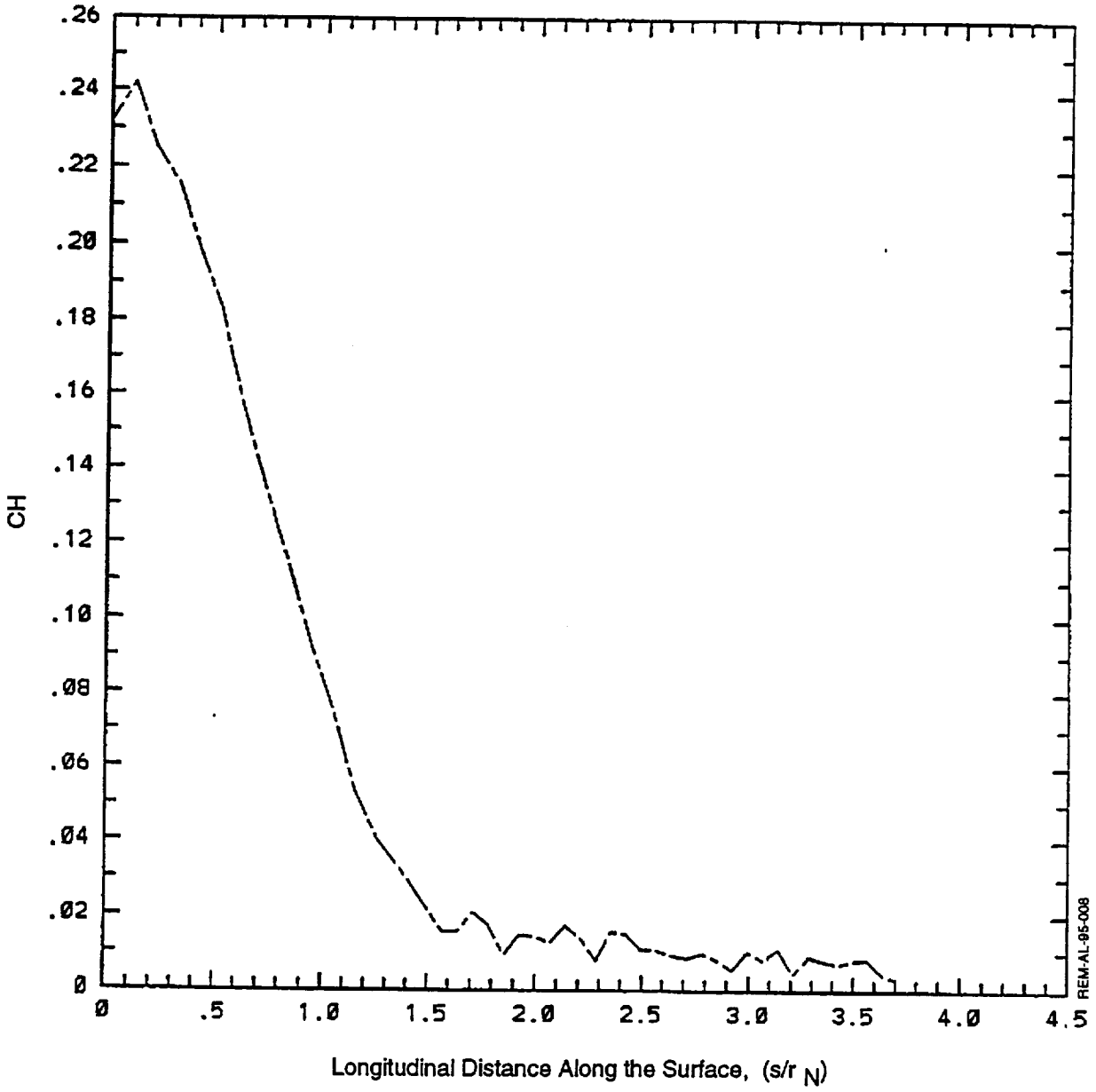

Figure 9.9: Variations of Heat Transfer Coefficient along the Surface of Sphere-Cylinder Configurations

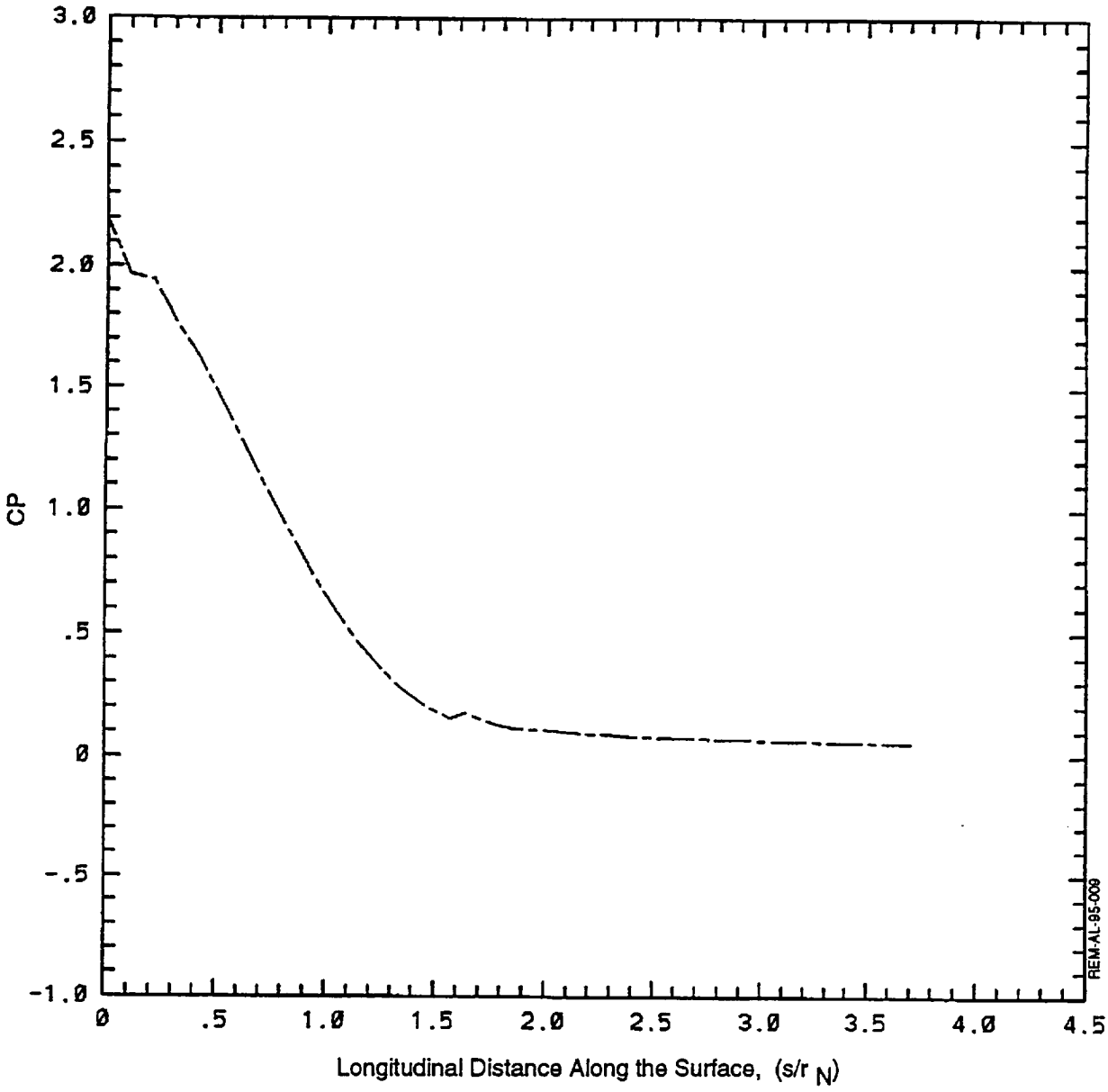

Figure 9.10: Variation of Pressure Coefficient along the Surface of Sphere-Cylinder Configuration

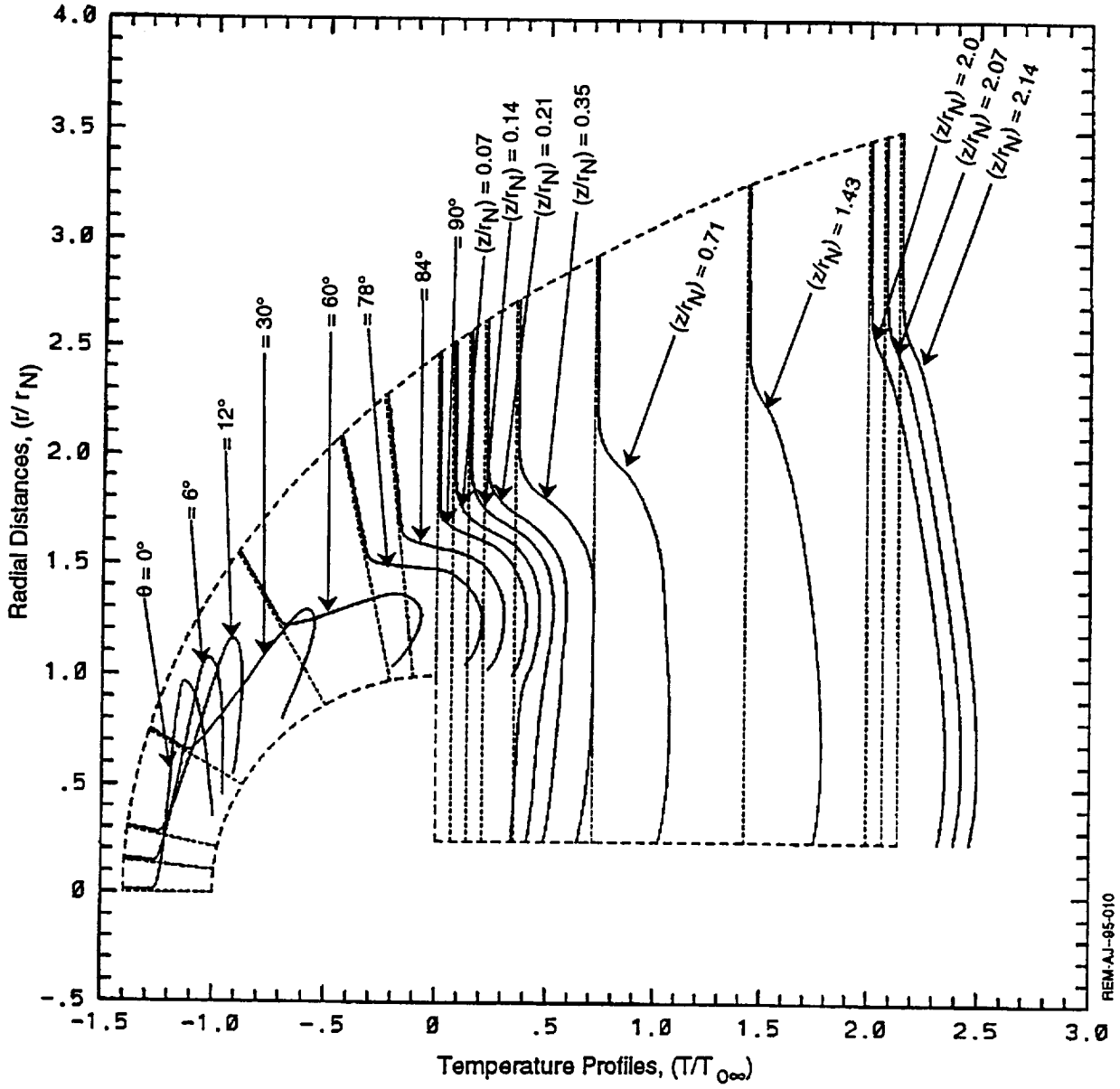

Figure 9.11: Temperature Profiles at Various Locations on a Generic AFE Configuration

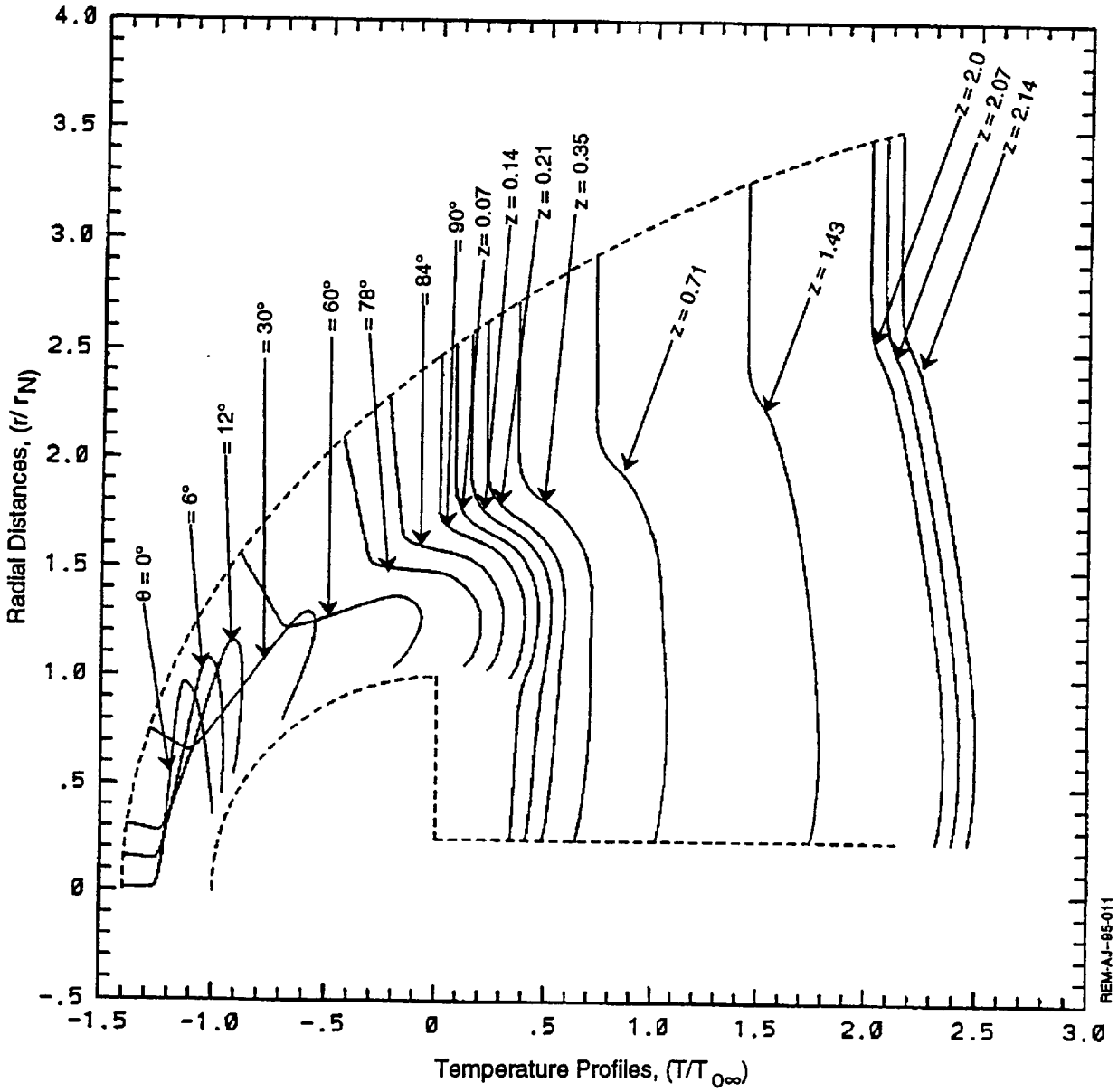

Figure 9.12: Temperature Profiles on a Generic AFE Configuration

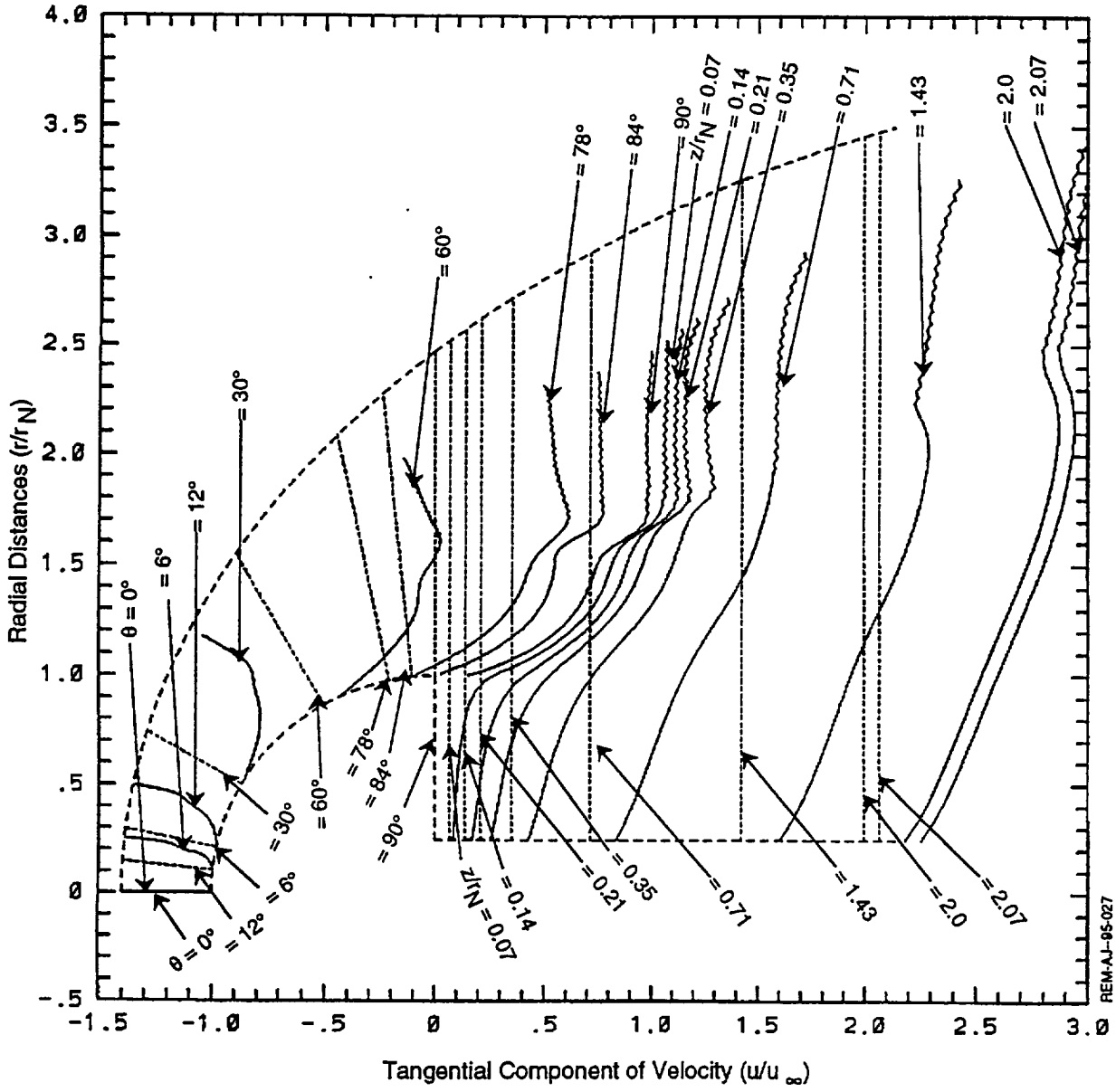

Figure 9.13: Profiles for Tangential Component of Velocity on Generic AFE Configuration

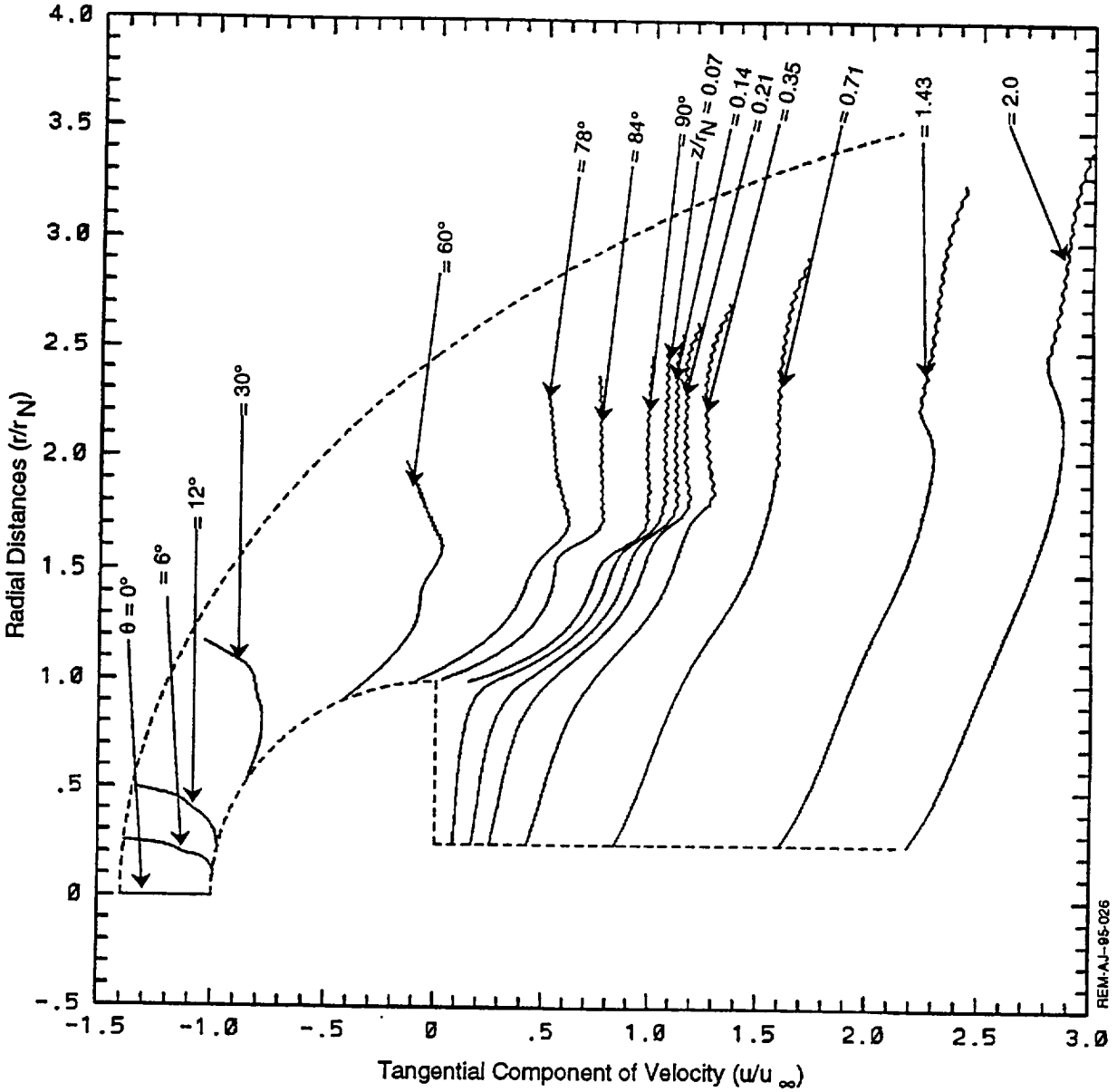

Figure 9.14: Profiles for Tangential Component of Velocity on Generic AFE Configuration

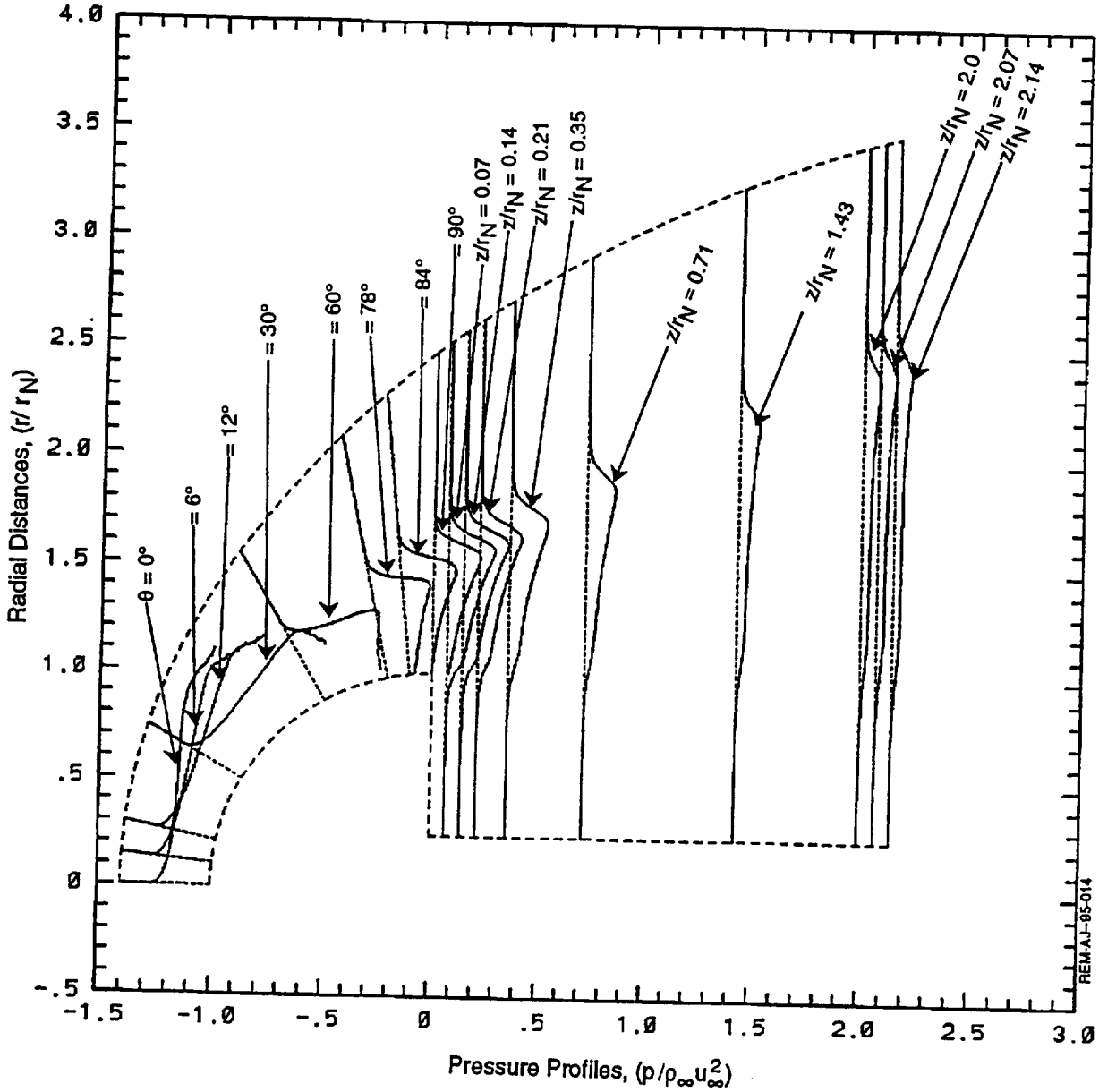

Figure 9.15: Pressure Profiles at Various Locations on a Generic AFE Configuration

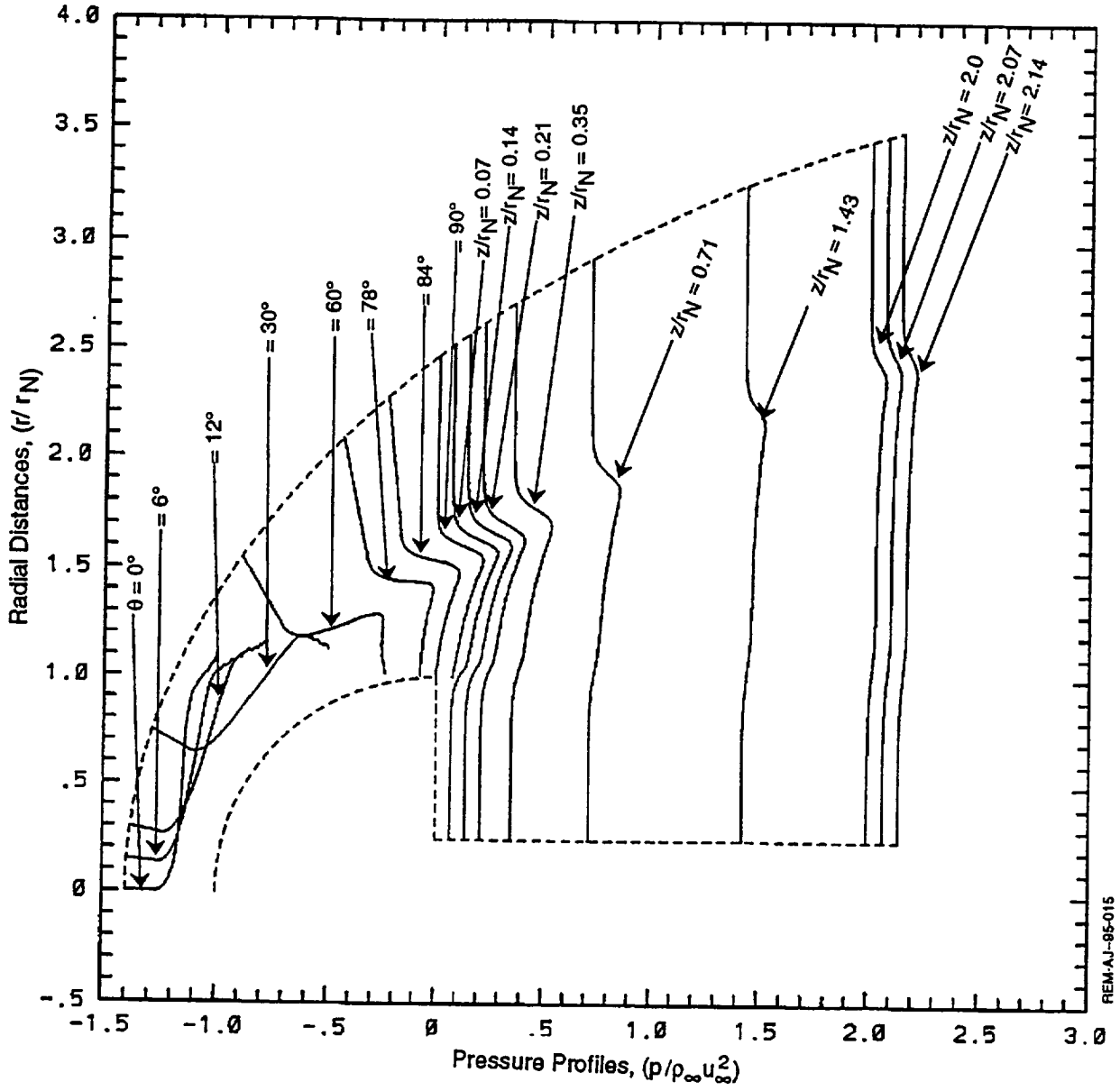

Figure 9.16 Pressure Profiles on a Generic AFE Configuration

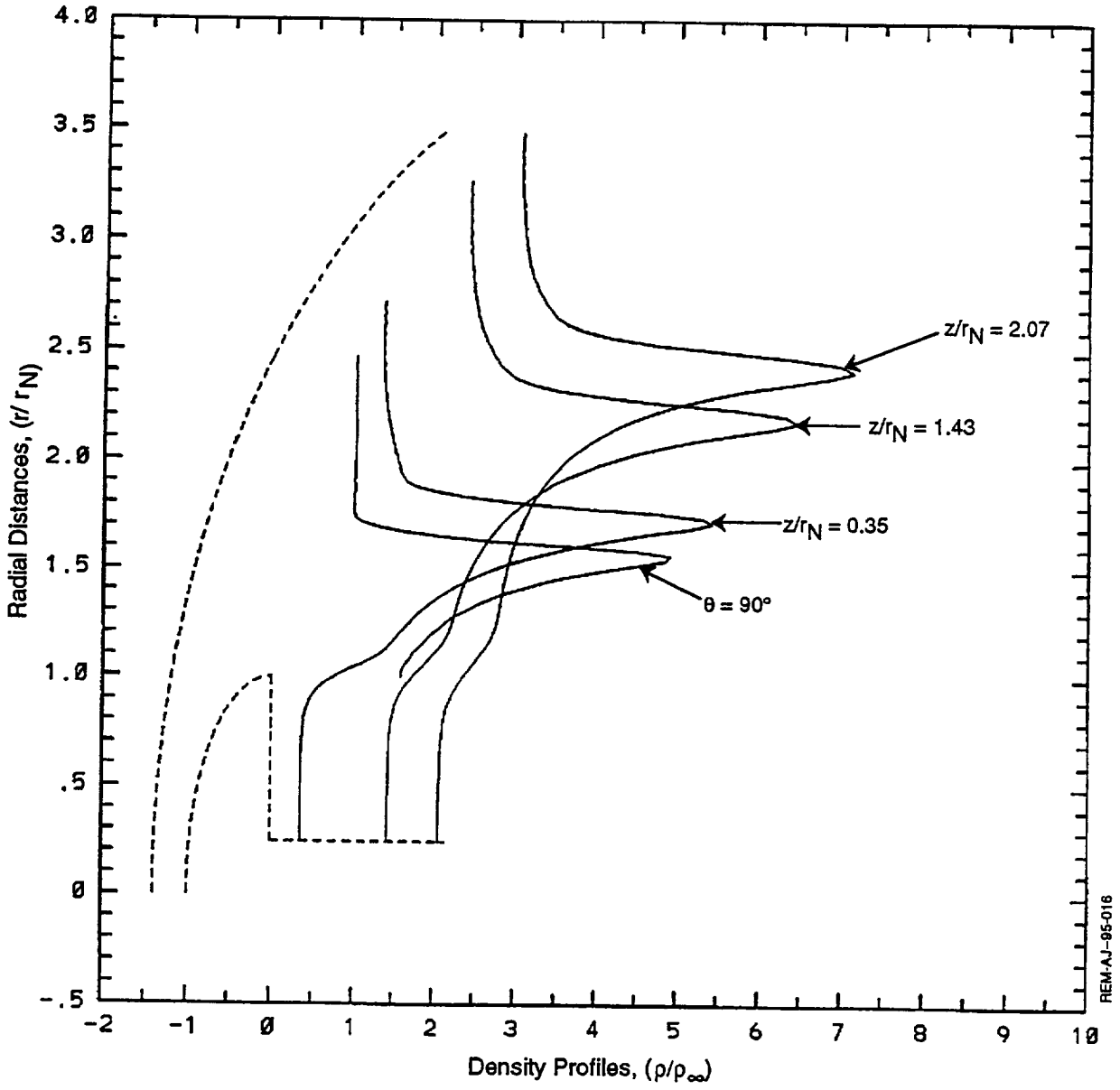

Figure 9.17: Density Profiles at Various Locations on a Generic AFE Configuration

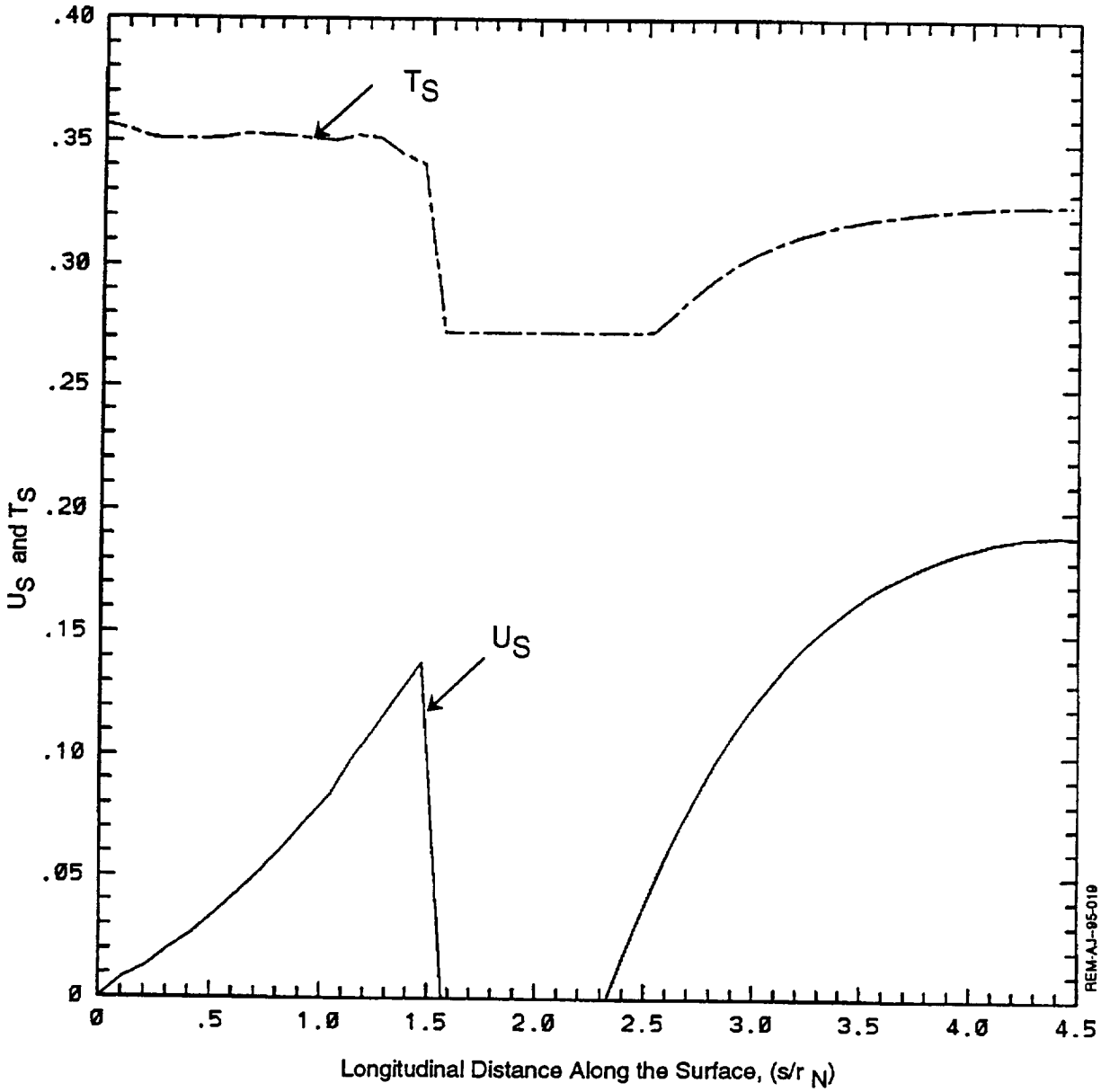

Figure 9.18: Surface Slip Velocity and Temperature Jump Values on the Surface of a Generic AFE Configuration

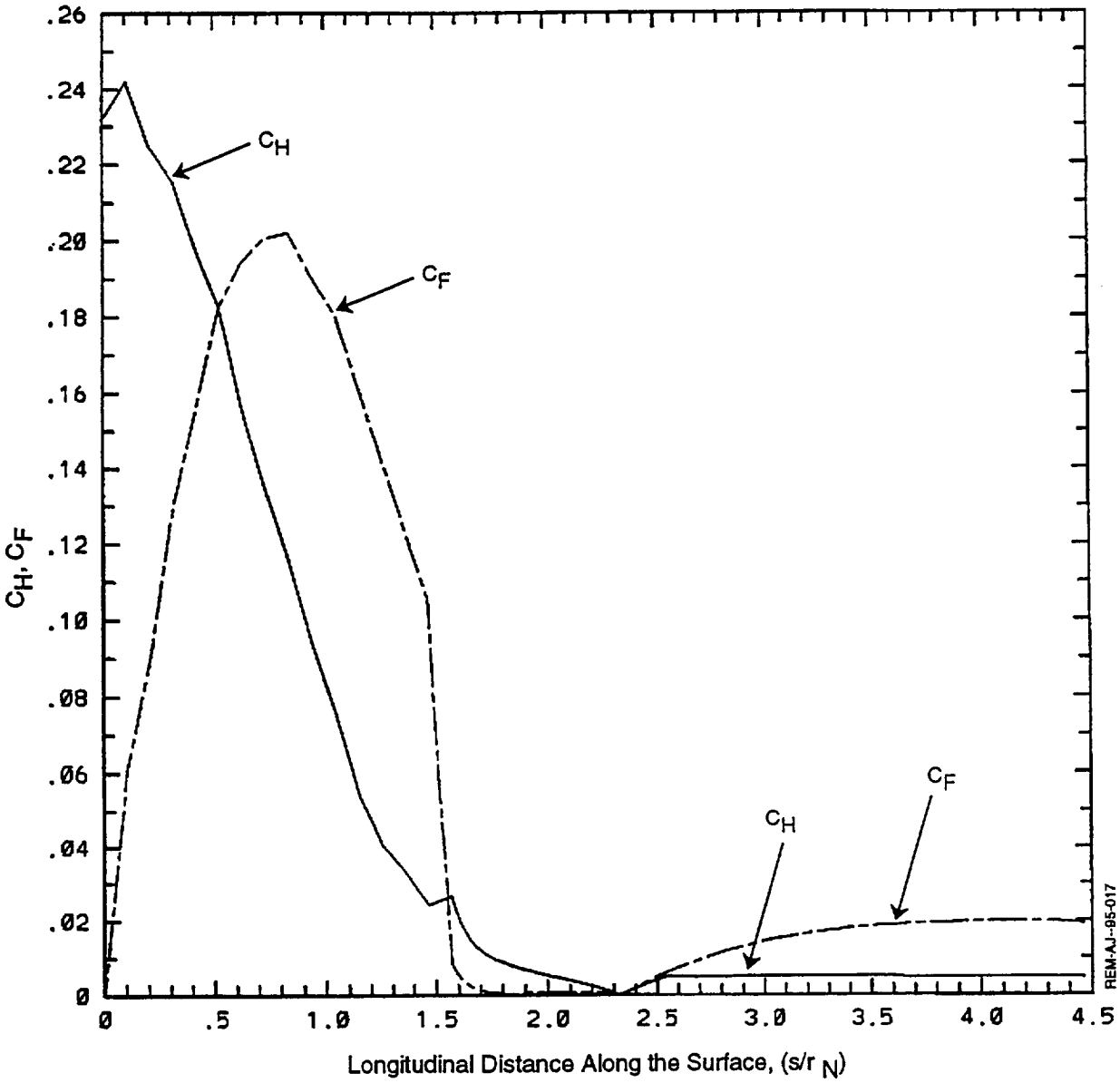

Figure 9.19: Variation of Heat Transfer and Skin-Friction Coefficient on a Generic AFE Configuration

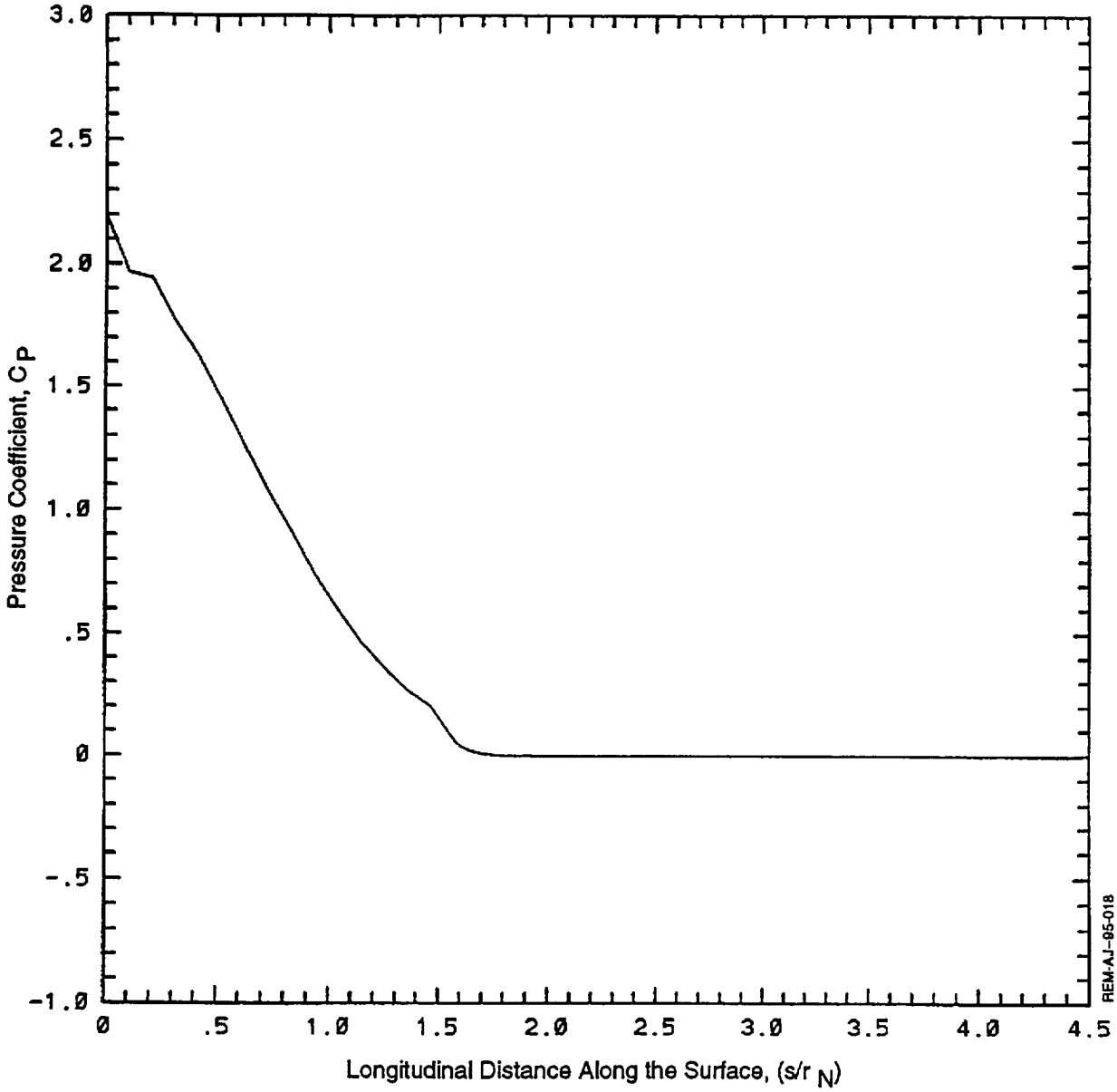

Figure 9.20: Variation of Pressure Coefficient Along the Surface of a Generic AFE Configuration

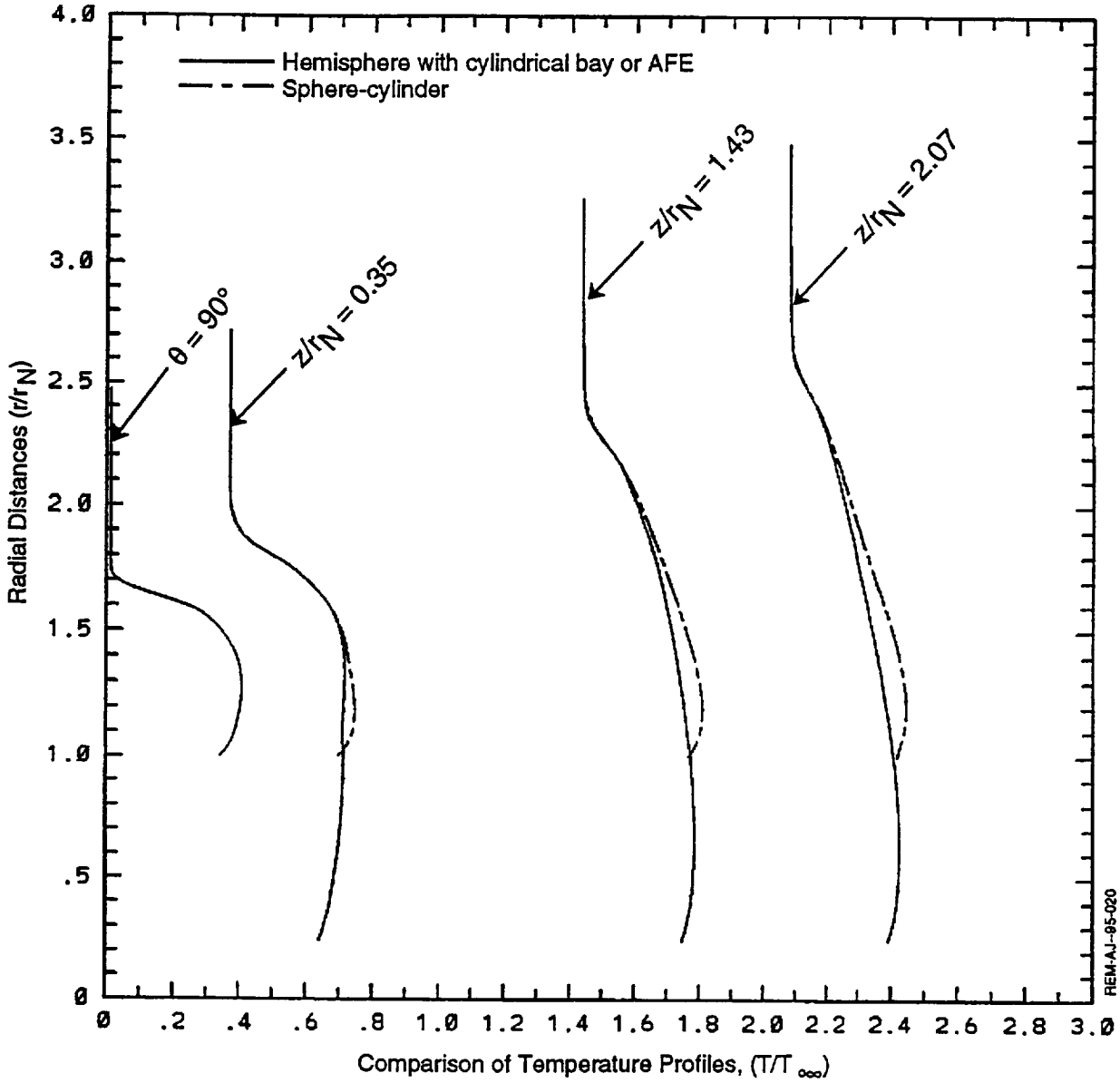

Figure 9.21 Comparison of Temperature Profiles on Generic AFE and Sphere-Cylinder Configurations

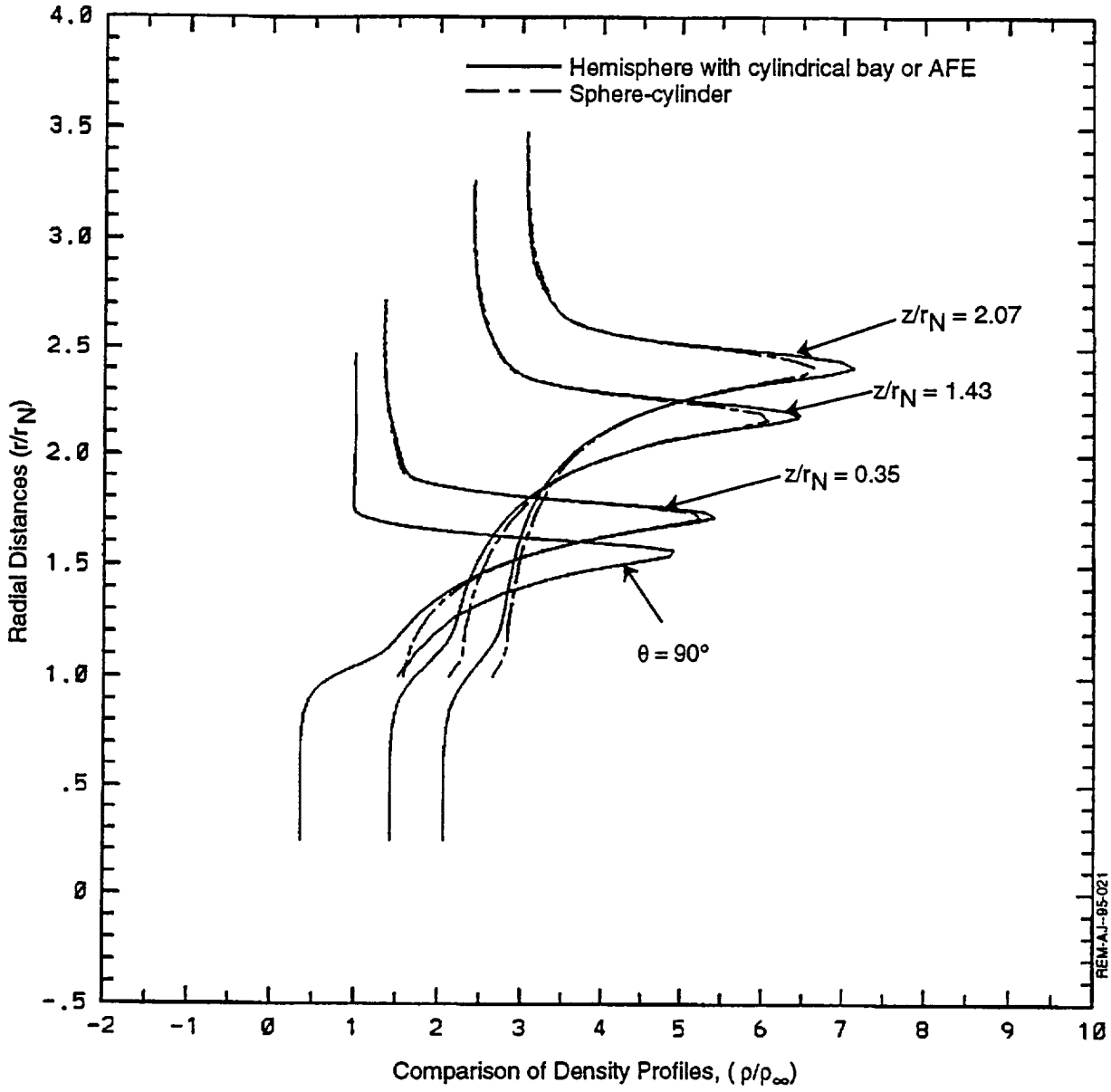

Figure 9.22: Comparison of Density Profiles on the Generic AFE and Sphere-Cylinder Bodies

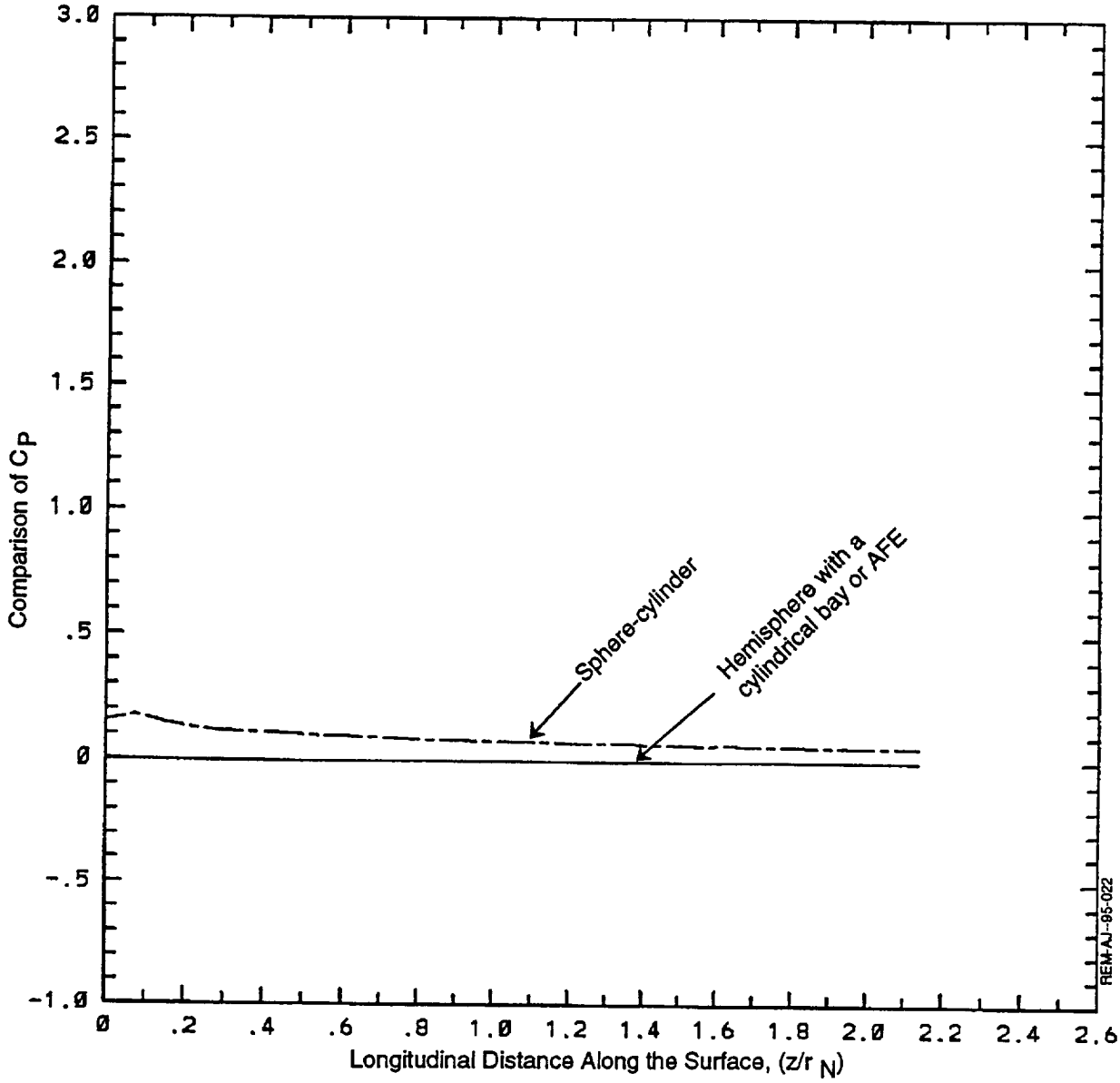

Figure 9.23: Comparison of Pressure Coefficient along the Cylindrical Portion of the Generic AFE and Sphere-Cylinder Bodies

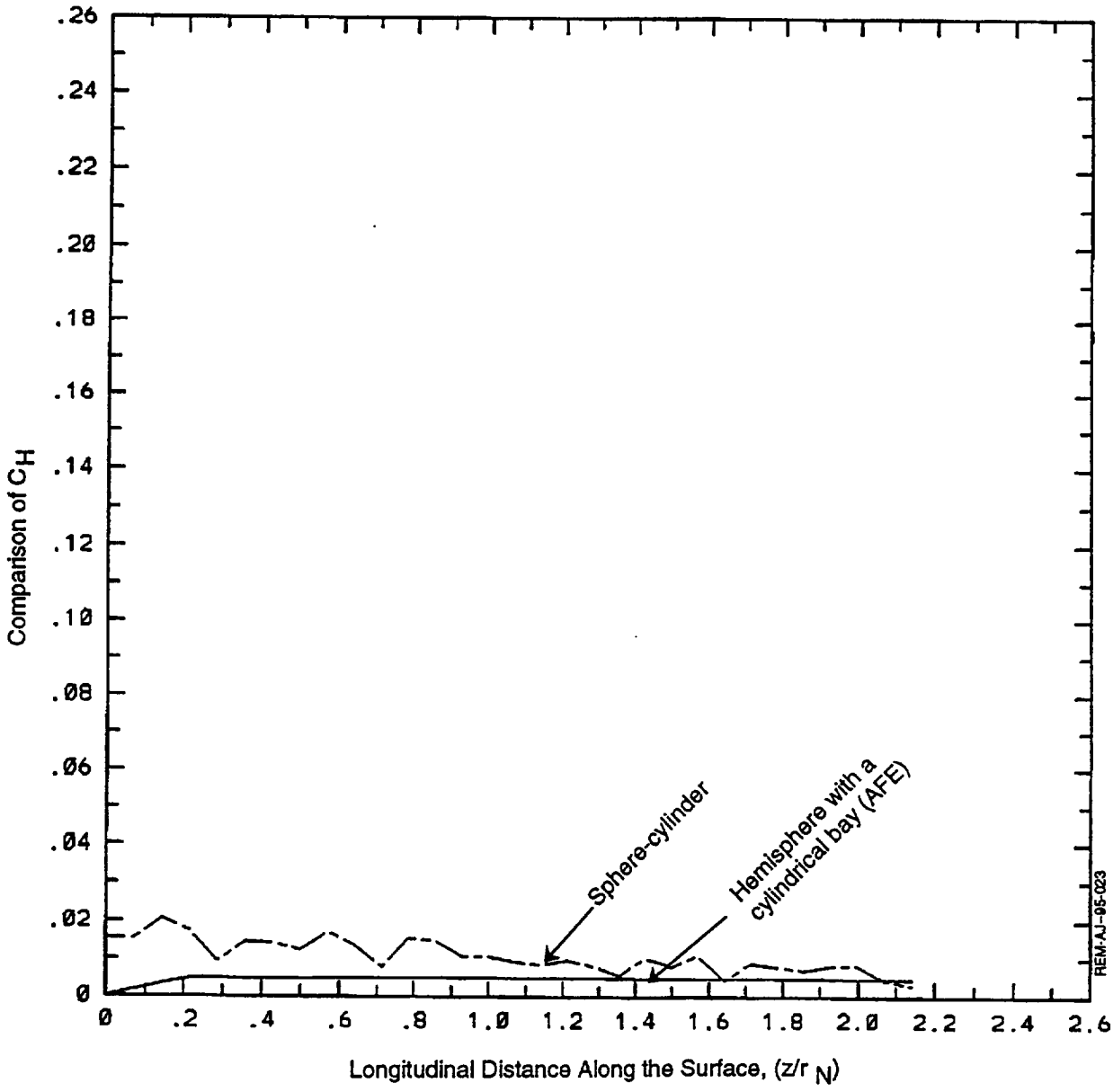

Figure 9.24: Comparison of Heat Transfer Coefficient along the Cylindrical Portion of Generic AFE and Sphere-Cylinder Bodies

Section 10
CONCLUSIONS

Extensive numerical computations have been carried out for a number of prescribed conditions, but for the sake of brevity, the results of computations for SR3 tunnel conditions of CNRS, Meudon, France, are reported here. Computations have been carried out on a cylindrical body with a spherical nose (also called sphere-cylinder body) and on a hemisphere with a cylindrical bay with radius equal to a quarter of radius of the base of hemisphere, to simulate a generic AFE configuration. Comparison of the results on sphere-cylinder and on the generic AFE body help us to understand the rarefaction effects and the effect of the wake flow on the main flowfield. It is found that under rarefied conditions, wake flow defined as the flow between the shear layer and the bay has little influence on the main flow between the shear layer and the shock wave. Comparison of our results with the DSMC data from NASA LaRC indicates general agreement about the nature of wake, but our results differ quantitatively with the DSMC results. At the present moment, the results from the CNRS tunnel are not available. As such, a quantitative comparison of the present results with the experimental data is not possible.

In general, it is found that under the prescribed conditions, wake is a slowly moving, high temperature, low density and low pressure fluid.

Section 11
REFERENCES

[1] Jain, A. C., "Hypersonic Stagnation Line Merged Layer Flow on Blunt Axisymmetric Bodies of Arbitrary Shape," AIAA 93-2723, 1993.

[2] Jain, A. C., "Hypersonic Merged Layer Flow on a Sphere," *J. of Thermophysics*, Vol. 1, No. 1, 1987, pp 21-27.

[3] Jain, A. C. and Dahm, W. K., "Hypersonic Merged Layer Blunt Body Flows With Wakes," *Proc. 17th Int. Sym. On Rarefied Gas Dynamics*, edited by Alfred E. Beylich, Aachen, Germany, VCH, 1991, pp 578-587.

[4] Brewer, E. B., "Hypersonic Rarefied Wake Characterization," NASA Technical Paper No. 3327, Jan. 1993

[5] Dogra, V. K., Moss, J. N., Wilmoth, R. G., and Price, J. M., "Hypersonic Rarefied Flow Past Spheres Including Wake Structure," AIAA 92-0495, 1992.

[6] Moss, J. N., Mitcheltree, R. A., Wilmoth, R. G., and Dogra, V. K., "Hypersonic Blunt Body Wake Flow Computations Using DSMC And Navier-Stokes Solvers," AIAA 93-2807, 1993.

[7] Dogra, V. K., Moss, J. N., and Joseph, M. P., "Near Wake Structure For A Generic ASTV Configuration," AIAA 93-0271, 1993.

[8] Wilmoth, R. G., Micheltree, R. A., Moss, J. N., and Dogra, V. K., "Zonally Decoupled Direct Simulation Monte Carlo Solutions of Hypersonic Blunt-Body Wake Flows," *J. of Spacecraft and Rockets*, Vol. 31, No. 6, pp. 971-979. Also, AIAA 93-2808, 1993.

[9] Moss, J. N., Dogra, V. K., and Wilmoth, R. G., "DSMC Simulations of Mach 20 Nitrogen Flows about a 70 Blunted Cone and its Wake," NASA Technical Memorandum 107762, Aug., 1993.

[10] Jain, A. C., "Rarefied Gas Effects on Aerobraking/Reentry Vehicles With Wakes," REMTECH RTR No. 238-01, July 1991.

[11] Liberstein, M. H., *A Course of Numerical Analysis*, Harper & Row, New York, International Edition, 1969.